UT GSBS Dissertations and Theses (Open Access)   Graduate School of Biomedical Sciences

5-2017

MOLECULAR DETERMINANTS OF RESIDUAL DISEASE IN OVARIAN CANCER

Kshipra M. Gharpure

Follow this and additional works at: http://digitalcommons.library.tmc.edu/utgsbs_dissertations

Part of the Neoplasms Commons, and the Translational Medical Research Commons

The TMC LIBRARY
Health Sciences Resource Center

MOLECULAR DETERMINANTS OF RESIDUAL DISEASE IN OVARIAN CANCER

By

Kshipra M. Gharpure, M.S.

APPROVED:

_____

Anil K. Sood, M.D.
Advisory Professor

_____

Gary E. Gallick, Ph.D.

_____

Menashe Bar-Eli, Ph.D.

_____

Dihua Yu, M.D., Ph.D

_____

Jinsong Liu, M.D., Ph.D.

APPROVED:

_____

Dean, The University of Texas
MD Anderson Cancer Center UTHealth Graduate School of Biomedical
Sciences

MOLECULAR DETERMINANTS OF RESIDUAL DISEASE IN OVARIAN CANCER

A

DISSERTATION

Presented to the Faculty of

The University of Texas

MD Anderson Cancer Center UTHealth

Graduate School of Biomedical Sciences

in Partial Fulfillment

of the Requirements

for the Degree of

DOCTOR OF PHILOSOPHY

by

Kshipra M. Gharpure, M.S.

Houston, Texas

May, 2017

Dedication

To my family for all the love and support they have

provided throughout my life

Molecular Determinants of Residual Disease in Ovarian Cancer

Kshipra M. Gharpure

Advisory Professor: Anil K. Sood, M.D.

The standard treatment for high grade serous ovarian cancer is primary cytoreductive surgery followed by adjuvant chemotherapy. Residual disease followed by surgery is associated with adverse overall and progression-free survival as well as poor response to adjuvant chemotherapy. Accurate identification of patients at high risk of residual disease will help avoid unnecessary surgeries and help in triaging these patients to neoadjuvant chemotherapy prior to interval surgical debulking. In this study, we address this clinical issue by identifying and validating molecular biomarkers that can predict the likelihood of residual disease in ovarian cancer patients. Using publically available databases and microarray datasets, we identify FABP4 and ADH1B as markers of residual disease since the high expression of these genes in tumor samples is directly associated with the incidence of residual disease. We then investigate the underlying biology of residual disease and further demonstrate that FABP4 is functionally responsible for aggressive phenotype of ovarian cancer cells that lead to residual disease in cancer patients. Using sophisticated bioinformatics techniques, several *in vitro* and *in vivo* experiments and analysis of patient samples, we explored upstream regulation of FABP4 and identified miR-409-3p as a key regulator of FABP4 expression. We further discover hypoxia as a main tumor micro-environmental factor regulating miR-409-3p and FABP4 in ovarian cancer. Using RPPA and DESI-MS imaging techniques, we explore the downstream pathways of

FABP4 and discovered that FABP4 regulates several pathways associated with metastasis as well as it affects several metabolites in ovarian cancer cells. Collectively, our study provides the mechanistic understanding of residual disease biology and identifies miR-409-3p and FABP4 as potential therapeutic targets for ovarian cancer treatment.

Table of Contents

List of Figures

List of Tables

Chapter 1: Introduction

1.1 Residual disease in ovarian cancer

Primary cytoreduction followed by adjuvant chemotherapy is the standard mode of treatment for ovarian cancer patients. Residual disease following the primary debulking surgery has been associated with worse overall and progression-free survival as well as poor response to adjuvant chemotherapy. Historically, surgeries resulting in the residual tumor of size 2 cm or more were labeled as suboptimal; whereas the one resulting in smaller tumors were regarded as optimal surgeries. The goal of the primary debulking was to achieve optimal cytoreduction since the survival rate was proven to be inversely proportional to the size of the residual tumor [1].

There were however differences in the definitions of 'optimal debulking'. In 1975, a study of 102 patients of stage 2 and 3 concluded 1.5 cm to be the threshold. Surgeries that left the patients with a residual tumor greater than 1.5 cm diameter were called 'suboptimal' whereas others were called 'optimal'. The study showed poor survival for patients with residual disease diameter greater than 1.5 [1]. Later studies by Chi et al. and Hoskins et al. (GOG 97), however concluded that patients with residual disease less than 1cm had better survival than the ones with larger tumor size [2, 3]. Other studies confirmed these observations and a threshold of 1 cm was used to determine whether a surgery was optimal or suboptimal [4, 5]. Advances in surgical techniques and postoperative care made aggressive cytoreduction more feasible and complete resection of residual disease became achievable. Recent studies thus focused on the survival differences between complete resection (no residual disease, R0) and any visible residual disease (R0). They noticed that each

10% increase in extent of debulking resulted in 5.5% or 2-3 months of increase in patient survival [6, 7]. GOG trials 104 and 172 further supported the data and concluded that significant survival differences exist between patients with no visible residual disease and patients with gross residual disease (< 0.5 cm or 0.5-2 cm) [8, 9]. Studies since then have identified complete cytoreduction as an independent prognostic factor for overall survival with data showing the longest survival (86 months) for patients with no gross residual disease compared to 37-46 months of survival for patients with 0.1-1cm and >1cm RD [10, 11]. An exploratory study of 3126 patients from 3 randomized trials by duBois et al. was one of the largest studies to establish the importance of R0. The study concluded that the patients with R0 had significantly better survival than patients with RD and there was no significant survival difference between patients with RD 0.1-1cm or greater than 1 cm. The study also showed the median recurrence time for patients with R0 was 15.5 months, whereas recurrence was shorter for patients with RD 0.1-1cm or greater than 1cm [12].

Though complete resection is the ultimate goal of the surgeries, it should be noted that even highly experienced gynecologic oncology surgeons end up leaving residual disease. Studies have shown that approximately two-thirds of the patients with advanced-stage ovarian cancer get residual disease after the PDS [13]. This can happen due to the presence of numerous, dense nodules that simply can't be removed, distant tumor metastasis, location of tumor near critical organs (e.g., porta hepatis), extensive mesenteric involvement etc. Thus, not only surgical skills but tumor biology also plays a crucial role in residual disease pathology.

1.1.1 Neoadjuvant chemotherapy vs primary debulking

While complete cytoreduction is potentially achievable at most in 30% of the cases using aggressive surgical procedures; not all patients can tolerate such an approach. Women with advanced stage disease, bulky tumor, widespread metastasis or women who are very weak and sick to undergo any surgery may not be good candidates for extreme surgical efforts. Neoadjuvant chemotherapy is thus being suggested as an alternative to primary debulking surgery. The idea is to reduce tumor burden using neoadjuvant chemotherapy and thus improve the chances of achieving R0 at the interval surgery.

A randomized clinical trial of 718 patients was conducted by EORTC (European Organisation for Research and Treatment of Cancer) and NCIC (National Cancer Institute of Canada). The patients were randomly assigned to primary debulking surgery (PDS) or to neoadjuvant chemotherapy (NACT) followed by interval debulking surgery (IDS). Although progression-free survival (PFS) and overall survival (OS) were similar in both the groups, the rate of achieving optimal cytoreduction was higher (80.6%) in patients after NACT-IDS than in the patients who received PDS (41.6%). Furthermore, patients who underwent NACT and IDS had improved quality of life as measured by lesser postoperative complications and infections compared to the patients who received PDS [14]. Results from another multicenter phase 3 clinical trial of patients with advanced stage disease showed that NACT resulted in higher chances of optimal debulking with similar OS and PFS. Several retrospective studies and meta-analyses have so far suggested that NACT is

equivalent to PDS in terms of survival and can be a better treatment option for patients in which optimal cytoreduction is not possible following PDS [15-18].

Although neoadjuvant chemotherapy is a potentially feasible alternative, there can be risks of side effects, drug resistance and refractory diseases that are associated with NACT. Further studies are thus essential before NACT can be included in the standard of care [17]. On the other hand, patients who are very sick or have tumor burden that cannot be optimally debulked, benefit little from the aggressive surgery. They might in fact suffer from the morbidities associated with such an approach. It is therefore extremely important to carefully determine whether a given patient will benefit from NACT or PDS.

1.1.2 Predictors of residual disease

To determine if a patient will or will not have a suboptimal resection or residual disease, various predictive tools have been developed and tested.

Given the importance of CA-125 as a marker for advanced stage ovarian cancer, many studies have evaluated the ability of CA-125 as a predictive marker for optimal cytoreduction [19-21]. Optimal debulking was achieved in 73% of the cases when CA-125 levels were lower than 500 U/ml, conversely when CA-125 levels were higher than 500U/ml, only 22% of the cases resulted in optimal cytoreduction [20]. Some studies also evaluated the changes in serum CA-125 after NACT and concluded that patients with CA-125 levels < 100 U/ml are likely to achieve R0 status after IDS than patients with higher CA-125 levels [22]. However, contradicting results from additional studies suggested that levels of CA-125 cannot be used as a reliable

predictor for suboptimal cytoreduction [23-26]. Another such serum marker (HE4) was also evaluated and retrospective analysis indicated HE4 levels of 264pmol/L and ascites volume < 500mL can predict optimal cytoreduction with 100% sensitivity and 89.5% specificity [27]. The studies however lack external validations.

Computed Tomography (CT) imaging is the most commonly studied modality to predict residual disease in patients. Several studies have tried to build prediction models based on the CT scans of ovarian tumors. In a retrospective study of 118 patients, Kim et al. identified extension of omental disease to stomach and spleen, and metastasis at inguinal and pelvic lymph nodes observed in CT scans as predictive markers for suboptimal cytoreduction in ovarian cancer patients [28]. Another study reported CT findings of attachment of the omentum to the spleen and tumor burden of greater than 2 cm on the diaphragm, liver surface, or parenchyma, pleura, mesentery, gallbladder fossa, or suprarenal para-aortic nodes to be predictors of residual disease with a positive predictive value of 67% and negative predictive value of 96% [29]. Similar retrospective studies by Bristow et al. and Dowdy et al. reported large volume of ascites and CT scan showing peritoneal thickening, omentum extensions and mesenteric tumor burden as predictors of suboptimal cytoreduction [30, 31]. A prospective, multicenter, non-randomized trial of advanced stage ovarian cancer patients was conducted to explore the combination of CA-125 and CT scan as a predictive tool for suboptimal primary debulking surgery. Advanced stage, CA-125> 500U/ml and metastasis at retroperitoneal lymph node, small bowel mesentery, superior mesenteric artery, perisplenic area, lesser sac and small bowel thickening were found to be indicators of suboptimal surgery. A predictive model using these

criteria had an accuracy of 0.758 [32]. In another retrospective study, Janco et al., analyzed data from 279 patients and built a predictive model based on age, Eastern Cooperative Oncology Group performance status (ECOG PS), American Society of Anesthesiologists (ASA) score, thrombocytosis, CA-125 levels, albumin levels and CT images of lymphadenopathy (LP), large-volume ascites, diffuse peritoneal thickening (DPT), omental cake, and spleen or liver involvement. ECOG PS, DPT, and LP were found to be markers of suboptimal surgery with c index value of 0.685[33].

Although studies have indicated that CT-based predictive models of residual disease are promising, they have not been extensively validated. Moreover, the predictive ability of CT scans depend largely on radiological skills, surgical techniques and surgeon's and radiologist's view and assessments of the scans [13, 34].

Since the previously described predictive models had limited success, laparoscopic methods were explored to assess the resectability of tumor burden. A pilot study comparing the predictive ability of laparoscopy and laparotomy revealed the overall accuracy of laparoscopy in predictive residual disease as 97%. In no cases, the prediction of suboptimal disease changed by the laparotomy performed later. Thus laparoscopy was proved to be as reliable as laparotomy while avoiding unnecessary cytoreduction and morbidity associated with laparotomy [35]. Fagotti et al. then developed a quantitative prediction model based on the laparoscopic findings of tumor metastasis. Table 1 describes the scoring schema formulated by Fagotti et al. to calculate predictive index value (PIV) for each patient [13, 36]. A score of 8 or above was said to predict the likelihood of suboptimal cytoreduction. The positive predictive value for the technique was 100% whereas the negative predictive value was 70%

[36]. This method of a score-based predictions of RD was evaluated by at least two other studies- A study by Angioli et al. reported that 96% of the patients predicted to have R0 resection, had optimal debulking [37]. Brun et al. reported that the specificity and positive predictive values for the Fagotti score were 89% and 89% respectively while the sensitivity and negative predictive values were 46% and 44% [38].

Tumour site distribution	Laparoscopic predictive index score = 2	Laparoscopic predictive index score = 0
Peritoneal carcinomatosis	Unresectable massive peritoneal involvement plus miliary pattern of distribution	Carcinomatosis involving a limited area surgically removable by peritonectomy
Diaphragmatic disease	Widespread infiltrating carcinomatosis or confluent nodules to most of the diaphragmatic surface	Isolated diaphragmatic disease
Mesenteric disease	Large infiltrating nodules or involvement of the root of the mesentery assumed based on limited movements of various intestinal segments	Small nodules potentially treatable with argon-beam coagulation
Omental disease	Tumour diffusion up to the large curvature of the stomach	Isolated omental disease
Bowel infiltration	Bowel resection assumed to be required or miliary carcinomatosis at the mesenteric junction	No bowel resection required and no miliary carcinomatosis at the mesenteric junction
Stomach infiltration	Obvious neoplastic involvement of the gastric wall	No obvious neoplastic involvement of the gastric wall
Liver metastasis	Any surface lesions	No surface lesions

Table 1 A scoring schema developed by Fagotti et al. to calculate predictive index value (Taken with permission from the copyright holder, Nick, A.M., R.L. Coleman, P.T. Ramirez, and A.K. Sood, *A framework for a personalized surgical approach to ovarian cancer.* Nat Rev Clin Oncol, 2015. 12(4): p. 239-45.)

To assess the accuracy of the laparoscopic measurements, Fagotti et al. conducted a multicenter, prospective trial (Olympia-MITO13) of 120 patients. Apart from mesenteric retraction, all other variables reached an accuracy rate of 80% or more thus establishing the reproducibility of laparoscopic scoring [39]. The Fagotti score was again used in the SCORPION trial where primary debulking and neoadjuvant chemotherapy followed by IDS were compared. Patients with scores between 8-12 were randomly triaged to receive either neoadjuvant chemotherapy or PDS. The primary results of the trial were promising. The study reported that rates of complete debulking (R0) were similar in both the groups and quality of life scores were better for the patients who received neoadjuvant chemotherapy [40]. The predictive index scoring is also a part of M.D. Anderson algorithm which was developed as a part of the women's cancer moon shot program. Figure 1 explains the algorithm. As a part of quality improvement initiative, a laparoscopic assessment is conducted for each patient and the scoring is done by two surgeons to ensure an agreement about tumor resectability. An additional opinion is considered if necessary. After this careful assessment of disease distribution by two or more surgeons, a patient is triaged either for PDS or NACT followed by IDS depending upon the scores. Thus PDS is recommended for patients only when R0 resection is potentially achievable. Novel therapeutic agents are offered to the patients after the laparoscopy and prior to the PDS (window of opportunity). Preliminary results have indicated increased rates of complete resection (20% pre-implementation versus 84% post-implementation) and improved chances of R0 after neoadjuvant chemotherapy (65% pre-implementation versus 100% post-implementation) [13].
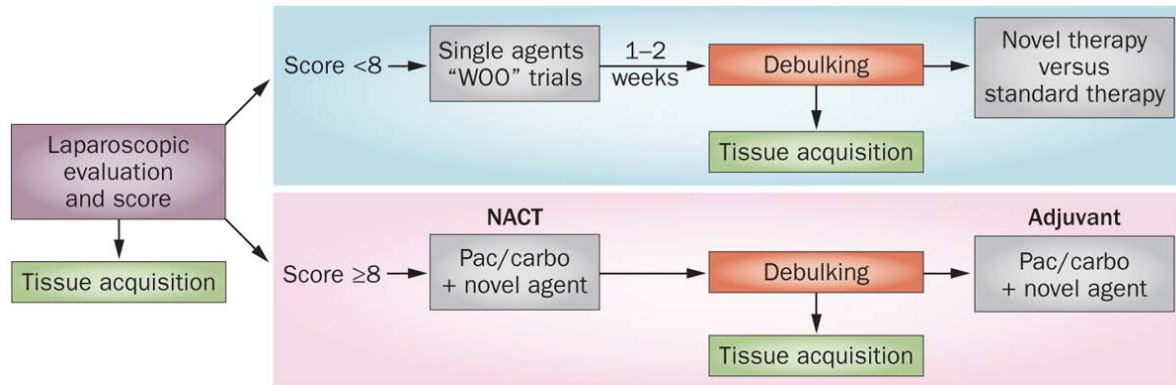
Figure 1 A schema for patients treated on the Anderson algorithm

(Taken with permission from the copyright holder, Nick, A.M., R.L. Coleman, P.T. Ramirez, and A.K. Sood, *A framework for a personalized surgical approach to ovarian cancer.* Nat Rev Clin Oncol, 2015. 12(4): p. 239-45.)

Residual disease could be a result of lack of surgical skills or location of nodules near critical organs or it could be because of invasive tumor biology. Considering that residual disease could be a consequence of biological characteristics of tumors, we hypothesized that tumor tissue based markers might be able to predict the likelihood of residual disease with high sensitivity. If a certain numeric threshold is established for the gene expression, then this method is essentially free of any subjective assessment seen in CT scans etc. Some studies have tried to develop molecular predictors for residual disease. They do however have certain limitations. Using stringent inclusion, exclusion criteria for tumor samples and validation studies, we discovered molecular biomarkers (FABP4 and ADH1B) to predict residual disease in ovarian cancer.

1.2 FABP4 (Fatty acid binding protein 4) and its biological functions

1.2.1 Role of FABP4 in various cell types

The FABP4 gene encodes fatty acid binding protein 4. It belongs to a family of fatty acid binding proteins that are intracellular lipid chaperons. They can reversibly bind to hydrophobic ligands such as fatty acids, eicosanoids and other lipids. The molecular weight of FABPs is 14-15 kDa and they share 20-70% sequence identity between different isoforms. Fatty acid binding protein 4 is also knowns as A-FABP4 or ap2 since it was first detected in adipocytes. Since then studies have shown that FABP4 is also present in macrophages, endothelial cells, dendritic cells and tumor cells [41-43]. In all these various cell types; FABP4 plays crucial roles in various cellular functions.

As a lipid chaperon, FABPs can transport fatty acids and lipids to various cell organelles. For example, it can transport lipids and fatty acids to mitochondria or peroxisome for oxidation, to the nucleus for lipid-mediated transcriptional regulation. The cells can secrete FABP4 and thus lipids outside the cells as a means of paracrine communication or it can store it in cytosol to regulate enzymatic activity. FABP4 can also send lipids to endoplasmic reticulum for membrane synthesis and signaling or it can transport fatty acids, lipids to lipid droplets for storage [44].
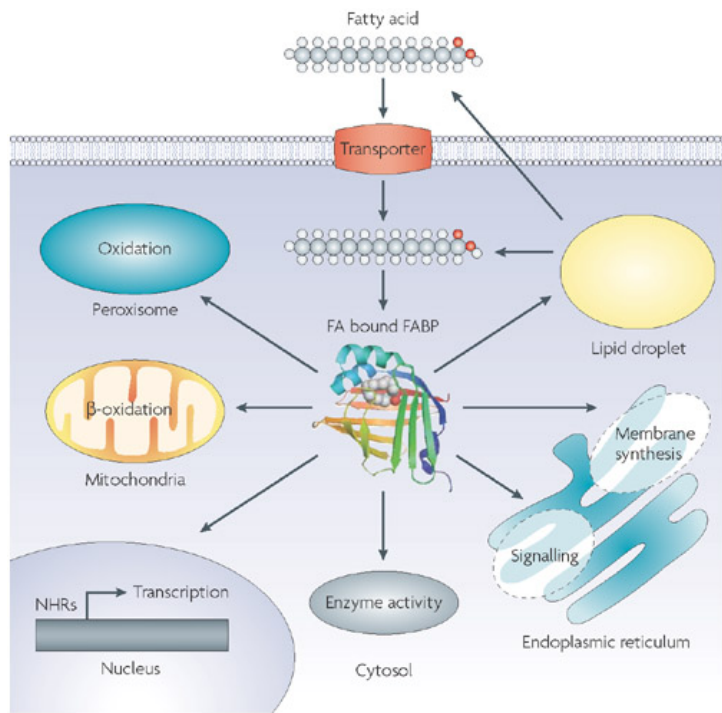
Figure 2 Functions of FABP in the cells [44]

(Taken with permission from the copyright holder. Furuhashi, M. and G.S. Hotamisligil,

Fatty acid-binding proteins: role in metabolic diseases and potential as drug targets.

Nat Rev Drug Discov, 2008. **7**(6): p. 489-503.)
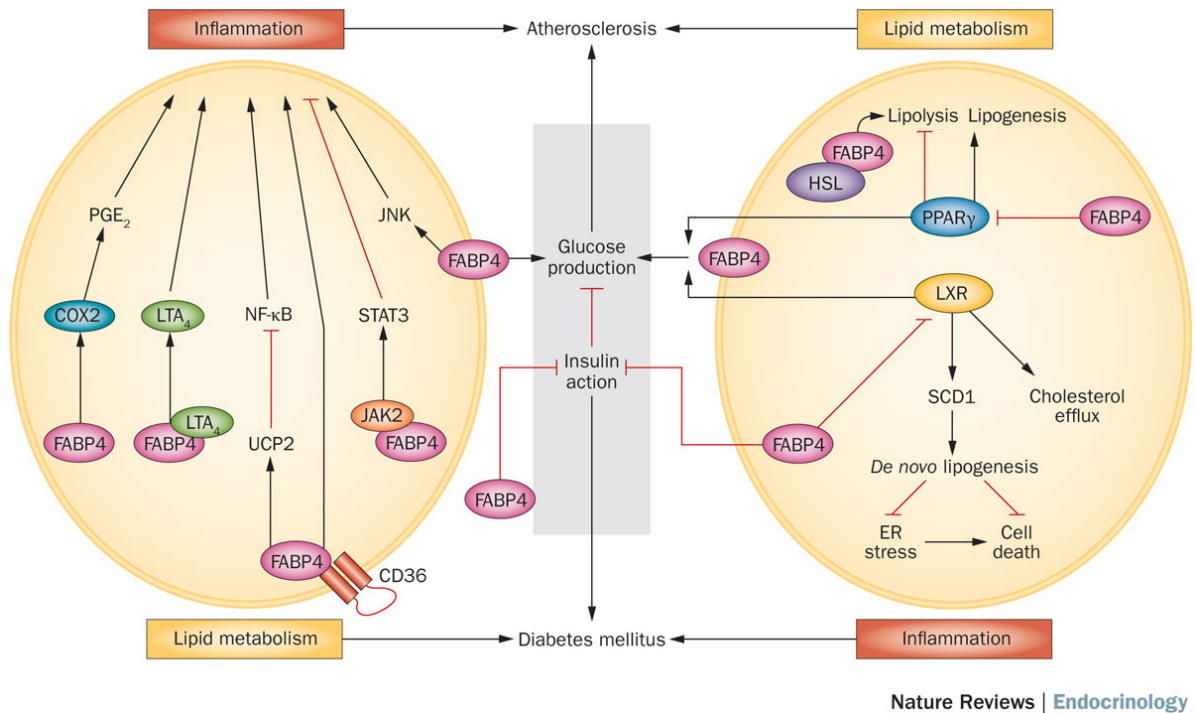
Figure 3 Role of FABP4 in lipid metabolism and inflammation[45]

(Taken with permission from the copyright holder. Hotamisligil, G.S. and D.A. Bernlohr, *Metabolic functions of FABPs--mechanisms and therapeutic implications.* Nat Rev Endocrinol, 2015. **11**(10): p. 592-605.)

FABP4 is known to be upregulated during differentiation of preadipocytes into adipocytes [46] and is known to regulate *de novo* lipogenesis [47]. It suppresses adipose tissue lipogenesis and increases lipolysis. It is also known to regulate eicosanoids, JAK2 and CD36 thus influencing various pathways related to inflammation. Increased levels of secreted FABP4 have been linked with obesity. FABP4 regulated lipid signaling has been known to influence glucose tolerance and insulin sensitivity.
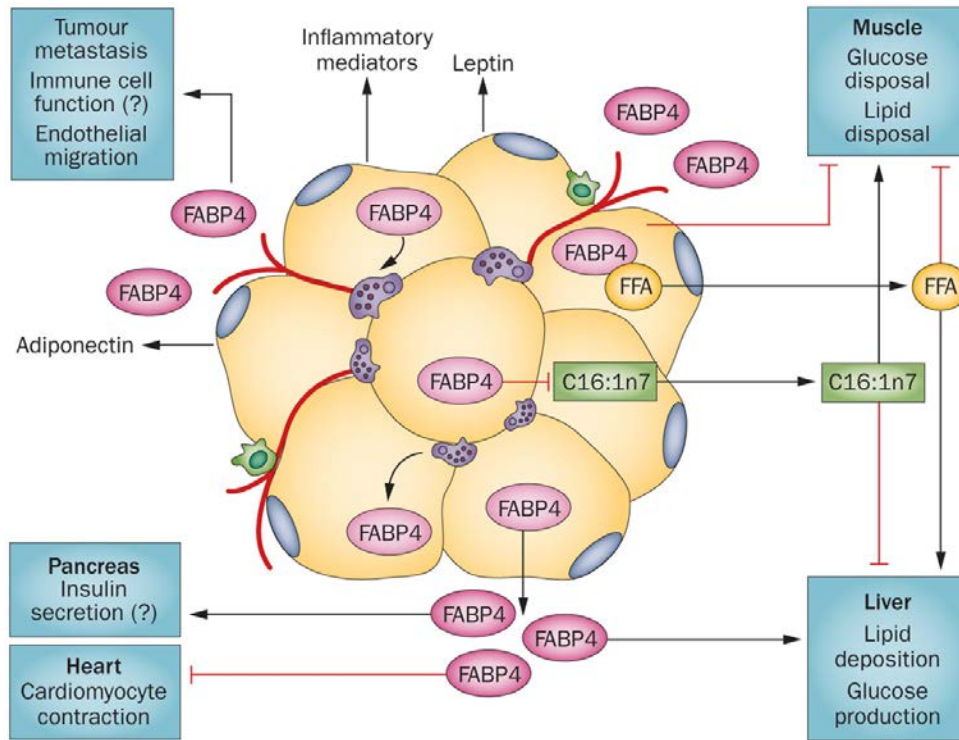
Figure 4 Functions of circulating FABP4[45]

(Taken with permission from the copyright holder. Hotamisligil, G.S. and D.A. Bernlohr, *Metabolic functions of FABPs--mechanisms and therapeutic implications.* Nat Rev Endocrinol, 2015. **11**(10): p. 592-605.)

FABP4 present in lung endothelial cells has been implicated in VEGF-induced airway angiogenesis and inflammation. Studies have thus shown that FABP4 plays a key role in vascular remodeling of airways and thus pathogenesis of asthma [48].

FABP4 is also expressed in differentiated and activated macrophages [44]. It regulates cholesterol accumulation in macrophages and also modulates inflammatory responses. It regulates several cytokines and pro-inflammatory enzymes such as tumor necrosis factor (TNF-1α), interleukin 1-β (IL1β), monocyte chemoattractant

protein 1 (MCP1), nitric oxide synthase (iNOS) and cyclooxygenase 2 (COX2). FABP4 has also been shown to regulate NF-kB and IKK (inhibitor of kappa kinase) and thus controls inflammatory and cytokine responses [49]. FABP4 also regulates foam cell formation and thus contributes to atherosclerosis [49, 50].

1.2.2 Role of FABP4 in cancer progression

Recent studies have highlighted the importance of FABP4 in tumor progression. In HUVEC cells, FABP4 regulates several pathways involving P38, eNOS, stem-cell factor (SCF)/c-kit and controls endothelial cell proliferation, migration and sprouting. In ovarian cancer, FABP4 has been shown to increase angiogenesis thus contributing to tumor progression [43]. In endothelial cells, inhibition of FABP4 increased reactive oxygen species and decreased angiogenesis. Knockdown of FABP4 *in vivo* using siRNA treatment, reduced proliferation (ki67), increased apoptosis (CC3) and reduced number of endothelial vessels (CD31) and thus had tumor inhibitory effects [51].

In ovarian cancer, FABP4 is known to play a key role in the interaction between cancer cell and adipocytes. Co-culture of adipocytes and cancer cells resulted in FABP4 mediated increased lipid content in cancer cells. Adipocytes thus provided lipids and induced β oxidation pathway in cancer cells, therefore promoting tumor progression by providing energy to cancer cells. The study further showed that knockout mouse model of FABP4 had lesser metastasis than the control mice [52]. In oral squamous cell carcinoma, FABP4 is predominantly expressed in tumor tissues compared to the non-tumorous tissues. Moreover, knockdown of FABP4 in SCC cancer cell line resulted in decreased cell proliferation possibly by inhibition of

phosphorylation of MAPK [53]. In breast cancer cells, treatment with exogenous FABP4 led to increased cell proliferation by inducing AKT-MAPK signaling cascade. Increase in FABP4 also led to an increase in the expression of fatty acid transport proteins in these cells which can also leads to increasing proliferation [54].

Our study focuses on FABP4 specifically present in the ovarian cancer cells and how it induces aggressive and infiltrative phenotype in the cells which ultimately results in residual disease.

1.3 Desorption electrospray ionization mass spectrometry

Since some of the proteins that were significantly altered in our RPPA analysis are also known to influence metabolic pathways and most importantly FABP4 is a fatty acid binding protein known to be involved in fatty acid oxidation pathways, we decided to investigate whether FABP4 affects the metabolic profile of ovarian cancer cell. Ovarian cancer metabolomics have been studied previously. Studies revealing glutamine dependency of cancer cells, importance of n-acetylaspartate pathway, amplification of USP13 or higher expression of fatty acid synthase; have all established the importance of metabolic changes occurring in cancer cells[55-58]. However, the studies do not provide spatial resolution of the metabolites. Without this information, it is difficult to pinpoint the exact compartment of the tumor (cancer cells or stroma) where the changes are occurring and hence it is difficult to fully comprehend the dynamics of these changes. Imaging techniques coupled with MS spectrometry, not only identify molecules or metabolites in a given sample but also provide information about their spatial distribution. DESI-MS imaging is one such

technique particularly used to analyze metabolites with low m/z values, such as lipids [59].

DESI-MS imaging has been used to analyze tissue extracts or plants or animal tissues [60-64]. Briefly, for the tissue analysis, a section of approximately 5-25 μm thickness is used. Then, a spray of solvents is directed onto the sample. When the droplets hit the tissue section, the analytes present in that area get dissolved in the solvent. A continuous spray of the solvent helps to generate secondary microdroplets containing the analytes that are then delivered to the mass spectrometry through an extended heated capillary[65]. Tandem MS is then used to identify the analytes. An image showing spatial distribution can then be made for each analyte. The most commonly used solvent system for DESI-MS imaging is a mixture of water and methanol or acetonitrile in combination with an acid modifier [61]. The composition of the solvent used for the analysis is critical since it can affect desorption and ionization of the molecules. The polarity of the solvent system also has an impact on the signals obtained from the species and can be adjusted to specifically focus on certain species [66, 67].
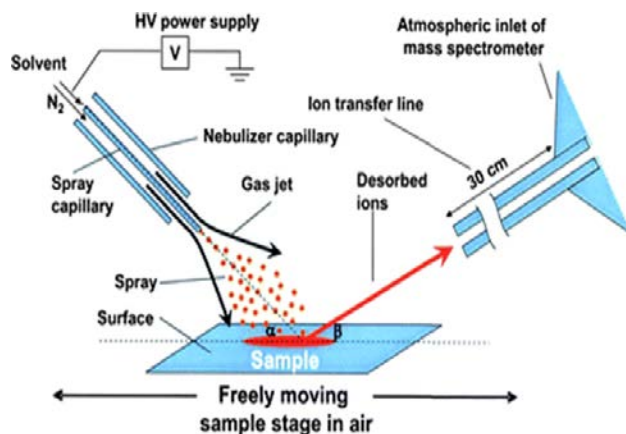
Figure 5 DESI-MS imaging methodology [68]

(Taken with permission form the copyright holder. Takats, Z., J.M. Wiseman, B. Gologan, and R.G. Cooks, *Mass spectrometry sampling under ambient conditions with desorption electrospray ionization.* Science, 2004. **306**(5695): p. 471-3.)

Since the technique does not require any staining or labelling procedures, the tissue morphology is maintained during the analysis [65]. This allows the images constructed from the MS data, to be directly compared with the H&E images of the tissue sections. Thus, it also helps to select the data from specific areas of the tissue sections, if needed. Figure 6 shows how DESI-MS images are analyzed along with H&E sections to know locations of a metabolite's signals.
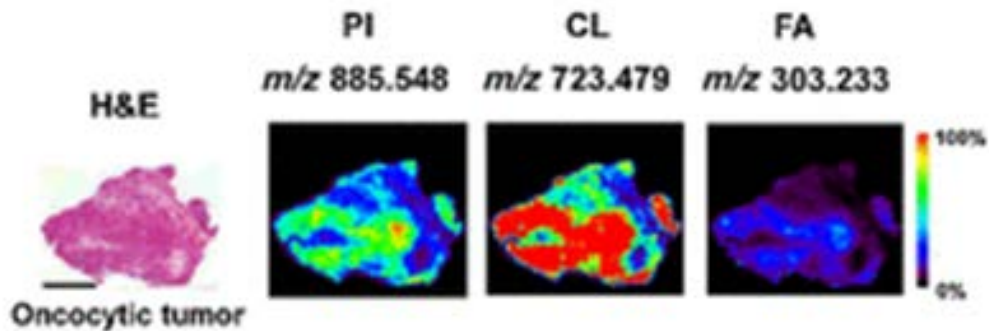
Figure 6 Example of DESI-MS images and comparison with H&E [69]

(Taken with permission from the copyright holder Zhang, J., W. Yu, S.W. Ryu, J. Lin, G. Buentello, R. Tibshirani, J. Suliburk, and L.S. Eberlin, *Cardiolipins Are Biomarkers of Mitochondria-Rich Thyroid Oncocytic Tumors.* Cancer Res, 2016. **76**(22): p. 6588-6597)

DESI-MS imaging has been mainly used to identify lipids present in the biological specimens. In case of spinal cord injury, it has been used to explore time-dependent chemical changes in the tissue and associate lipidomic profiles with the injury [70]. Sequential analysis of 2D images collected from DESI-MS has been used to construct 3D images of a mouse brain thus allowing to associate specific molecular moieties with the substructures of brain [71]. Recent studies have focused on using DESI-MS imaging as a diagnostic tool to differentiate between normal and cancerous tissues. For example, in bladder cancer, a study of patient tissue samples revealed that certain fatty acids, glycerophosphoinositols (PI) and glycerophosphoserines (PS) are elevated in tumors compared to adjacent normal tissue [72, 73]. DESI-MS analysis of prostate cancer tissues was also able to differentiate between cancerous and normal sections based on cholesterol sulfate expression [74]. Similar studies in glioblastoma, seminoma tissues and ovarian cancer have been conducted [75, 76]. In all these studies, DESI-MS imaging was able to provide a visual distinction between cancerous lesions and normal tissue section of a given specimen. Current work in the field is focused on using DESI-MS for more complex classifications such as tumor grading, differentiating between molecular subtypes of a cancer etc.

A comprehensive study of the determinants of residual disease is an unmet need in the field of ovarian cancer. In this study, we first aimed to identify molecular biomarkers that can predict the likelihood of residual disease with high sensitivity and selectivity. After discovering FABP4 as a biomarker for residual disease, we studied the upstream mechanism that leads to its upregulation in ovarian cancer. We then investigated the pathways regulated by FABP4 that eventually lead to residual disease in ovarian cancer.

Specific aims and hypothesis:

Aim 1: To identify a gene signature that will predict the residual disease status in ovarian cancer patients.

Hypothesis: A gene signature predictive of residual disease status can be identified through integrative analysis of patient database

Rationale: The standard treatment for ovarian cancer is to surgically remove as much tumor as possible, followed by chemotherapy. Recent reports suggest that patients most likely to benefit from surgery upfront are those with complete resection of disease (R0), which is among the strongest predictors of overall survival. The rates of R0 resection are approximately 30%. Unfortunately, all patients are currently subjected to a large incision for surgery when only 30% will have R0 resection and the remaining would ideally be treated with neoadjuvant chemotherapy. There are no reliable methods (e.g., imaging, biomarkers, etc.) that can accurately predict whether a given patient will have R0 resection at surgery. We therefore aim to identify molecular predictors of residual disease to allow reliable prediction of those most likely to benefit from surgery (i.e., achieve R0 resection).

Aim 2: To identify the mechanisms by which FABP4 is up regulated in ovarian cancer

Hypothesis: Decreased miRNA levels lead to elevated expression of FABP4 in ovarian cancer cells.

Rationale: High expression of FABP4 was found to correlate with high likelihood of residual disease. Analysis of TCGA data revealed there is no correlation between copy number and high FABP4 expression. After screening various micro-environmental factors, hypoxia seems to be the dominant factor related to upregulation of FABP4 in ovarian cancer cell lines. Through our *in silico* analysis, we discovered several miRNAs predicted to bind to 3'UTR of FABP4. Hence we propose that a miRNA is the main regulator of FABP4 in ovarian cancer and is the reason of its high expression in high grade serous ovarian tumors.

Aim 3: To determine the biological consequences of increased FABP4 expression on ovarian cancer growth and metastasis and investigate the underlying mechanisms.

Hypothesis: FABP4 promotes ovarian cancer metastasis by regulating key proteins and metabolites in cancer cells.

Rationale: One of the reasons that tumors cannot be resected is that they are widely disseminated or they are infiltrated into normal organs. Our preliminary results show that ectopic FABP4 promotes migration and invasion of cancer cells and silencing FABP4 inhibits these processes. We hence believe that higher expression of FABP4 makes the cancer cells more infiltrative and metastatic, leading to residual disease.

Chapter 2: Methods

Data for exploratory studies

For biomarker discovery, we used 2 large publicly available Affymetrix microarray datasets involving patients with HGSOCs and providing associated clinical information, including residual disease status. The first of these was the ovarian cancer cohort from The Cancer Genome Atlas [77]. We downloaded CEL files (level 1 data) for the ovarian samples (Affymetrix HT HG-U133A arrays, $n = 598$) on September 2, 2012; these represent the TCGA update that was current as of June 24, 2011 (revision 1007). We downloaded the associated clinical data ($n = 576$) on September 14, 2012. We excluded samples if they were from recurrent tumor, omental tumor, or normal tissue. When there were multiple primary tumor samples per patient, we retained data from just one sample. We also excluded cases if there was no information about residual disease status, if the tumor was not high grade, or if the patient received neoadjuvant chemotherapy. The second dataset was from the study of Tothill and colleagues [78]. We downloaded CEL files (Affymetrix U133+2 arrays, $n = 285$) and clinical data from the Gene Expression Omnibus (GSE9891) on September 13, 2012. We excluded cases from this dataset if tumor samples were low grade, of low malignant potential, non-serous histology, or non-ovarian or peritoneal origin. Cases were also excluded if the patient received neoadjuvant chemotherapy or if residual disease status was not provided. Accordingly, biomarker discovery was performed using only data from primary tumors of chemotherapy naïve patients with HGSOC.

For each of the datasets described above, we quantified expression at the probeset level with R statistical software (version 2.15.1) using the robust multi-array average procedure as implemented in the subroutine justRMA in the R "affy" package (version 1.34.0). We only considered probesets common to the array platforms used in the first 2 datasets. Except for the 4 samples marked for exclusion by TCGA, our sample filtrations described above were performed subsequent to the quantification step.

Validation studies

Following identification of candidate genes having a wide dynamic range and with high expression levels associated with high risk of residual disease in exploratory analyses, we performed validation studies in an independent cohort. Following Institutional Review Board approval, we obtained primary ovarian tumor samples from archived surgical material at The University of Texas MD Anderson Cancer Center (Houston, TX; $n = 84$) and the Pacific Ovarian Cancer Research Consortium at the Fred Hutchinson Cancer Research Center (Seattle, WA; $n = 55$). We also included 41 samples of omental tumor tissue from MD Anderson for comparison. All samples were selected from chemotherapy naïve tumors. Information about residual disease status in the validation cohort was extracted from patient medical records by clinical members of the team and was scored as R0 versus any residual disease. This information was kept blinded from all other team members until after predictions were made concerning identification of a subset of patients at high risk for residual disease.

These predictions were made on the basis of expression levels of a candidate gene of interest relative to 18S, assayed using qRT-PCR.

Exploratory data analyses.

We used 2-sample *t* tests to compare expression levels by residual disease status (R0 vs. any residual disease) in the TCGA and Tothill datasets, separately. We analyzed the resulting collections of nominal *P* values to identify probesets significant at a 10% or 5% false discovery rate (FDR) in each data set separately. We selected probesets meeting the specified criterion in both subsets. We produced density plots for these probesets, as well as heatmaps using hierarchical clustering, to illustrate patterns of expression. We examined the resulting plots to identify probesets with (i) wide dynamic range and (ii) high levels of expression associated with particularly high incidence of residual disease. We examined similar plots for the selected probesets in the Bonome and CCLE datasets to see whether the qualitative expression patterns were also observed there.

Selecting a sample size and prediction threshold for the validation study.

Following identification of genes for which high expression levels were associated with high risk of residual disease, we wished to select an *a priori* decision threshold for "calling" a patient in the validation cohort to be at high risk of residual disease based on elevated biomarker expression measured by qRT-PCR. Patients with expression of a candidate biomarker gene above the selected threshold would be in the predicted high-risk group for residual disease. To select a decision threshold,

we first computed the positive predictive values (PPV) in the TCGA and Tothill datasets at thresholds defined by varying quantiles of biomarker expression. We assumed that similar PPVs would apply to the validation cohort and performed numerical simulations to determine a decision threshold at which we would be maximally powered to detect a difference in incidence of residual disease in the validation set. We chose a threshold with an estimated power of at least 80% to detect a difference in incidence of residual disease significant at $P < 0.05$ using a 1-sided Fisher exact test. We used similar simulations for our initial sample size computations before collecting the validation set.

Statistical assessment of success.

We constructed a 2 × 2 table showing our calls (high risk of residual disease vs. lower risk of residual disease) compared with actual surgical outcomes (residual disease vs. R0) in the validation cohort. We used a 1-sided Fisher exact test to test the null hypothesis of equivalent rates of residual disease in the 2 groups against the alternative of increased incidence of residual disease in the predicted high-risk group.

Quantitative RT-PCR analysis.

Total RNA was extracted from the tumor tissues using the TRIzol® extraction method. RNA was then quantified using a nanodrop method and the 260/280 ratios were also checked to determine quality. RNA (1µg/sample) was reverse transcribed into cDNA using the Verso cDNA kit (Thermo Scientific, West Palm Beach, FL) according to the manufacturer's protocol.

qRT-PCR was performed on a 7500 PCR system (Applied Biosystems, Warrington, UK) using 1µL of cDNA for each sample. SYBR green (Applied Biosystems) was used to detect the products and 20pmoles of primer were used for the reaction. All reactions were carried out with 20µL of reaction mix and were performed in triplicate. We used the following primers: For *FABP4*, 5'-TGATGATCATGTTAGGTTTGGC-3' (forward) and 5'-TGGAAACTTGTCTCCAGTGAA-3' (reverse). For *ADH1B*, 5'-AGGGTAGAGGAGGCTGAAGA-3' (forward), 5'-ACCTGCTTCACTCTGGGAAA-3' (reverse). The PCR reactions were run under the following conditions: 50°C for 2 minutes, 95°C for 15 minutes, followed by 40 cycles at 95°C for 1 minute each. All reactions were analyzed with the 7500 Applied Biosystems PCR software (v.2.0.5). The cycle threshold (Ct) values of the target genes were initially normalized to the Ct values of 18S rRNA and melt curves were checked to determine the specificity of the reactions.

Cell line maintenance and siRNA and miRNA transfection

All cancer cell lines were maintained at 37°C and 5% CO_2 in culture with RPMI-1640 or Dulbecco's modified Eagle medium supplemented with 15% fetal bovine serum and 0.1% gentamicin sulfate (Gemini Bio-Products, Calabasas, CA, USA). The cell lines were obtained from American Type Culture Collection and were routinely tested for absence of *Mycoplasma* and were validated using Short Tandem Repeat DNA fingerprinting. All the *in vitro* experiments were performed at 60-80% cell confluence.

All siRNA transfections were conducted using Lipofectamine as a transfecting agent. SiRNA concentration of 100 nM was used, and the ratio of Lipofectamine (Life Technologies, Carlsbad, CA, USA) to a specific siRNA was 3:1. The cells were treated with siRNAs for 4 hrs in serum-free media before incubation in complete media for the specified time frame. For miRNA transfections (mimic and anti-miRNA), RNAiMAX (Life Technologies, Carlsbad, CA, USA was used as a transfection agent, and the ratio of RNAiMAX to a specific miRNA was 2:1. The concentration of miRNA-mimic or anti-miR was 40 nM concentration and the transfections were conducted in serum-free conditions. After 4 hrs, the cells were incubated in complete media for the specified time frame. The sequences for siRNAs and miRNAs are listed in Table 2.

In vivo models

Female athymic nude mice were purchased from Taconic Farms (Hudson, NY) and housed in pathogen-free conditions. The mice were cared for according to the guidelines of the American Association for Accreditation for Laboratory Animal Care International and the US Public Health Service Policy on Humane Care and Use of Laboratory Animals. All *in vivo* experiments and protocols were approved by MD Anderson's Institutional Animal Care and Use Committee.

For all *in vivo* experiments, cells were trypsinized at 60-80% confluence, neutralized with FBS-containing media and centrifuged at 1200 rotations per minute at 4°C for 6 minutes. The cells were then washed with phosphate-buffered saline (PBS) and reconstituted in Hank's balanced salt solution (HBSS, Gibco, Carlsbad, CA, USA) to the desired concentration (1×10^6 cells/mouse in 50 µl for A2780 cells,

8×10^5 cells/mouse in 50 µl for luciferase-labelled HeyA8 MDR cells, 1×10^6 cells/mouse in 50 µl for luciferase-labelled Ovcar 5 cells). Mice were anesthetized with ketamine, and an incision was made above the left ovary. The cells were directly injected into the ovary using a 1-ml tuberculin syringe with a 30-gauge needle. The incision was then closed using surgical clips and sutured to ensure complete closure of the surgery site. The mice were returned to cages until full recovery. Mice were given sustained-release buprenorphine subcutaneously for pain management, and the clips were removed after a week when the incision was completely healed.

No therapeutic intervention was conducted in the experiment in which FABP4-overexpressing cells were injected. For all therapeutic experiments, a siRNA or miRNA dose of 200 µg/kg was used, and the treatments were started 1 week after cell injections. The mice were divided into two groups: control and treatment, 10 mice/group. Mice in the control group received control siRNA or control miRNA incorporated into neutral DOPC liposomes. Mice in the treatment group received FABP4 siRNA or a miR-409-3p mimic incorporated into DOPC liposomes. The doses were given twice weekly intraperitoneally. The mice were monitored daily for any toxic effects. Luciferase imaging was conducted to observe the effect of treatments on the metastasis as described previously [79]. Briefly, Imaging and data acquisition were performed with the IVIS Spectrum *in vivo* imaging system coupled to Living Image Software (Xenogen). The mice were first anesthetized in an acrylic chamber with a mixture of 1% isoflurane. They were then injected intraperitoneally with luciferin potassium salt (15 mg/ml) in PBS at a dose of 150 mg/kg body weight. A digital grayscale image was initially acquired, which was then overlaid with a pseudocolor

image representing the spatial distribution of detected photons emerging from active luciferase present within the animal. Signal intensity was expressed as a sum of all photons detected per second. Once a mouse in any group became moribund, all mice were euthanized. Mouse weight, tumor weight, number of nodules and locations of metastasis were recorded. Tumor tissues were then frozen in optimal cutting temperature media, fixed in formalin for paraffin embedding or snap-frozen.

Liposomal nanoparticle preparation

Incorporation of siRNA or miRNA into DOPC liposomes was achieved as previously described [80]. Briefly, DOPC and siRNA or miRNA were mixed at a ratio of 1:10 (w/w) in the presence of tertiary butanol. Tween 20 was added to the mixture at a ratio of 1:19. The mixture was vortexed and frozen in an acetone/dry ice bath and lyophilized. The lyophilized preparations were hydrated with PBS at room temperature to a concentration of 200 µg of siRNA or miRNA/kg per injection per mouse.

MiRNA-mRNA expression association in TCGA OV samples

TCGA cases were included if the patients had high-grade disease and no history of pre-treatment. TCGA gene expression quantification were produced using justRMA applied to the CEL files from TCGA (Affymetrix HT HG-U133A arrays, n = 598) ([4]). TCGA miRNA microarray level 3 data (Agilent 8 x 15K Human miRNA-specific microarray) was obtained from the Data Access Matrix. Data was available for 799 miRNAs. There were 541 samples meetings the inclusion criteria who had both gene expression and miR data available. The association between each probe

for the gene of interest and each available miRNA was assessed using the Maximal Information Coefficient (MIC) computed using MINE software of Reshef et al. [81].

MiRNA-mRNA Interactions

We retrieved miRNA-target interaction information from miRWalk2.0 (http://www.umm.uni-heidelberg.de/apps/zmf/mirwalk/) that hosts miRNA-target predictions from twelve programs. We selected the cases predicted by at least seven algorithms (half of the total number of programs checked+1). The interaction between miR-409-3p and FABP4 (NM_001442) (3' UTR) was predicted by nine programs (miRWalk, Microt4, miRanda, miRMap, miRNAMap, PITA, RNA22, RNAhybrid, Targetscan). We used Perl to sort the information available and Latex to present the sites most probably to interact.

Luciferase reporter assays, and FABP4 3′UTR site mutagenesis

Luciferase assays were conducted as described previously [82]. Briefly, a GoClone pLightSwitch luciferase reporter for the 3'UTR of FABP4 was purchased from Switchgear Genomics (Menlo Park, CA, USA).

HeyA8 MDR cells were transfected with control miRNA or miR-409-3p mimic (100 nM; Life Technologies, Carlsbad, CA, USA) with the help of FuGENE HD transfection agent. The cells were also transfected with 3'UTR reporter constructs and Cypridina TK controls (pTK-Cluc). After 24 h, the LightSwitch Dual Luciferase assay kit was used and the luciferase signal was measured using a microplate luminometer, as per the manufacturer's guidelines (Biotek, Winooski, VT, USA). Luciferase activity

was normalized using the Cypridina TK control, and an empty 3'UTR construct was used as a negative control. The ratios were then normalized to the scrambled control miRNA. Mutant FABP4 3'UTR was created for the predicted binding site mentioned in Figure 21 using a QuickChange lightning multi-site-directed mutagenesis kit (Agilent Technologies, Santa Clara, CA, USA) using the primers mentioned in Table 2. The mutation was then confirmed using Sanger DNA sequencing before the mutant FABP4 3'UTR was used for the luciferase assay.

Immunoblotting

Protein lysates from tumor tissues or cultured cells were prepared using modified RIPA buffer containing proteinase and phosphatase inhibitors. Protein concentrations were determined using the BCA protein assay reagent kit (Pierce Biotechnology, Rockford, IL, USA). Lysates were loaded and separated on SDS-polyacrylamide gels. The proteins were then transferred to a nitrocellulose membrane using a semidry electrophoresis procedure (BioRad Laboratories, Hercules, CA, USA). The membrane was blocked at room temperature for 1 h in 5% milk powder in Tris-buffered saline with Tween 20 (TBST) and then incubated at 4°C overnight with primary antibodies; FABP4 (catalog number HPA002188; Sigma) and vinculin as a loading control (catalog number V9131; Sigma). After washing with TBST, the membranes were incubated with horseradish peroxidase-conjugated horse anti-rabbit IgG (for FABP4) or anti-mouse IgG (for vinculin) (catalog numbers NA834 and NA931; 1:2000; GE Healthcare) at room temperature for 2 h. An enhanced

chemiluminescence detection kit (catalog number NEL104001EA; Pierce Biotechnology) was used to visualize the horseradish peroxidase signal.

Migration and invasion assay

Modified Boyden chambers (Coster, MA, USA) were coated with 0.1% gelatin (migration) or defined basement membrane matrix (invasion). Defined basement membrane matrix (for invasion) was prepared in a 10-ml stock solution with laminin (50 µg/ml), 1 ml of type IV collagen (50 µg/ml), 0.2 ml of gelatin (2 mg/ml), and 4 ml and 4.8 ml of PBS. In the upper chamber, HeyA8 MDR and Ovcar 5 cells (0.7×10^5) suspended in 200 µl of serum-free media were added 48 h after siRNA/miRNA transfections or Tamoxifen treatments. In the upper chamber, complete media for cells containing 10% fetal bovine serum (500 µl) was added as a chemo-attractant. The chambers were incubated at 37°C in 5% CO_2 for 6 h (migration assay) or 24 h (invasion assay). After incubation, the cells in the upper chamber were removed with cotton swabs. Cells were fixed, stained, and counted using light microscopy. Cells from five random fields were counted. Experiments were done in triplicate.

Tumor samples

High-grade ovarian tumor samples which are chemotherapy naïve were obtained after the study was approved by the Institutional Review Board, and written consent was obtained for the use of patient samples for research.

miR-409-3p expression in patient tumor samples as taken from GEO dataset

The detailed method can be found in [83]. Briefly, 4 samples of HOSE (Normal primary ovarian surface epithelial cells taken from normal postmenopausal women) and 19 serous epithelial ovarian cancer samples were analyzed. The tumor samples were of high-grade and contained more than 70% malignant epithelial cellularity. The cloning frequency of a specific miR expressed as a fraction of total reads from a given samples was used to compare the relative expression of miRNAs between samples.

***In situ* hybridization**

In situ hybridization was done as previously described in [82] . High grade serous ovarian cancer tissues which are chemotherapy naïve were selected. Xylene and an ethanol dilution series were used for deparaffinization and rehydration of the formalin-fixed, paraffin-embedded tissue sections. Tissue sections were digested with 15 µg/ml proteinase K for 20 minutes at room temperature and then loaded onto Ventana Discovery Ultra (Tucson, AZ) for *in situ* hybridization analysis. The tissue slides were then incubated with a double-digoxigenin-labeled miRCURY LNA miRNA probe (Exiqon, Woburn, MA, USA) for 2 h at 55°C. Three percent H_2O_2 was used to inactivate endogenous peroxidases. After incubation with polyclonal anti-digoxigenin antibody and horseradish peroxidase-conjugated secondary antibody (Ventana), a tyramine-conjugated fluorochrome (TSA) reaction was performed for 12 minutes. Sequential TSA rounds were performed for the detection of proteins using the same protocol. Slides were mounted with antifading ProLong Gold Solution (Life Technologies).

Immunostaining

Paraffin-embedded sections (5 μm) of tumor tissues were cut and used for detection of FABP4. Formalin-fixed sections were deparaffinized by sequential washings with xylene, 100% ethanol, 95% ethanol, 80% ethanol, and PBS. A suitable antigen retrieval method was used. Endogenous peroxidase was blocked by incubating the slides with 3% hydrogen peroxide in PBS. Nonspecific binding was prevented by incubating the slides with 4% fish gelatin. This was followed by incubation with primary antibody overnight at 4°C. The next day, the slides were washed with PBS and incubated with suitable secondary antibody (goat anti-rabbit horseradish peroxidase antibody diluted in protein block solution) for 1 h at room temperature. The slides were then washed with PBS followed by development with 3,3'-diaminobenzidine. The nuclei were stained with Gill's hematoxylin solution and the slides were then mounted.

Quantitative real-time PCR

Total RNA was extracted from the tumor tissues using the Direct-Zol RNA extraction kit (Zymo Research, Irvine, CA, USA). RNA was then quantified using a NanoDrop spectrophotometer method and the 260 nm/280 nm ratios were checked to determine quality. RNA (1 μg per sample) was reverse-transcribed into cDNA using the Verso cDNA kit (Thermo Scientific, West Palm Beach, FL, USA) according to the manufacturer's protocol.

Quantitative real-time PCR was performed on a 7500 PCR system (Applied Biosystems, Warrington, UK) using 1 μl of cDNA for each sample. SYBR green

(Applied Biosystems) was used to detect the products, and 20 pmol of primer was used for the reaction. All reactions were carried out with 20 µl of reaction mix and performed in triplicate. We used the primers mentioned in Table 2. The following conditions were used for PCR: 50°C for 2 minutes, then 95°C for 15 minutes, followed by 40 cycles at 95°C for 1 minute each. All reactions were analyzed using the 7500 Applied Biosystems PCR software (v.2.0.5). The cycle threshold values of the target genes were initially normalized to the cycle threshold values of 18S rRNA, and melt curves were checked to determine the specificity of the reactions.

For miRNA quantifications, Taqman miRNA assays (Life Technologies) were used and reverse-transcription real-time PCR was performed, according to the manufacturer's instructions. RNU6B was used as a housekeeping gene.

Copy number analysis

TCGA mRNA microarray (Agilent 244K Custom Gene Expression G4502A-07, Affymetrix Human Genome U133A 2.0 Array, Affymetrix Human Exon 1.0 ST Array) and RNASeqv2 level 3 and clinical data were retrieved from Broad GDAC Firehose http://gdac.broadinstitute.org/. Putative copy-numbers from GISTIC were retrieved from cbio portal (http://www.cbioportal.org/). To find the relationship between FABP4 expression and copy number, we first employed a Shapiro-Wilk test and verified that the data doesn't follow a normal distribution. The nonparametric test Kruskal-Wallis test, was applied and no relationship between FABP4 and copy-number could be established. A box-and-whisker plot (Box plot represents first (lower bound) and third

(upper bound) quartiles, whiskers represent 1.5 times the interquartile range) was used to visualize the data (log2(x)).

Correlation of FABP4 with genes from hypoxia metagene signature

The Spearman's rank-order correlation test was applied to measure the strength of the association between FABP4 and the genes from the Winter et al. hypoxia metagene[84]. We imposed a cut-off of functional relevance on the Spearman correlation coefficient in absolute value of 0.2 based on the method published previously [85].

Correlation of FABP4 expression with metabolites present in patient tumor samples.

The metabolomics data and the gene expression data (normalized log values) were taken from [58, 86, 87]. High grade serous ovarian cancer tumor samples (n=66) were analyzed. The samples were divided into high or low FABP4 group based on the median expression of FABP4 in all the samples. Similarly a median value for each metabolite was calculated for high or low FABP4 samples. The comparison is presented as antilog values.

DESI-MS imaging

DESI-MS imaging was conducted as described previously [88]. A 2D Omni Spray (Prosolia Inc., Indianapolis, IN) coupled to an LTQ-Orbitrap Elite mass spectrometer (Thermo Scientific, San Jose, CA) was used for tissue imaging. DESI-

MS imaging was performed in the negative and positive ion mode from *m/z* 100 to 1500, using a hybrid LTQ-Orbitrap mass spectrometer which allows for tandem MS experiments, high mass accuracy (<5 ppm mass error), and high mass resolution (240,000 resolving power) measurements. The spatial resolution of the imaging experiments was 200 µm. Spatially accurate ion images were assembled using BioMap and MSiReader software. The histologically compatible solvent system dimethylformamide:acetonitrile (DMF:ACN) 1:1 (v/v) was used for negative ion mode analysis, at a flow rate of 1.2 µl/min. For positive ion mode analysis, pure ACN was used, at a flow rate of 3 µl/min. The N_2 pressure was set to 185 psi. For ion identification, high mass resolution/accuracy measurements using the same tissue sections analyzed were conducted. Tandem MS analyses were performed using both the Orbitrap and the linear ion trap for mass analysis.

Histopathology and light microscopy

The same tissue sections analyzed by DESI-MS imaging were subjected afterwards to standard H&E staining protocol. Light microscopy images of the H&E stained slides were taking using the EVOS FL Auto Cell Imaging System (Invitrogen, Thermo Fisher Scientific, Waltham, MA, USA).

Effect of Tamoxifen on expression of FABP4

The drug was dissolved in DMSO and physiologically achievable concentrations were used for the experiments. HeyA8 MDR cells were plated in 24

well plates and serum starved before tamoxifen treatment. The cells were collected and RNA was extracted for qRT-PCR.

Free fatty acid uptake assay

The experiment was conducted as per the manufacturer's instructions (Free Fatty Acid Uptake Assay Kit (Fluorometric, ab176768) Cambridge, MA, USA). The cells were serum starved and treated with tamoxifen at a desired concentration. Then the fatty acid dye loading solution was added (100µl/ well of a 96 well plate). The florescence signal was measured at Ex/Em 485/515 nm using a bottom read mode after 30 minutes incubation at room temperature.

Survival analysis

Survival analysis was performed in R (version 3.2.5) using Tothill data set. The relationship between overall survival, respectively progression free survival and covariates (mRNA expression levels and clinical parameters (age and stage) was examined using a Cox proportional hazard model. A multivariate Cox proportional hazard model was fitted, including the clinical parameters and mRNA expression significant in the univariate analysis.

Statistical Analysis

MS data corresponding to the areas of interest were extracted using MSiReader software. The *m/z* range was discretized by performing hierarchical clustering and cutting the resulting dendrogram at distance 0.05. Peaks appearing in

more than 10% of the pixels were kept for analysis. Logistic regression was performed with Lasso regularization using the "glmnet" package (26) in the R language. Regularization parameters were determined by 3-fold cross-validation analysis. The data were randomly equally divided into training and validation sets of samples, 50-50 per patient basis. For other assays, Student's *t*-test was performed to examine the difference between the control and treatment groups. A *P* value less than 0.05 was deemed statistically significant. All the statistical tests were two-sided. Error bars represent standard error from triplicates.

siRNA	Sequence
Control siRNA	5'-UUAUGCCGAUCGCGUCACATT-3' 3'-TTAAUACGGCUAGCGCAGUGU-5'
FABP4 siRNA seq 1	5'-GACGUUGACCUGGACUGAAdTdT-3' 3'-UUCAGUCCAGGUCAACGUCdTdT-5'
FABP4 siRNA seq 2	5'-GUGGGAUAUAUUGUUCAAAdTdT-3' 3'-UUUGAACAAUAUAUCCCACdTdT-5'

Primers	Primer sequences
18S	5'CGCCGCTAGAGGTGAAATTC3' (forward) and 5'TTGGCAAATGCTTTCGCTC3' (reverse)
FABP4	5'-TGATGATCATGTTAGGTTTGGC-3' (forward) and 5'- TGGAAACTTGTCTCCAGTGAA-3' (reverse)
Mutated	CAACAATATCTTTTTGAACAATATATCCCACAGGCGACGGTAGAGTTCAAT GCGAACTTCAGTCCAGGTCAA (forward) TTGACCTGGACTGAAGTTCGCATTGAACTCTACCGTCGCCTGTGGGATAT ATTGTTCAAAAAGATATTGTTG (reverse)

Table 2 siRNA and primer sequences used in the study

Chapter 3: Molecular biomarkers for prediction of residual disease in ovarian cancer

We used two publicly available datasets –TCGA and Tothill [77, 78] containing samples of HGSOC (High grade serous ovaria cancer). We set up specific inclusion and exclusion criteria for our analysis. We excluded samples if they were from recurrent tumors, metastatic sites or normal tissues. We also excluded the tumors that were not of high grade serous histology or were taken from patients who had undergone neoadjuvant chemotherapy. From the two datasets, we thus selected 491 (TCGA) and 189 (Tothill) cases that met our criteria (Tumors that were taken from primary site i.e. ovary, are chemotherapy naïve and are of stage 3 and above from high grade serous histological subtypes).

From the TCGA dataset, 77% of the patients had RD while 74% of the patients from the Tothill dataset had residual disease. We then analyzed the patient survival data for these cases. We initially grouped them into 4 groups based on the size of the residual disease   >20mm (n=102), 11-20mm (n=34), 1-10mm (n=242), No macroscopic disease (n=113) for TCGA and macro-size NK/ exact size unknown (n=13), >1cm (n=57), <1cm (n=66), nil (n=50) for Tothill dataset. Figure 7 (a and b) shows the survival differences among these different groups. When we compared overall survival of patients with R0 versus any RD (other 3 groups combined), we noticed that R0 patients had significantly better overall survival compared to the rest (Figure 7 c and d), $p<0.0001$ and $p<001$ for TCGA and Tothill respectively.
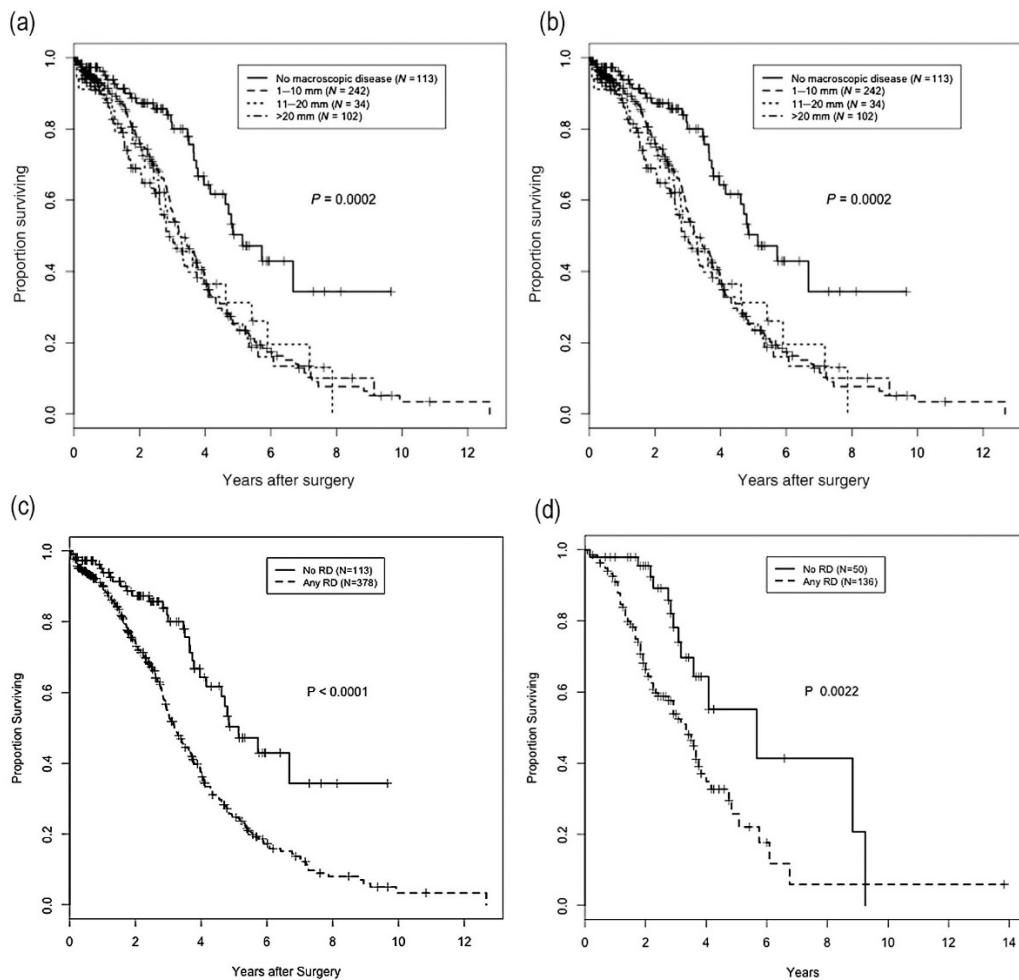
Figure 7 Overall survival for the patients with high grade serous ovarian cancer, grouped according to the size of the residual disease after primary debulking surgery. TCGA (a) and Tothill (b) datasets were investigated. Analysis of TCGA (c) and Tothill (d) patient datasets from the comparison of R0 to any residual disease (RD).

We then used the clinical information of RD status and gene expression data for the tumor samples collected from TCGA and Tothill datasets to identify genes associated with increased incidence of residual disease. We only used the probe sets that are common in TCGA and Tothill sets and recorded the mean expression of the gene in RD group and R0 group. Table 3 shows the list of 47 probe sets (associated with 38 genes) that have differences in their expression between RD and R0 group at 10% false discovery rate.

Gene	Probe set
ADAM12	213790_at
ADH1B	**209612_s_at**
ADH1B	**209613_s_at**
ADIPOQ	207175_at
ALDH1A3	203180_at
ALDH5A1	203609_s_at
AQP1	209047_at
BCHE	205433_at
COL11A1	37892_at
COL16A1	204345_at
COL3A1	201852_x_at
COL5A1	203325_s_at
COL6A2	213290_at
COL8A1	214587_at
CRISPLD2	221541_at

CXCL12	203666_at
CXCL12	209687_at
CYR61	201289_at
DCN	201893_x_at
DCN	209335_at
DCN	211813_x_at
DCN	211896_s_at
ETV1	221911_at
FABP4	**203980_at**
FAP	209955_s_at
GADD45B	207574_s_at
GADD45B	209304_x_at
GADD45B	209305_s_at
GFPT2	205100_at
GREM1	218468_s_at
GREM1	218469_at
KCNE4	222379_at
LUM	201744_s_at
NBL1	201621_at
NBL1	37005_at
NFYA	204107_at
OMD	205907_s_at
PDGFD	219304_s_at

PDLIM3	209621_s_at
PDPN	221898_at
POLR1C	207515_s_at
PTGIS	208131_s_at
SVEP1	213247_at
TIMP3	201150_s_at
VGLL3	220327_at
VSIG4	204787_at
XYLT1	213725_x_at

Table 3 List of 47 probe sets that have different expression in R0 and RD groups and are common between TCGA and Tothill datasets (10% false discovery rate)

When the false discovery rate was lowered to 5%, we identified 8 genes that differed in their expression between RD vs. R0 groups and were common in TCGA and Tothill dataset. Figure 8 shows the heatmaps of the expression of those 8 genes for TCGA (a) and Tothill (b) sets.
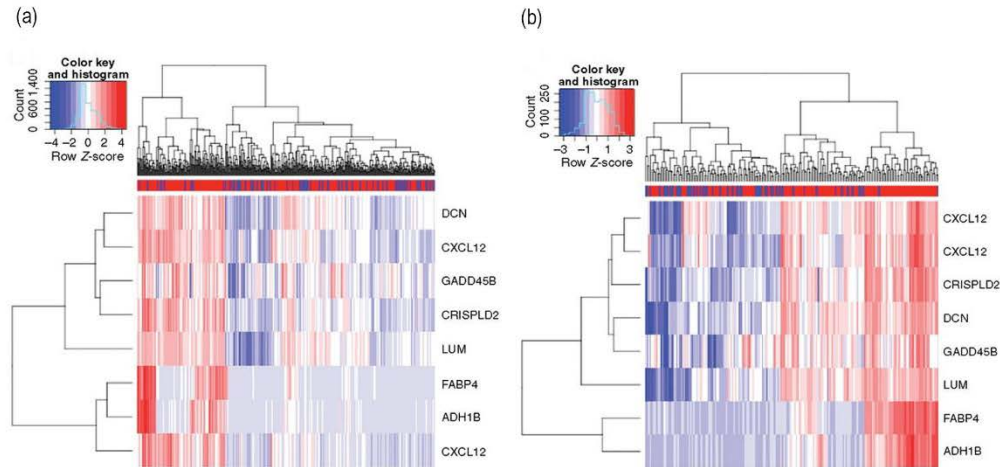
Figure 8 Heatmaps showing expression of top 8 genes that have different expression between R0 and RD groups as observed in TCGA (a) and Tothill (b) datasets. (<5% false discovery rate). The color bars at top indicate residual (red) or non-residual (blue) cases. The red and blue bars within the map indicate high and low gene expression respectively. High expression of FABP4 and ADH1B correlate with residual disease incidences while low expression correlate with R0 incidences. The expression of FABP4 and ADH1B correlate well with each other.

We then investigated the density plots of the 8 genes presented in Figure 7. We noticed that for FABP4 and ADH1B, the expression distribution was bimodal, as opposed to the distribution of other genes which did not show a qualitative shift in their expressions in RD and NoRD cases. For FABP4 and ADH1B, many samples had low expression of these genes, however for a small set of samples, the expression was very high. Nearly all the samples above a certain level of expression have RD. Figure 9 shows gene expression and RD status for FABP4, ADH1B in TCGA and Tothill sets.

(a)

Expression of FABP4 in TCGA

(b)

Expression of FABP4 in Tothill

(c)

Expression of ADH1B in TCGA

(d)

Expression of ADH1B in Tothill
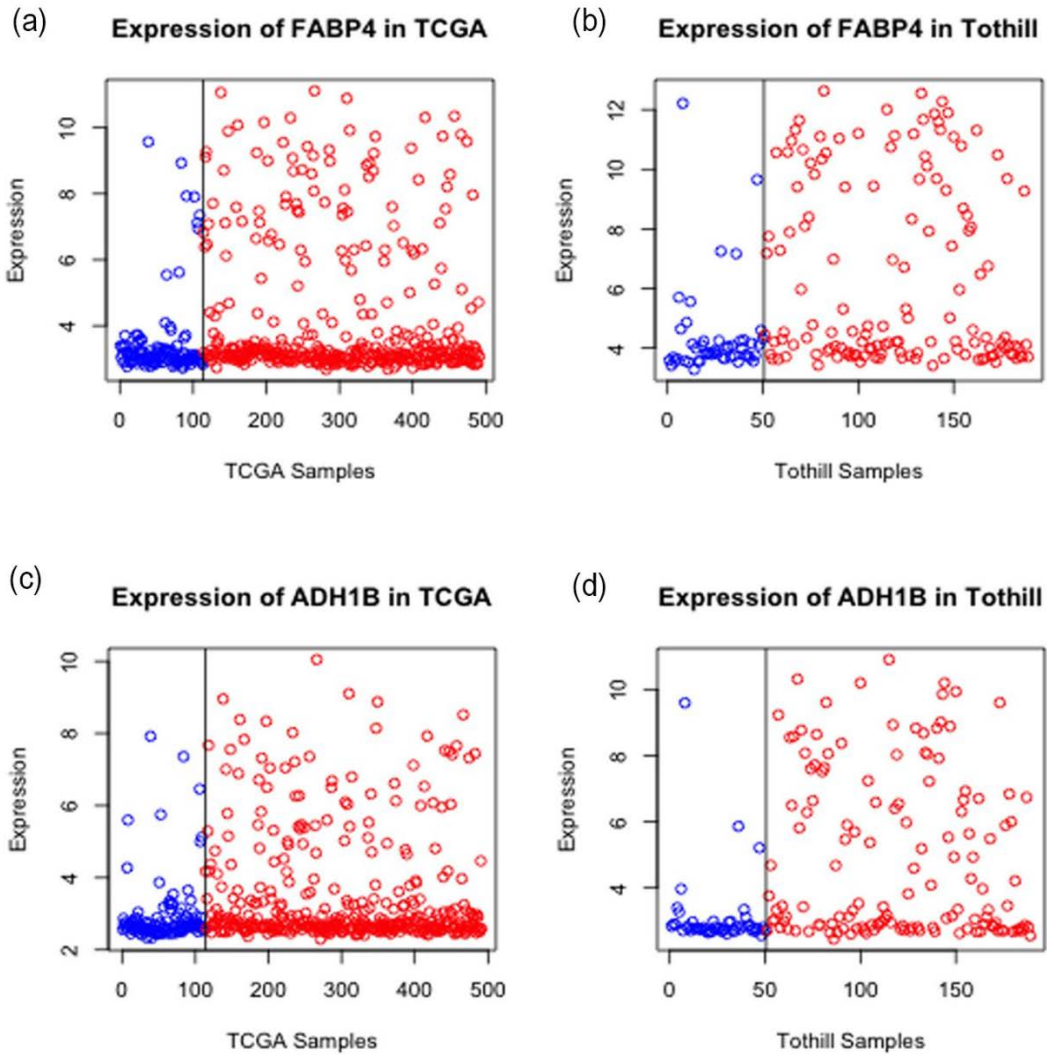
Figure 9 Dot and density plots for FABP4 (TCGA (a) and Tothill (b)) and ADH1B (TCGA (c) and Tothill (d)) Cases with residual disease are represented in red while non-residual disease is indicated in blue. Y axis represents normalized expression of FABP4 or ADH1B and X axis represents number of samples from TCGA or Tothill datasets. Increased rates of RD (red dots) is observed at high expression of FABP4 and ADH1B.

We then decided to explore the joint distribution of gene expression of FABP4 and ADH1B (Figure 9). We measured the RD status when the expression of both-ADH1B and FABP4 was high (using 3.5 as a cut of for both the genes). In TCGA samples, 97 out of 107 (90.6%) samples belonging to the 'high expression' group had RD whereas 281 out of 384 (73.2%) samples having low gene expression of ADH1B and FABP4 had RD. Among the Tothill samples, 59 out of 63 samples (93.7%) of high expression group had RD while 80 of 126 samples (63.5%) of low expression had RD.
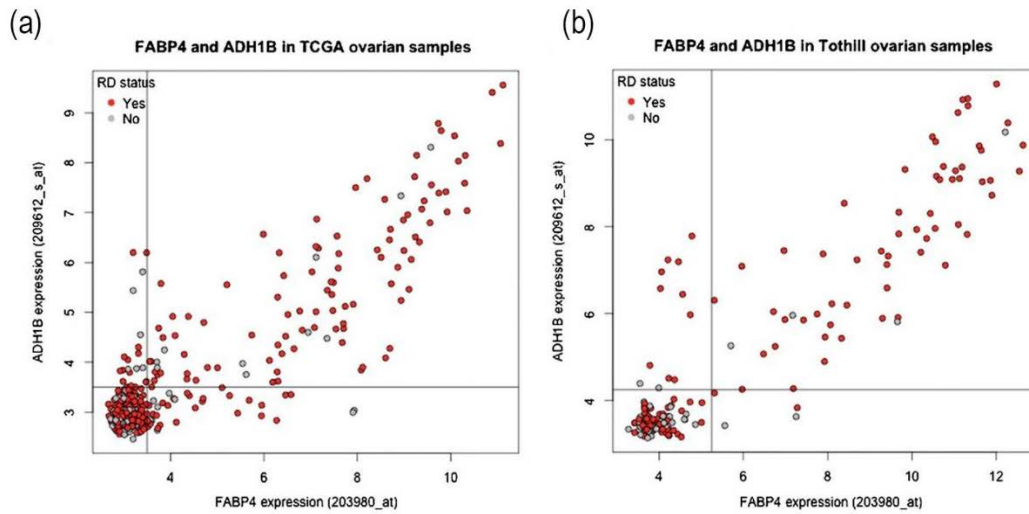
Figure 10 Plots of FABP4 and ADH1B for TCGA (a) and Tothill (b) datasets. The rates of residual disease (red dots) are higher when both the genes are elevated

After identification of 2 possible biomarkers from the computational analysis, we decided to perform validation studies in an independent cohort using qRT-PCR method to determine gene expression. We examined 139 patient tumor samples from two institutes- MD Anderson Cancer Center and Fred Hutchinson Cancer Research Center. All the samples were chemotherapy naïve. We initially checked the expression of ADH1B and FABP4 in omental samples as well and compared the gene expression between ovarian and omental samples. Figure 11 shows the density plots for ADH1B and FABP4 for both the tissues. For both the genes, the expression was higher in omental tissues compared to ovarian tissues.
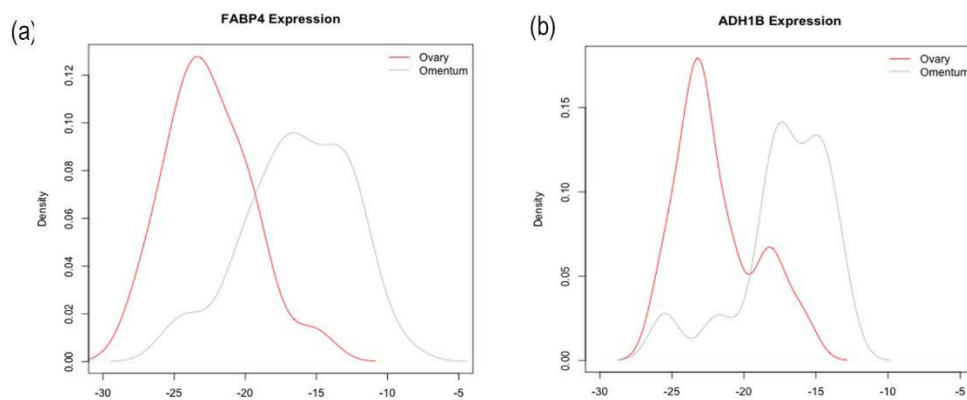
Figure 11 Density plots of FABP4 (a) and ADH1B (b) in ovary (red) and omental (gray) as observed in qRT-PCR experiments

We also checked FABP4 expression for 4 cases for which paired ovarian and omental samples were available. In all these samples, omental gene expression was higher than ovarian gene expression. (Percent difference- 2%, 85%, 110%, 131%). We therefore decided to only focus on the samples from primary site a) To be consistent with TCGA and Tothill data set b) The gene expressions were not comparable between these two sites and cannot be analyzed using a same cut-off values. The analyses of gene expression and RD were double-blinded. The qRT-PCR values for ADH1B and FABP4 gene expression and RD statuses are presented in Figure 11. As observed in the TCGA and Tothill datasets, the expression levels of ADH1B and FABP4 were highly correlated with each other. However, the distribution of these genes was different from the one observed in the microarray data of TCGA and Tothill sets. The data from qRT-PCR analysis was not bimodal as observed in the previous microarrays. Therefore, we decided to specify a threshold to determine which samples will be grouped in high or low expression groups. Based on the power calculations, we decided that 25% of the samples with the highest FABP4 expression will be grouped together and we predicted that this group will have higher probability of having RD compared to the rest of the samples. After unblinding the data and correlating gene expression with RD statuses, we noticed that 30 out of 35 patients predicted to have RD, had residual disease (PPV 86%). On the other hand, 54 out of 104 from the low FABP4 group had residual disease (PPV 52%). The odds ratio was 5.5 and the difference was significant (p=0.0002) using one sided Fischer's exact test
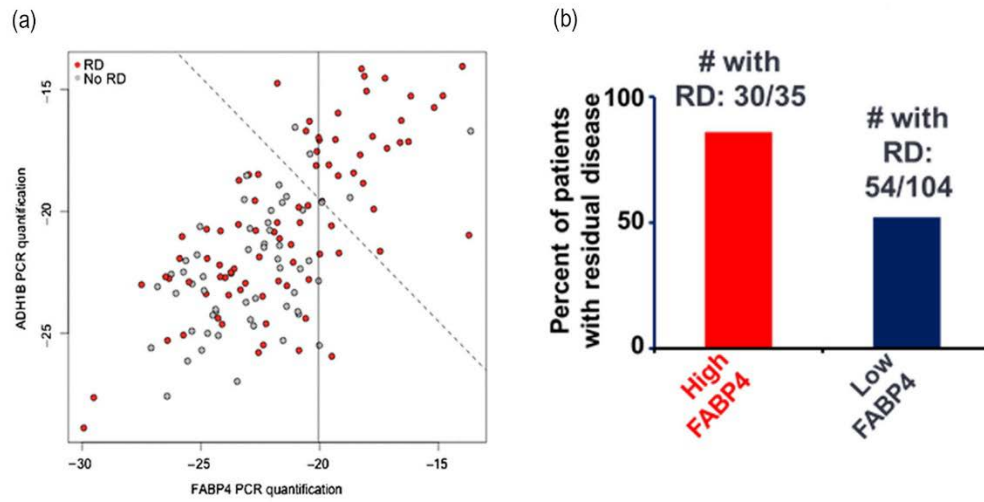
Figure 12 (a) Plot of qRT-PCR values for FABP4 and ADH1B for the ovarian validation

samples. The solid line is the cutoff used for blinded validation while the dashed line

is the cutoff determined after weighting two genes equally (b) Prediction results for the

validation cohort after dividing the samples in high and low FABP4 groups

When we further explored the relationship between ADH1B or FABP4 gene expression and residual disease status (Figure 13 a and b), we noticed a continuous trend of increasing incidence of RD observed with increase in gene expression. For example, RD rate across the 4 groups of FABP4 genes was 41% (14/34, lowest quartiles), 63% (22/35), 51% (18/35) and 86% (30/35, top most quartile)
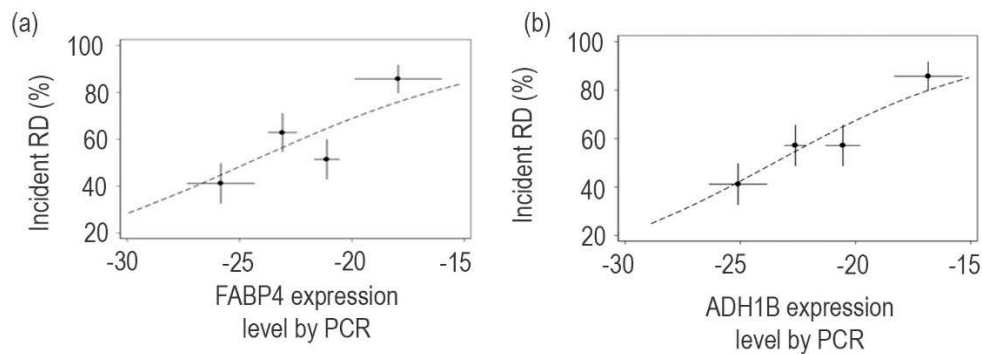
Figure 13 Plots showing incidence of RD as a function of expression of FABP4 (a) and ADH1B (b), based on qRT-PCR values from the validation cohorts. The points show the incidence of RD for each group plotted at the mean value of FABP4 or ADH1B per group. Horizontal and vertical lines indicate standard deviations

Our molecular biomarkers thus accurately predicted RD incidences in high grade serous ovarian cancer.

Chapter 4: Effects of FABP4 on tumor progression

After establishing the importance of FABP4 as a molecular biomarker, we next explored if it has any functional role in tumor progression. We first silenced FABP4 in HeyA8 MDR cells using FABP4 siRNA and made sure that we have achieved significant FABP4 inhibition. We then conducted migration and invasion assays to examine the effect of FABP4 knockdown on key steps in tumor metastasis.

After FABP4 siRNA transfection, there was 85-90% knockdown of FABP4. As seen in Figure 14 (a and b) there was a significant reduction in the ability of cells to migrate ($p<0.01$) or invade ($p<0.01$) after FABP4 knockdown. We also conducted proliferation assay to make sure that the effect on migration and invasion is not a result of stunted cell proliferation. There was no significant difference in cell proliferation after FABP4. We then investigated the effect of ectopic expression of FABP4 in cancer cells. In A2780 cells, ectopic FABP4 expression led to increase in migration ($p<0.05$) and in invasion ($p<0.01$) (Figure 14 c and d).

The effect was also observed in additional cell lines such as Ovcar 5 and when we used additional siRNA sequence. In Ovcar 5 cells, knockdown of FABP4 resulted in significant reduction in migration ($p<0.05$) and inhibition ($p<0.05$) of the cells treated with siFABP4 (Figure 14 e and f). The second sequence of siRNA was able to ~60% decrease in migration ($P<0.01$) and ~65%decrease in invasion ($p<0.01$) (Figure 14 g and h). Figure 14 i, j, k show the validation of FABP4 knockdown in the cells.

.
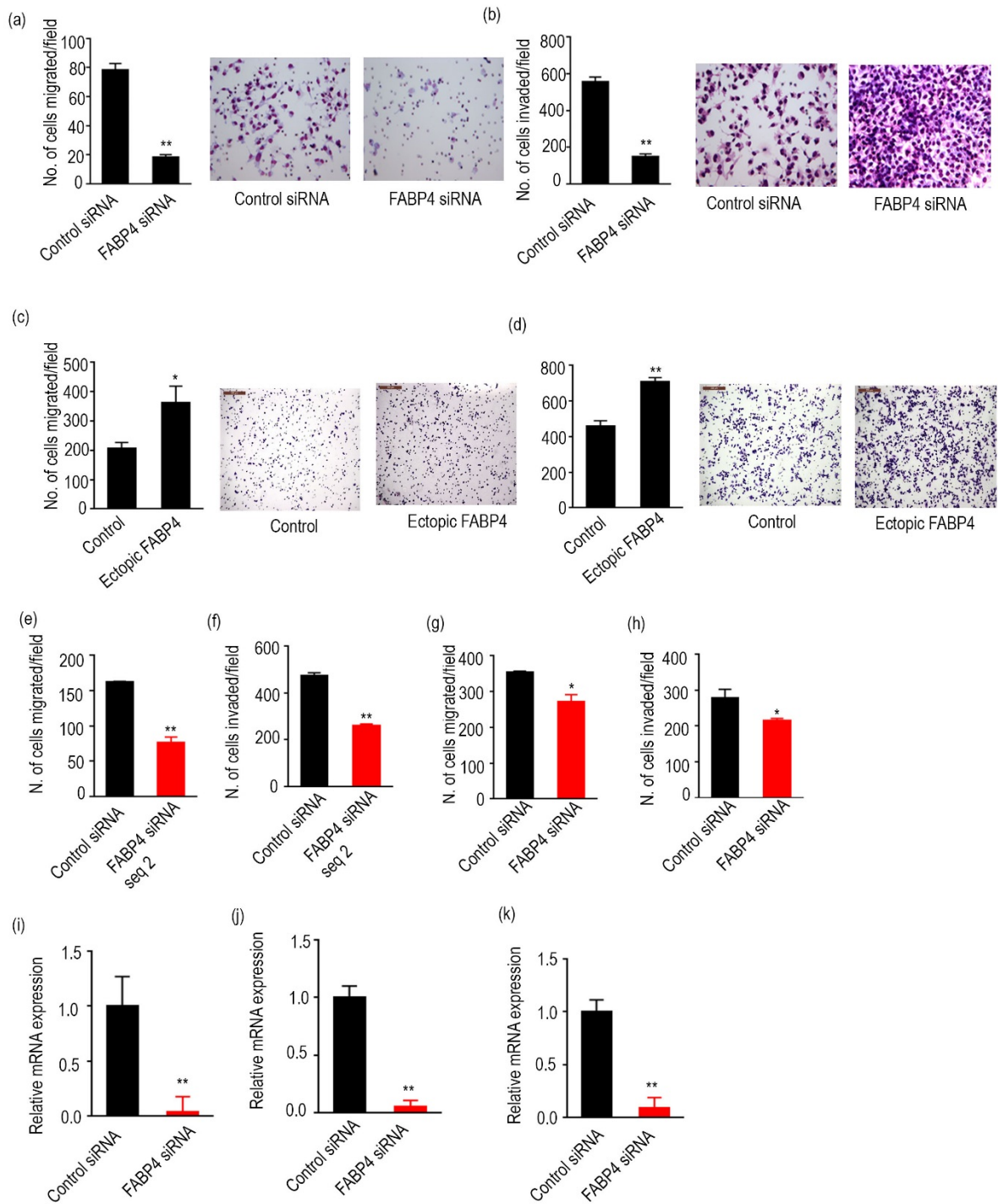
Figure 14 (a, b) Effect of knockdown of FABP4 on the (a) migration and (b) invasion of ovarian cancer cells (HeyA8 MDR). **p < 0.01. (c, d) Effect of increased expression

of FABP4 on the (c) migration and (d) invasion of cancer cells (A2780-ip1). *p<0.05. **p < 0.01. (e, f) Effect of FABP4 knockdown on (e) migration and (f) invasiveness using a second siRNA sequence. **p<0.01. (g, h) Effect of FABP4 knockdown on (g) migration and (h) invasion in Ovcar 5 cells. *p < 0.05. Validation of FABP4 knockdown is shown for HMDR cell line FABP4 sirna (i) seq 1 (j) seq 2 (k) Ovcar 5 cell line

Since the in *vitro* studies were promising, we decided to see if FABP4 promotes tumor progression in *in vivo* settings. We first established a cell line (A2780) ectopically expressing FABP4. We then injected control cells and cells ectopically expressing FABP4 in the ovaries of nude mice and examined the effect of FABP4 on promoting tumor burden and metastasis. Compared to subcutaneous or intra-peritoneal injections, this orthotopic model closely mimics the cancer progression as seen in ovarian cancer patients [89, 90]. There was no therapeutic intervention for this study and the mice were sacrificed when any mouse became moribund. There was a significant difference in tumor weight and number of nodules between control and ectopic FABP4 group (Figure 15 a and b).We then analyzed H&E sections of the tumors collected from these mice. We noticed that while tumors in the control group did not invade the normal tissues, tumors from ectopic FABP4 group were highly infiltrative (Figure 15 d). The metastatic pattern was also unique in the ectopic FABP4 group (Figure 15 e). In the control group, the tumor was mainly located in ovary, peritoneum and mesentery whereas the metastasis in ectopic FABP4 was also observed in diaphragm, liver, pelvis. As expected, immunohistochemical analysis showed that FABP4 was indeed overexpressed in the tumors from ectopic FABP4 group (Figure 15 f).
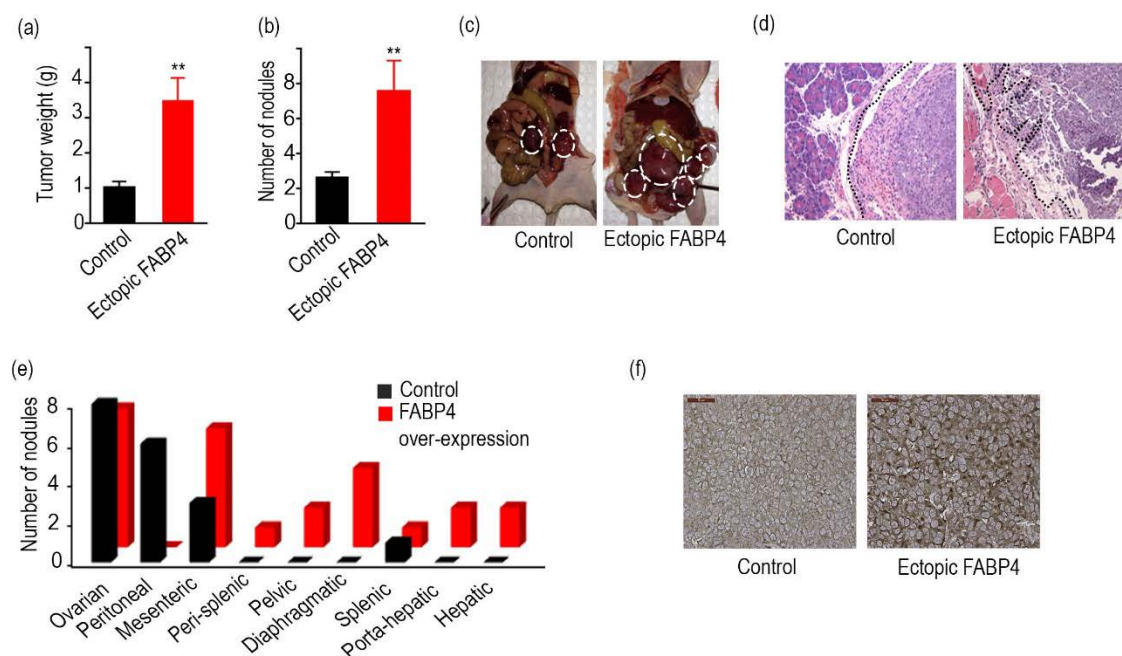
Figure 15 (a) Aggregate mass of tumors in orthotopic mouse models involving A2780-ip1 cells transfected with control and FABP4 ectopic expression vectors (n = 10 mice per group, Student *t* test). **p < 0.01. (b) Effect of ectopically expressed FABP4 on the number of nodules in orthotopic mouse models involving A2780-control and A2780-FABP4 ectopic expression (n = 10 mice per group, Student *t* test). **p < 0.01. (c) Representative images of nodules are shown on the right. (d) Representative hematoxylin and eosin-stained sections of tumor tissues from mice injected with control A2780-ip1 cells or A2780-ip1 cells transfected with FABP4-expressing vector. (e) Distribution of metastatic nodules present in the groups (f) Immunohistochemical expression of FABP4 in tumor tissues from mice injected with control A2780-ip1 cells or A2780-ip1 cells with ectopic expression of FABP4.

The next step was to investigate the effects of FABP4 knockdown on tumor progression. We used luciferase labeled HeyA8 MDR cell lines and performed intra-ovarian cell injections to establish orthotopic mouse model of ovarian cancer. A week after the cell injections, we randomly divided the mice in two groups, one would receive control siRNA encapsulated in DOPC nanoliposomes while the other group would receive FABP4 siRNA encapsulated in DOPC nanoliposomes. The intra-peritoneal DOPC injections were given twice weekly and the mice were sacrificed when any mouse became moribund. At the end of the study, tumor weight, number of nodules, locations of metastasis and weight of the mice were measured. As shown in Figure 16 a and b, FABP4 knockdown led to a significant reduction in tumor weight and number of nodules. The metastasis was widespread in the control mice but was only observed in the ovaries and peritoneal areas of mice injected with FABP4 siRNAs (Figure 16 e). Bioluminescence images also supported the results. There was a significant difference in luciferase readings between control mice and mice injected with FABP4 siRNA (Figure 16 f). We also examined the tumor tissues for FABP4 expression. The treatment with FABP4 siRNA achieved significant knockdown of FABP4 in mice as shown with immunohistochemistry and western blot (Figure 16 g and h). We also recorded weight of the mice in these two groups and noticed that the treatment did not have any effect on the mice weight (Figure 16d).
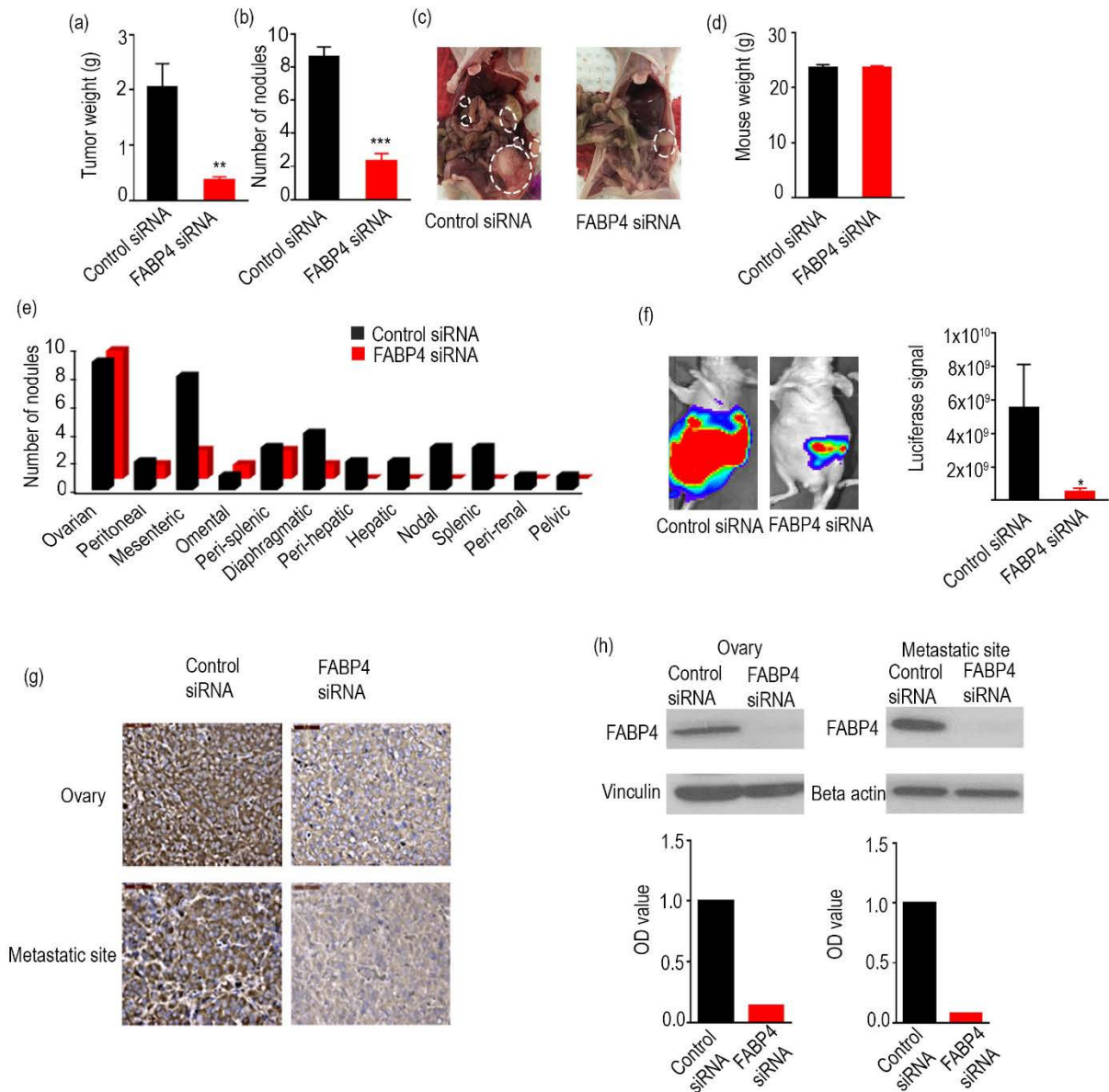
Figure 16 (a) Aggregate mass of tumors in orthotopic mouse models involving HeyA8 MDR cells. Mice were treated with control or FABP4 siRNA encapsulated in DOPC liposomes (n = 10 mice per group). **p < 0.01. (b) Effect of knockdown of FABP4 on the number of metastatic nodules in HeyA8 MDR orthotopic mouse models. ***p <

0.001. (c) Representative images are shown on the right. (d) Mouse weight in the control and treatment groups. (e) Distribution of metastatic nodules present in individual mice after treatment with control or FABP4 siRNA encapsulated in DOPC liposomes. (f) Representative images of metastatic lesions revealed by luciferase imaging, and quantitative assessment of luciferase signal from mice treated with control or FABP4 siRNA encapsulated in DOPC nanoliposomes. *p<0.05. (g) Immunohistochemical staining showing FABP4 protein expression levels at the primary site (ovary) and metastatic sites after treatment with control or FABP4 siRNA. (h) FABP4 protein expression levels at the primary site (ovary) and metastatic sites after treatment with control or FABP4 siRNA, as shown in Western blot analysis. OD-Optical Density.

We also examined additional orthotopic mouse model. This time, we used Ovcar 5 cell line, the siRNA treatment was similar to the one described above. At the end of the study, we noticed significant inhibition of tumor progression in FABP4 siRNA treatment group. There was a significant reduction in tumor weight (Figure 17 a), number of nodules (Figure 17 b) and metastasis was also restricted to ovary and mesentery unlike the extensive metastasis seen in control mice (Figure 17 c). The treatment did not have any deleterious effect on body weight of mice (Figure 17 d).
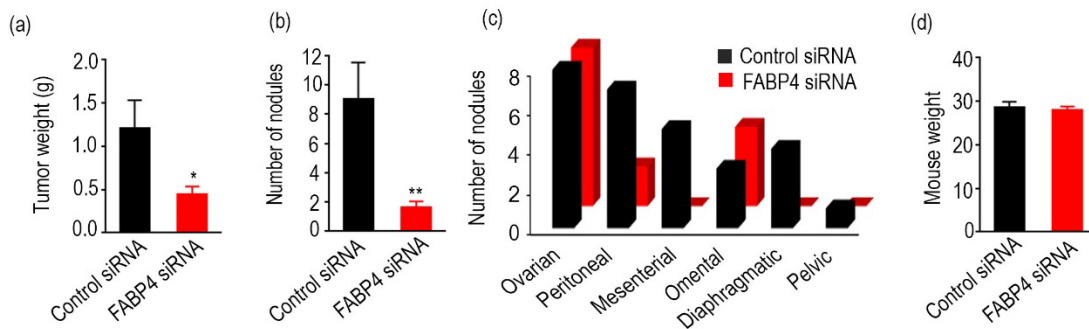
Figure 17 (a) Aggregate tumor weight for mice injected with Ovcar 5 cell line. The mice were treated with control siRNA or FABP4 siRNA encapsulated in DOPC nanoliposomes. *p<0.05. (b) Effect of knockdown of FABP4 on the average number of nodules. **p<0.01. (c) Pattern of metastasis in the control and treated mice. (d) Mouse weight in the control and treatment groups.

Aggressive cytoreduction as attempted in patients is not feasible in mice. To determine if FABP4 knockdown affects the likelihood of achieving no residual status, we calculated a score based on the metastasis pattern seen in the orthotopic mouse models. We based our scoring schema on the one developed by Fagotti et al. [36]. The original schema assigns a score between 0-2 based on the extent of metastasis at a given location. Studies have shown that the scores correlate with the residual disease status in ovarian cancer patients [37, 38]. Figure 1 represents original schema. Like Fagotti score, our modified scoring system (Figure 18 a) assigns a score of 2 for each metastasis location and if the combined score for a specific mouse is greater than or equal to 8, it was considered a case of residual disease. Conversely, score below 8 indicated that R0 status. We calculated scores for each of the mouse from the two *in vivo* experiments described above. Ectopic expression of FABP4 led to higher scores in mice compared to the control mice (Figure 18 b). In the second *in vivo* experiment, most of the mice treated with control siRNA had scores of 8 indicating increased likelihood of residual disease; while all the mice treated with FABP4 siRNA had scores below 8 (Figure 18 c). All the in *vitro* and *in vivo* experiments thus established the key role FABP4 plays in residual disease occurrences in ovarian cancer.

(a)

Modified Fagotti score	
Sites of metastasis	**Score**
Peritoneum	2
Diaphragm	2
Mesentery	2
Omentum	2
Splenic area	2
Renal / pelvic area	2
Liver/para-hepatic area	2
Lymph nodes	2

(b)
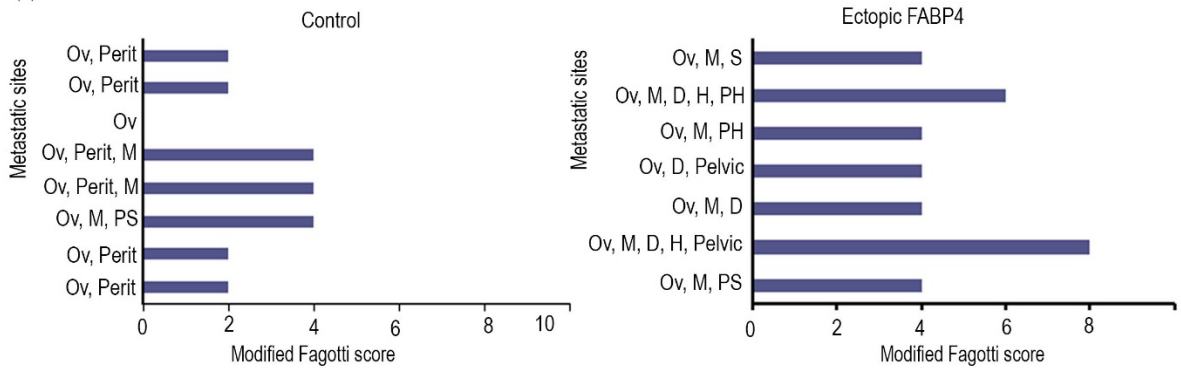
(c)
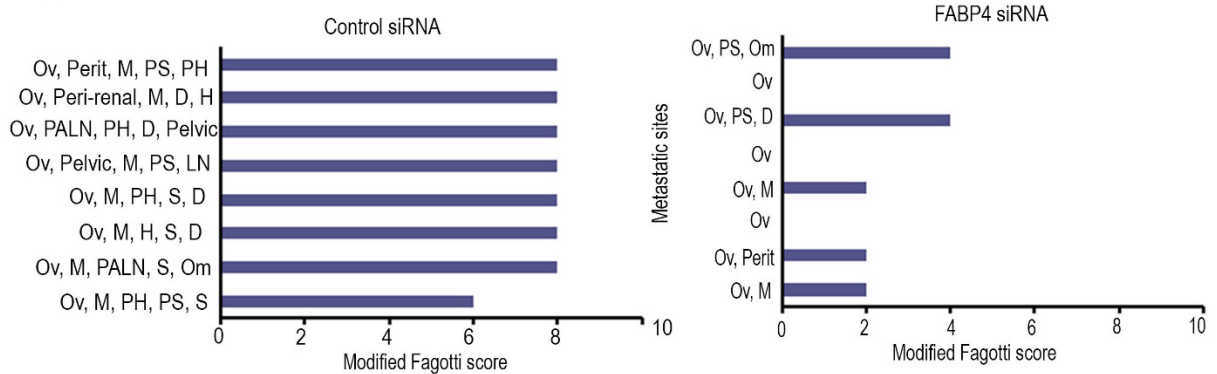
Figure 18 (a) Scoring schema for the modified Fagotti score (b) Modified Fagotti scores for each mouse in the control and ectopicFABP4 groups. (c) Modified Fagotti scores for each mouse in the control siRNA and FABP4 siRNA groups. (Ov-Ovary,

Perit-Peritoneum, M-Mesentery, S-Spleen, PS-Para-splenic area, H-Liver, PH-Para-hepatic area, D-Diaphragm, LN-Lymph node, PALN-Para-aortic lymph nodule, om-Omentum)

Chapter 5: Upstream regulation of FABP4

We next investigated the upstream regulation of FABP4 in ovarian cancer. We first analyzed TCGA data and checked if there is any correlation between copy number and mRNA expression of FABP4. We investigated the data across various platforms (Affymetrix Agilent, RNAseq2) however, there was no correlation between copy number and FABP4 expression in TCGA ovarian cancer samples (Figure 19).
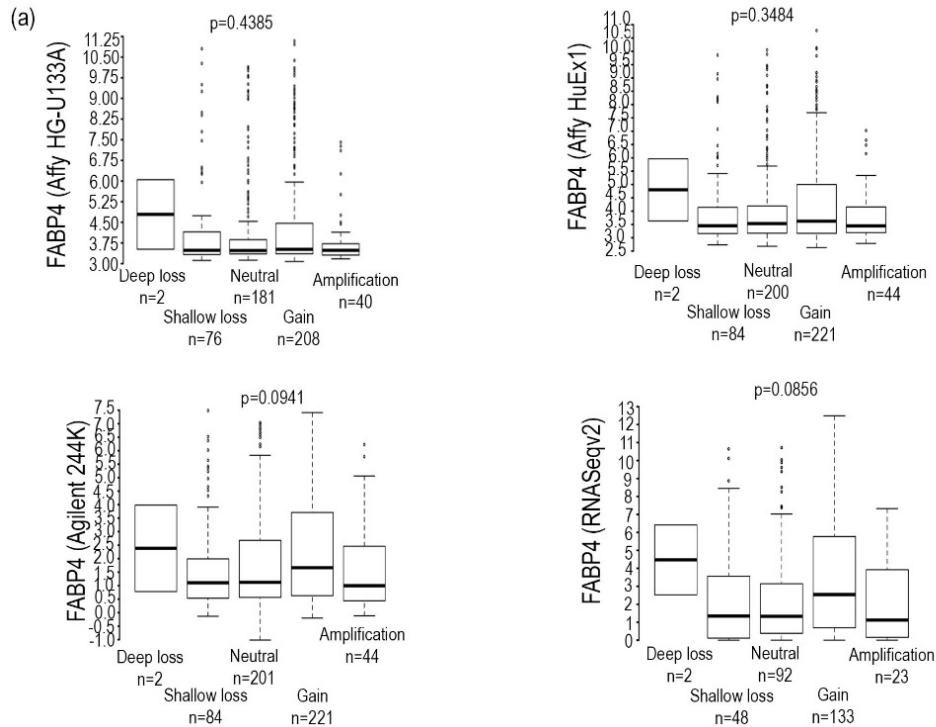
Figure 19 Correlation between copy number and mRNA expression levels of FABP4 across platforms (Affymetrix, Agilent, RNAseqv2) using data from The Cancer Genome Atlas.

We then compared FABP4 expression in ovarian cancer cell lines and compared it with that of the tumor tissues taken from mice injected with the same cell line. We noticed that FABP4 expression in tumor tissues is significantly higher compared to its expression in the cell lines. We thus checked the effect of tumor micro-environmental factors on the expression of FABP4. We checked if 3D arrangement of cells in the tumor tissue has any role in increasing FABP4 expression *in vivo*. The effect was significant when compared to the cells grown in 2D condition, however it was not consistent and did not validate in other cell lines. Effect of stromal cell lines and hypoxia (Figure 24a) is discussed later in the next chapter. We also tested the possibility of transcriptional regulation of FABP4. We analyzed TCGA dataset and selected transcriptional factors (ISX, MSX, FOXA1) that had the highest correlation with FABP4 expression across 3 platforms (Affymetrix, Agilent and Illumina). Knockdown of some transcription factors resulted in downregulation of FABP4 thus suggesting possible regulation by these factors but the chromatin immunoprecipitation assay did not show binding between the selected transcription factor and the promoter region of FABP4.

We thus decided to explore the possibility of miRNA regulation. We systematically analyzed TCGA data to select the potential miRNAs regulating FABP4. The selection process is explained in Figure 20a. We selected chemotherapy naïve, high grade serous ovarian cancer samples from TCGA set. We then probed miRNA data and selected miRNAs that have some association with FABP4 mRNA. We used MIC (maximal information coefficient) scores to select miRNAs. In this system, a score of 0 represents there is no association between a given miRNA and the expression of

gene while a score 1 indicates a perfect association between a miRNA and a gene. The miRNAs with MIC $\geq$ 0.2 were selected for further analysis. We used prediction softwares to investigate which of these selected miRNAs are predicted to target 3'UTR of FABP4. Table 4 lists the 32 miRNAs that had MIC scores of $\geq$ 0.2 with FABP4 and also lists the number of prediction softwares that predicted their interaction with FABP4. After 2 selection criteria, we selected miR-409-3p which was predicted to target FABP4 by the highest number of softwares (9 prediction softwares).
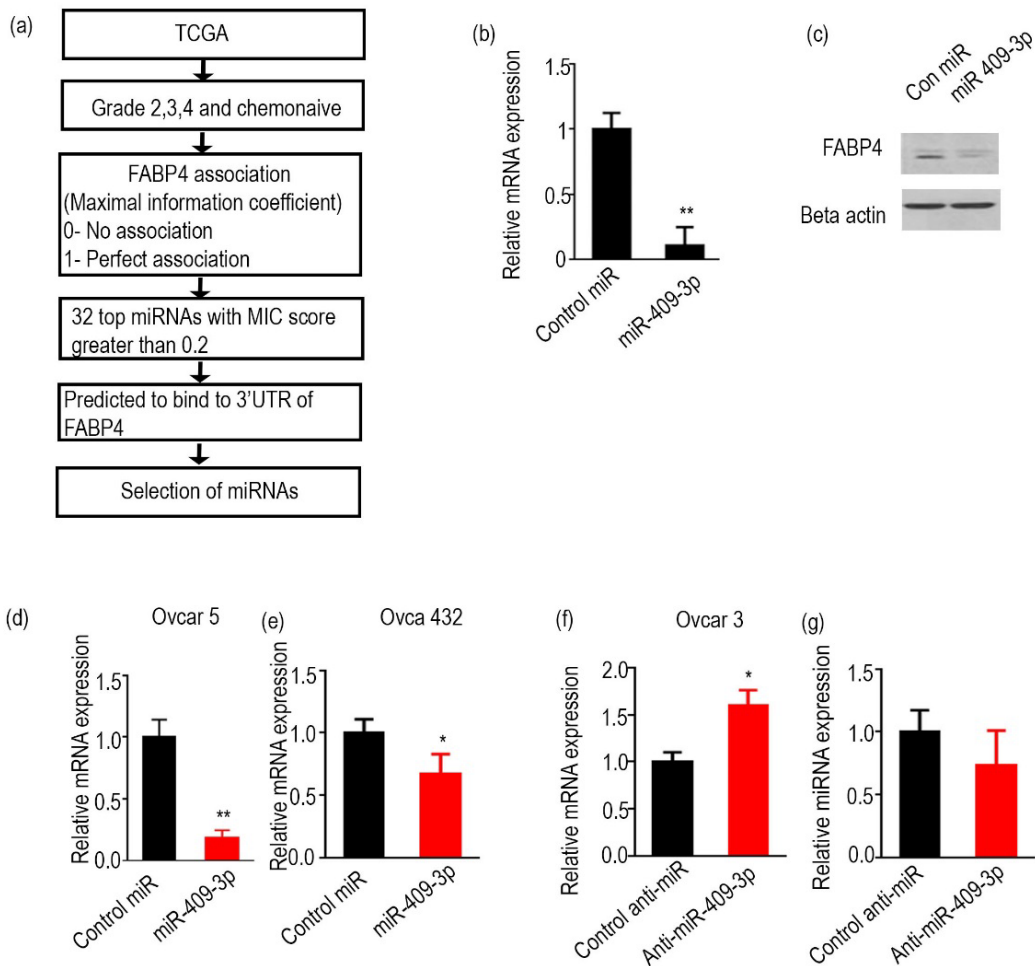
Figure 20 (a) Flowchart showing the methods used to identify microRNAs (miRNAs) that target FABP4 in ovarian cancer. (b) Effect of miR-409-3p mimic transfection specifically on FABP4 expression levels (RNA) in HeyA8 MDR cells. (c) Effect of miR-409-3p mimic transfection on FABP4 expression levels (protein) in HeyA8 MDR cells.(d) Effect of miR-409-3p mimic transfection on the expression of FABP4 in Ovcar 5 cells. **p<0.01. (e) Effect of miR-409-3p mimic transfection on the expression of FABP4 in Ovca 432 cells. *p<0.05. (f) Effect of miR-409-3p inhibitor on the expression of FABP4 mRNA (left) and on the level of miR-409-3p (right) in Ovcar 3 cells. *p < 0.05.

MicroRNA	MIC score	Number of softwares predicting miR-409-3p and 3' UTR of FABP4
hsa-miR-143	0.270601	2
hsa-miR-126	0.22939	5
hsa-miR-214*	0.22323	1
hsa-let-7g*	0.22284	1
hsa-miR-199a-5p	0.22044	1
hsa-miR-409-3p	**0.21971**	**9**
hsa-miR-507	0.21927	1
hsa-miR-145*	0.21636	1
hsa-miR-214	0.21551	1
hsa-miR-1225-3p	0.21542	-

hsa-miR-431	0.21531	2
hsa-miR-342-3p	0.21100	1
hsa-miR-199b-5p	0.21077	1
hsa-miR-145	0.21002	1
hsa-miR-150	0.20990	4
hsa-miR-133a	0.20808	1
hsa-miR-409-5p	0.20784	0
hsa-miR-199b-3p	0.20771	2
hsa-miR-22	0.20767	1
hsa-miR-22*	0.20705	1
hsa-miR-133b	0.20703	1
hsa-miR-1	0.20599	2
hsa-miR-1225-5p	0.20435	1
hsa-miR-514	0.20427	-
hsa-miR-132	0.20395	1
hsa-miR-152	0.20356	3
hsa-miR-432	0.20268	1
hsa-miR-508-3p	0.20240	2
hsa-miR-139-5p	0.20203	1
hsa-miR-379	0.20181	1
hsa-miR-182	0.20142	1
hsa-miR-143*	0.20019	1

Table 4. miRNAs with MIC scores greater than 0.2 for association with FABP4 gene expression

We then checked the effect of miR-409-3p on FABP4 expression in *vitro*. We transfected HeyA8 MDR cells with miR-409-3p mimic and observed 85% reduction in FABP4 mRNA levels (p<0.01) (Figure 20 b). We saw a similar effect at protein level (Figure 20 c). The effect was also observed in additional cell lines. In Ovcar 5 (Figure 20 d) and Ovca 432 cells (Figure 20 e), FABP4 levels were reduced after miR-409-3p mimic transfection (p<0.01 and p<0.05 respectively).Conversely, when we transfected Ovcar 3 cells with anti-miR-409-3p, we observed an increase in the expression of FABP4 (Figure 20 f). There was 40% inhibition (Figure 20 g) after anti-miR-409-3p transfection which resulted in a significant increase in FABP4 expression (p<0.05).

The next step was to investigate whether miR-409-3p binds to 3'UTR of FABP4. The binding site for miR-409-3p on 3'UTR of FABP4 is shown in Figure 21 a and the mutated sequence is shown in Figure 21 b. We conducted luciferase assays to answer this question. We transfected HeyA8 MDR cells with plasmids containing empty 3'UTR or 3'UTR of FABP4. The cells were then transfected with control miR or miR-409-3p. When the luciferase activity was measured, we observed that the activity was significantly lower for cells transfected with 3'UTR of FABP4 and miR-409-3p compared to the controls (Figure 21 c) thus indicating that miR-409-3p binds to 3'UTR of FABP4. We then mutated the sequence of 3'UTR of FABP4 where miR-409-3p is predicted to bind. As observed earlier, there was a significant reduction in the luciferase activity in the cells transfected with 3'UTR of FABP4 and miR-409-3p however there was no significant difference between the controls and the cells transfected with mutated 3'UTR of FABP4 suggesting that miR-409-3p can longer to

bind to the mutated binding site of 3'UTR of FABP4 (Figure 21 d) . Thus luciferase assay confirmed that miR-409-3p can bind to 3'UTR of FABP4.

We next assessed the expression of miR-409-3p in ovarian cancer cell lines and compared it with its expression in normal ovarian cell line (HIO180). We noticed that the expression of miR-4093p is significantly lower in the cancer cell lines compared with the normal ovarian cell line (Figure 21 e). We also compared miR-409-3p expression in ovarian tumor tissues and normal ovarian tissue using Gene Expression Omnibus dataset (GSE15190) [83] (Figure 21 f). This data set also revealed that tumor samples have low expression of miR-409-3p compared to the normal tissues. We then examined 8 ovarian cancer patient tumor samples from the Gynecology Oncology Dept. of M.D. Anderson Cancer Center. We used *in situ* hybridization technique to analyze the expression of FABP4 and miR-409-3p. We saw a distinct inverse association between miR-409-3p and FABP4 expression levels in the *in situ* hybridization images (Figure 21 g).
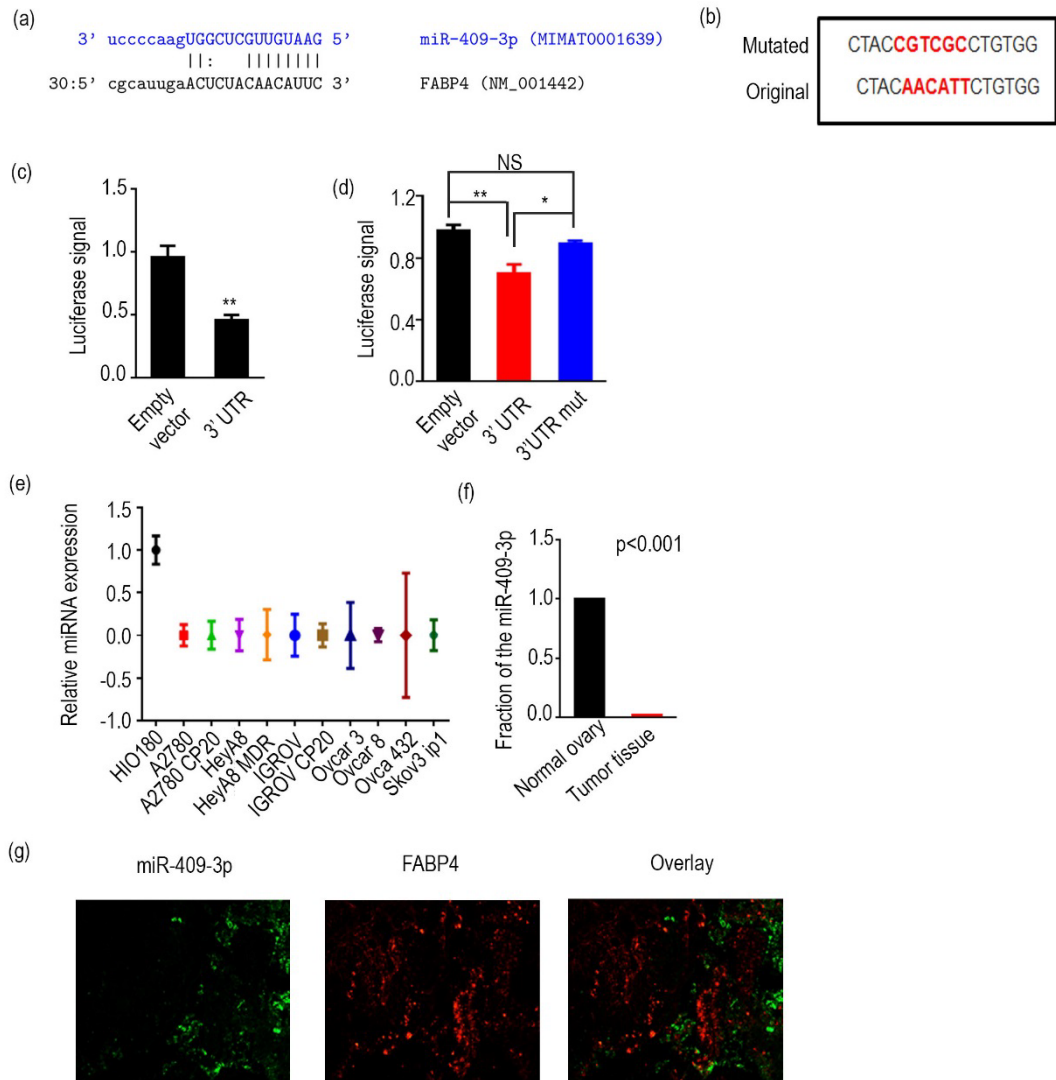
Figure 21 (a) Predicted binding site of miR-409-3p on the 3' untranslated region (UTR) of FABP4. (b) Original and mutated 3' untranslated region (UTR) sequence of FABP4, where miR-409-3p is predicted to bind. (c) Relative luciferase activity normalized to that of cells transfected with an empty control and cells transfected with control miRNA. HeyA8 MDR cells were transfected with empty control, wild-type FABP4and

then transfected with a control miRNA mimic or a miR-409-3p mimic. **$p < 0.01$. (d) Relative luciferase activity normalized to that of cells transfected with an empty control and cells transfected with control miRNA. HeyA8 MDR cells were transfected with empty control, wild-type FABP4 (red bar), or FABP4 with mutated 3'UTR (blue bar) and then transfected with a control miRNA mimic or a miR-409-3p mimic. Activity was measured 48 hours after transfection. *$p < 0.05$; **$p < 0.01$; NS indicates not significant. (e) Expression of miR-409-3p in various ovarian cancer cell lines compared with normal ovarian cells (HIO180). (f) Expression of miR-409-3p in normal ovarian tissue and ovarian tumor samples in the GSE15190 dataset. (g) *In situ* hybridization for miR-409-3p (green) and FABP4 (red) in tumor tissues from patients with ovarian cancer (n = 8). Representative image is shown. Effect of miR-409-3p on tumor progression.

To investigate the effects of miR-409-3p on the metastatic abilities of cells, we transfected HeyA8 MDR cells with control miR and miR-409-3p and 48 hours later conducted migration and invasion assays. There was a significant reduction in the number of cells migrated ($p<0.01$) and invaded ($p<0.01$) after miR-409-3p mimic transfection (Figure 22 a and b). The effect was consistent in additional cell line and Ovcar 5 cells decreased migration ($p<0.05$) and invasion ($p<0.05$) after miR-409-3p transfection. On the other hand, when transfected with anti-miR-409-3p, there was an increase in migration ($p<0.05$) and invasion of cancer cells (Figure 22 c and d).

To investigate whether the functions of miR-409-3p are mediated through FABP4, we performed a rescue experiment (Figure 22 e). We initially established a cell line (SKOV3 ip1) stably overexpressing a FABP4 construct lacking the 3'UTR. Thus it would not be sensitive to a miR-409-3p mimic. We conducted luciferase experiment as described above. SKOV3ip1 cells with FABP4 were significantly more invasive ($p < 0.05$) compared to the controls. Transfection of the cell line ectopically expressing FABP4 with miR-409-3p mimic did not lead to a significant decrease in invasion compared to the control miR transfected cells. Thus, we concluded that FABP4 could be the main target for miR-409-3p's actions related to metastasis
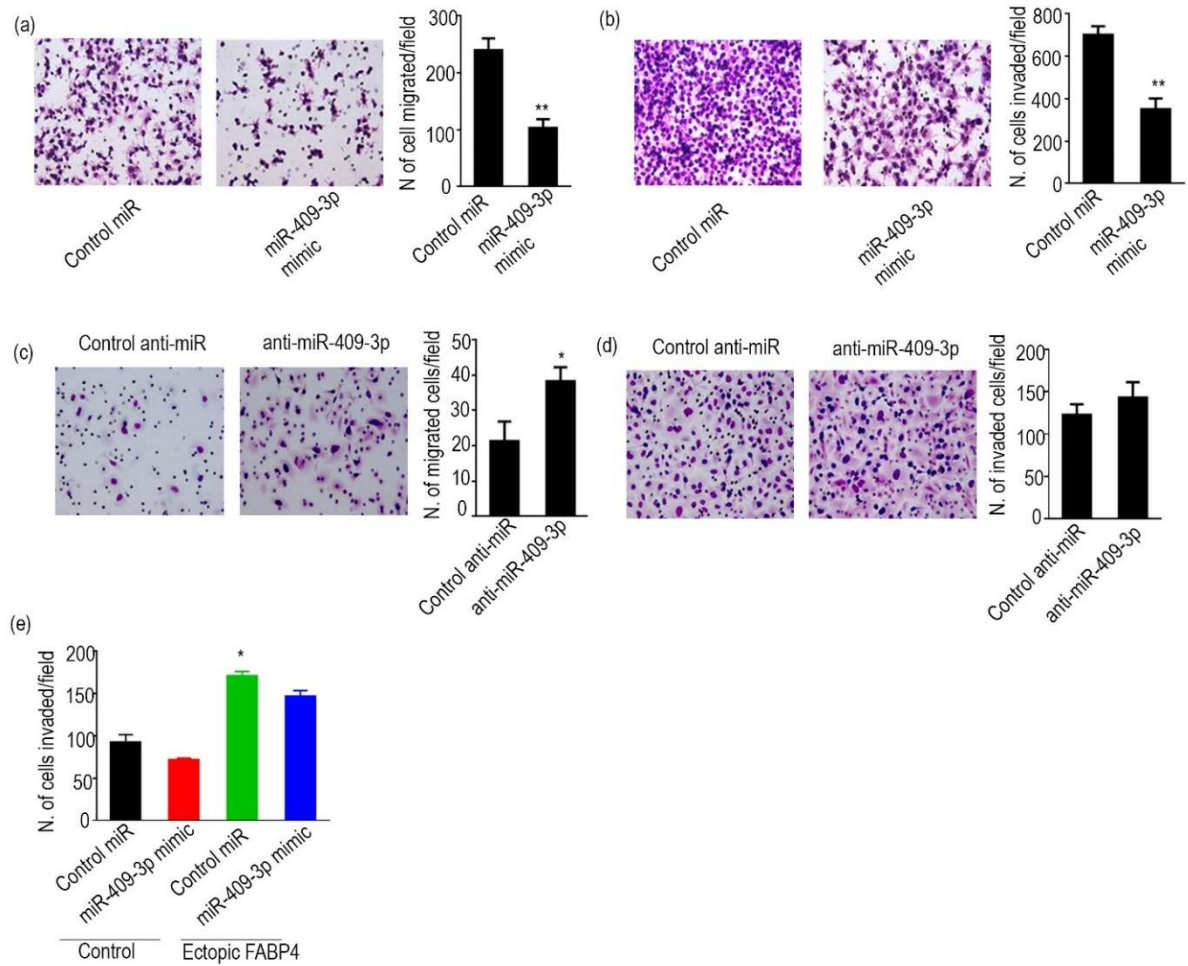
Figure 22 (a,b) Effect of miR-409-3p mimic transfection on the (a) invasiveness and (b) migration of HeyA8 MDR cells. **p < 0.01. (c,d) Effect of anti-miR-409-3p transfection on (c) migration and (d) invasiveness of Ovcar 3 cells. *p < 0.05. (e) Invasion potential of SKOV3 ip1 cells was assessed in control cells or cells ectopically expressing FABP4 after transfection with control miRNA mimic or miR-409-3p mimic.

Having established the tumor suppressive role of miR-409-3p in *vitro*, we examined its effect *in vivo.* Similar to the previous experiments, we performed intra-ovarian cell injections of HeyA8 MDR to establish orthotopic mouse model. A week after cell injections, mice were intraperitoneally injected with DOPC nanoliposomes encapsulating control miR or miR-409-3p mimic twice weekly. At the end of the study, mice were sacrificed and tumors were collected, weighed and location of metastases were recorded. There was a significant reduction in the tumor burden as well as in the number of nodules in the mice treated with miR-409-3p mimic (Figure 23 a and b). In the control mice, the metastasis was observed at diaphragm, lymph nodes, pelvis, perihepatic and perisplenic areas conversely in the mice treated with miR-409-3p mimic the metastasis was mainly localized at ovary and mesentery (figure 23 c). We also recorded the mice weight and noticed no harmful effects of the treatment on the weight of the mice (figure 23 d).

We next checked the expression of FABP4 in tumor samples collected from mice treated with miR-409-3p mimic. miR-409-3p mimic was able to significantly reduce FABP4 expression in the *in vivo* setting. FABP4 mRNA expression decreased after the miR-409-3p mimic injections ($p < 0.05$) (Figure 23 e) but the effect was more pronounced at the protein level as seen in western blot and immunohistochemical staining (Figure 23 f and g respectively).
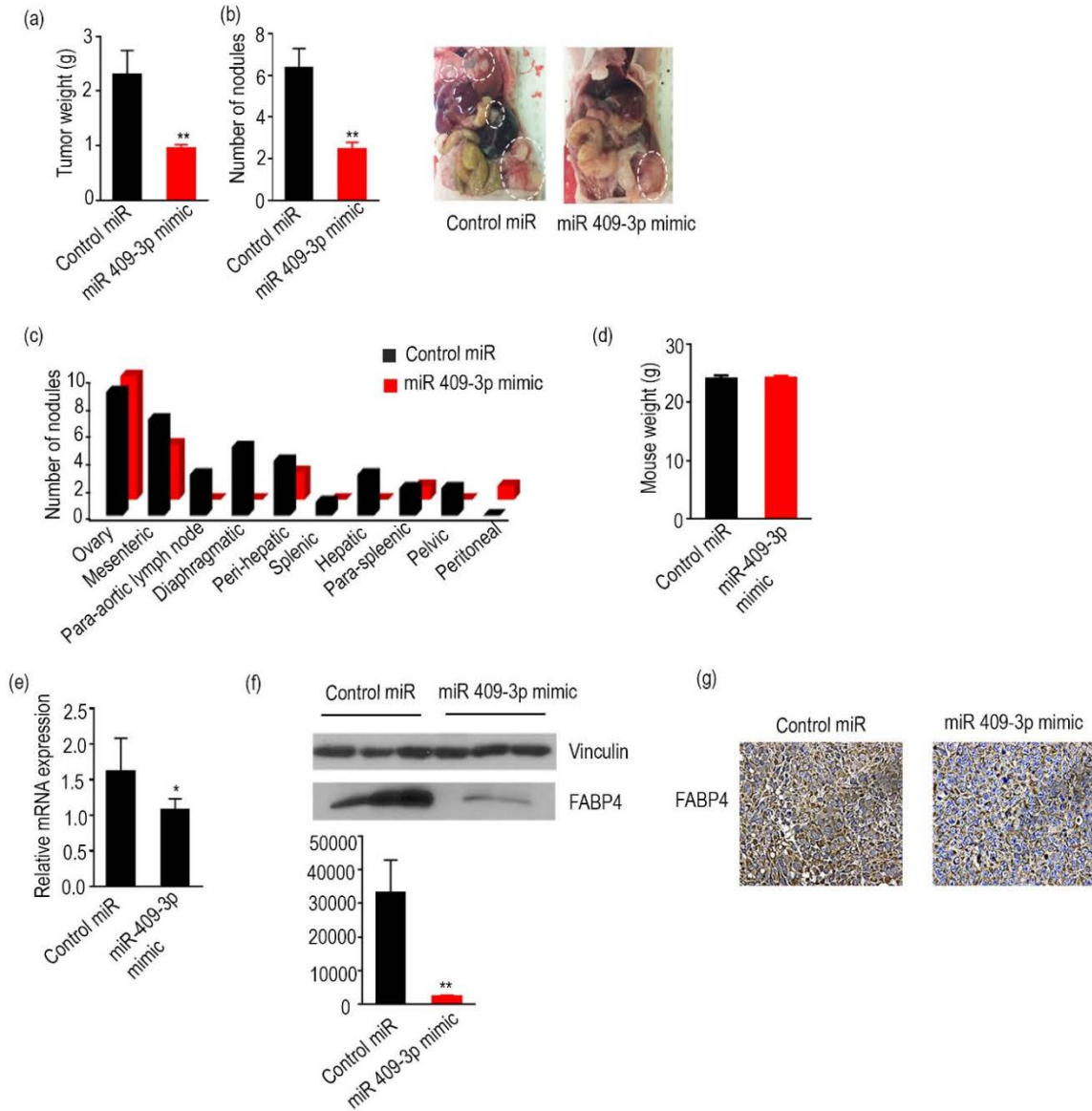
Figure 23 (a) Aggregate mass of tumors in orthotopic mouse models of ovarian cancer (HeyA8 MDR cell line) injected with control miRNA or miR-409-3p mimic encapsulated in DOPC liposomes. **p < 0.01. (b) Effect of miR-409-3p mimic on the number of nodules. Representative images are shown on the right. **p < 0.01. (c) Distribution of tumor nodules in individual mice after treatment with control miRNA or

miR-409-3p mimic. (d) The weight of the control and treated mice at the end of the experiment. (e) Expression of FABP4 in tumor tissues after treatment with miR-409-3p mimic treatment. *p < 0.05 (f) Effect of treatment with miR-409-3p mimic on the expression of FABP4 (protein) in tumor samples (n = 3). **p < 0.01. (g) Representative images of immunohistochemical analysis of FABP4 expression in mice treated with control miRNA or miR-409-3p mimic.

We next calculated the modified Fagotti scores for the mice in both the groups. Figure 24 shows the scores for individual mice from the control and miR-409-3p mimic groups. Most of the mice from the control group had a score of 8 and above, thus indicating increased likelihood of residual disease. On the other hand, mice treated with miR-409-3p mimic had scores lower than 8, thus indicating that no residual disease is likely to be achieved in these cases.
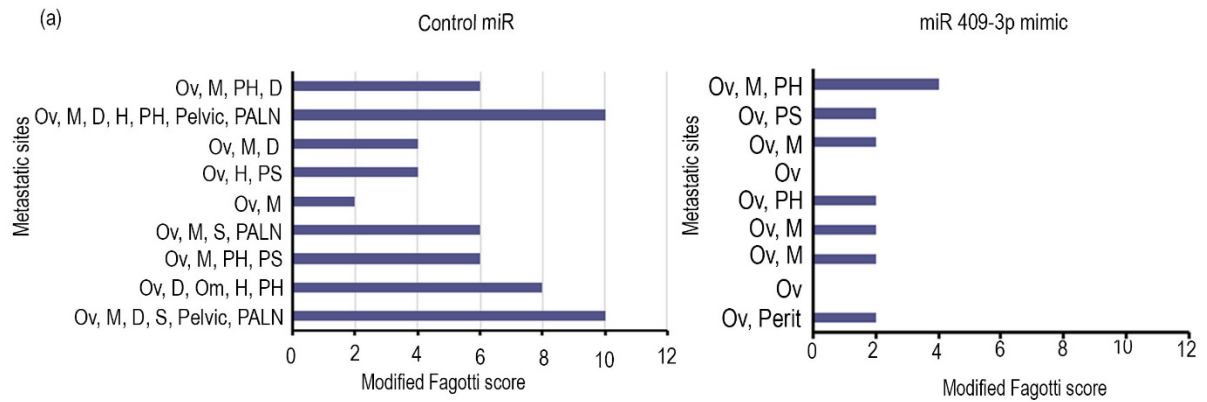
Figure 24 Modified Fagotti scores for individual mice from control miRNA and miR-409-3p mimic groups.

Chapter 6: Tumor micro-environmental factors regulating FABP4 and miR-409-3p

We next decided to explore the tumor micro-environmental factors that can affect the expression of miR-409-3p and FABP4. We examined the effect of stromal components such as fibroblasts, mesothelial cells, endothelial cells and macrophages on cancer cells and also studied the effect of hypoxic conditions on the expression of FABP4 in ovarian cancer cells. We incubated cancer cells with the conditioned media taken from endothelial fibroblasts, mesothelial cells or macrophages. For hypoxia experiments, we subjected cancer cells to 1% hypoxia for 48 hours and collected the cells for assessing FABP4 expression. Out of all the factors examined, hypoxia consistently increased FABP4 expression in the cancer cells (Figure 25 a). In HeyA8 MDR cells, hypoxia treatment led to ~3 fold increase in FABP4 level ($p<0.05$) (Figure 25 b). The same effect was also observed in an additional cell line, Ovca 432. Hypoxia treatment led to ~4 fold increase in FABP4 expression ($p<0.05$) (Figure 25 c). We then decided to check the expression of miR-409-3p in these cells. Interestingly, miR-409-3p expression was low in the hypoxia-treated cells compared to the control ($p<0.05$) (Figure 25 d). The same effect was also observed in Ovca 432 cells, miR-409-3p expression was inhibited by after hypoxia treatment ($p<0.05$) (Figure 25 e)

(a)

Tumor microenvironmental factor	Upregulation of FABP4 (Fold change)
Hypoxia	**3**
Endothelial cells	2
Fibroblast cells	1.5
Mesothelial cells	No change
Macrophages	1.5
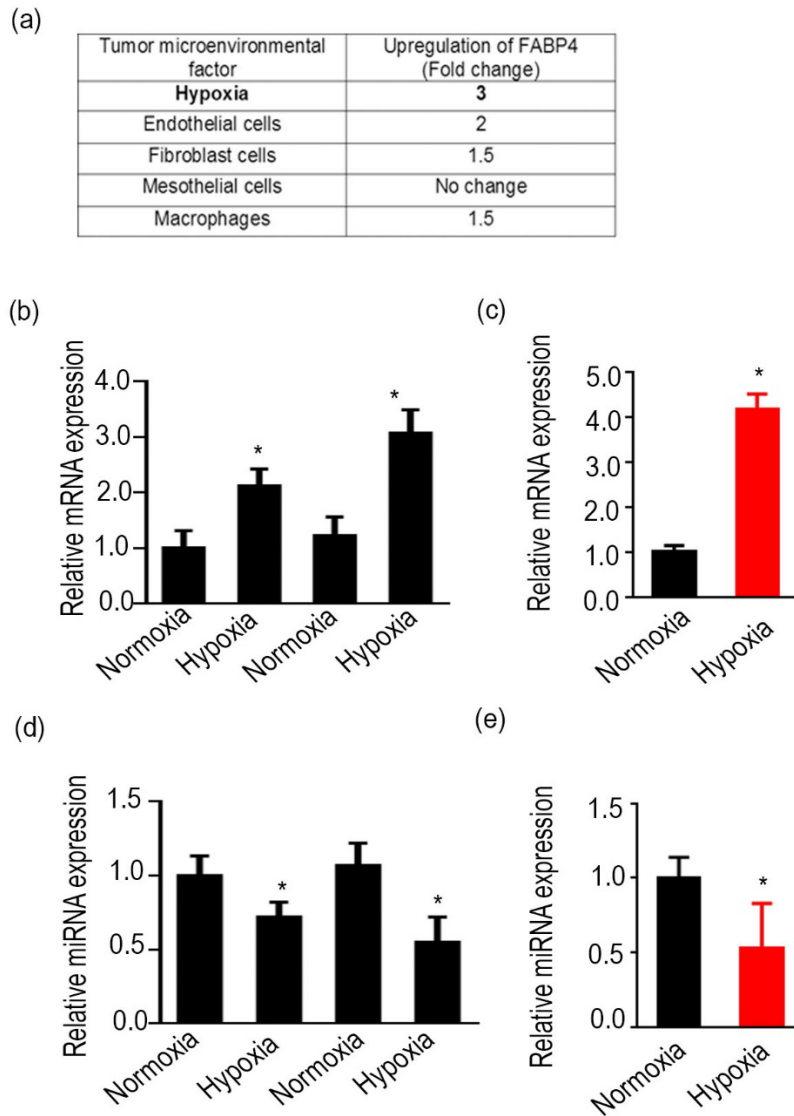
Figure 25 (a) Effect of tumor micro-environmental factors on the expression of FABP4 (b c) Effect of hypoxia on (b) FABP4 expression and (c) expression of miR-409-3p in HeyA8 MDR cells. (d, e) Effect of hypoxia on (d) miR-409-3p expression and (e) FABP4 expression levels in Ovca 432 cells. *p < 0.05.

We then decided to see if the similar effects can be seen *in vivo*. We used the tumor samples that are collected from mice treated with bevacizumab. Bevacizumab is anti-vascular endothelial growth factor and has been shown to increase hypoxia in ovarian cancer patients [91]. We conducted immunohistochemical analysis of the tumor sections with CA9 (Carbonic anhydrase 9, a hypoxia marker) and FABP4 antibodies. We observed consistent co-localization of CA9 and FABP4 in these tissues (Figure 26 a). We further used the same samples for qRT-PCR analysis. We checked the expression of miR-490-3p in the tumor samples treated with bevacizumab and compared it with tumors treated with control antibody. The expression of miR-409-3p was lower in the tumors treated with bevacizumab compared to the control tumors (Figure 26 b).

After in *vitro* and *in vivo* experiments, we decided the check if the similar regulation can be seen in the patient samples. We probed TCGA and Tothill datasets for this analysis. We also used the hypoxia metagene signature as described in [84]. We extracted the gene expression data for FABP4 and for the genes mentioned in the hypoxia metagene signatures. We saw a positive correlation between FABP4 expression and the expression of many genes from the signature across various platforms. Table 5 shows these correlations. Of particular mention was the gene PLAU, plasminogen activator, urokinase. There was a significant correlation between FABP4 and PLAU across all the platforms. Figure 26 c shows spearman correlations between FABP4 and PLAU. We further checked if silencing of dicer affects the expression of miR-409-3p. The qRT-PCR results indicated that knockdown of dicer resulted in significant downregulation of miR-409-3p levels (Figure 26 d). Thus *in vitro*,

in vivo and patient data, all point to the regulation of FABP4 and miR-409-3p by hypoxia.
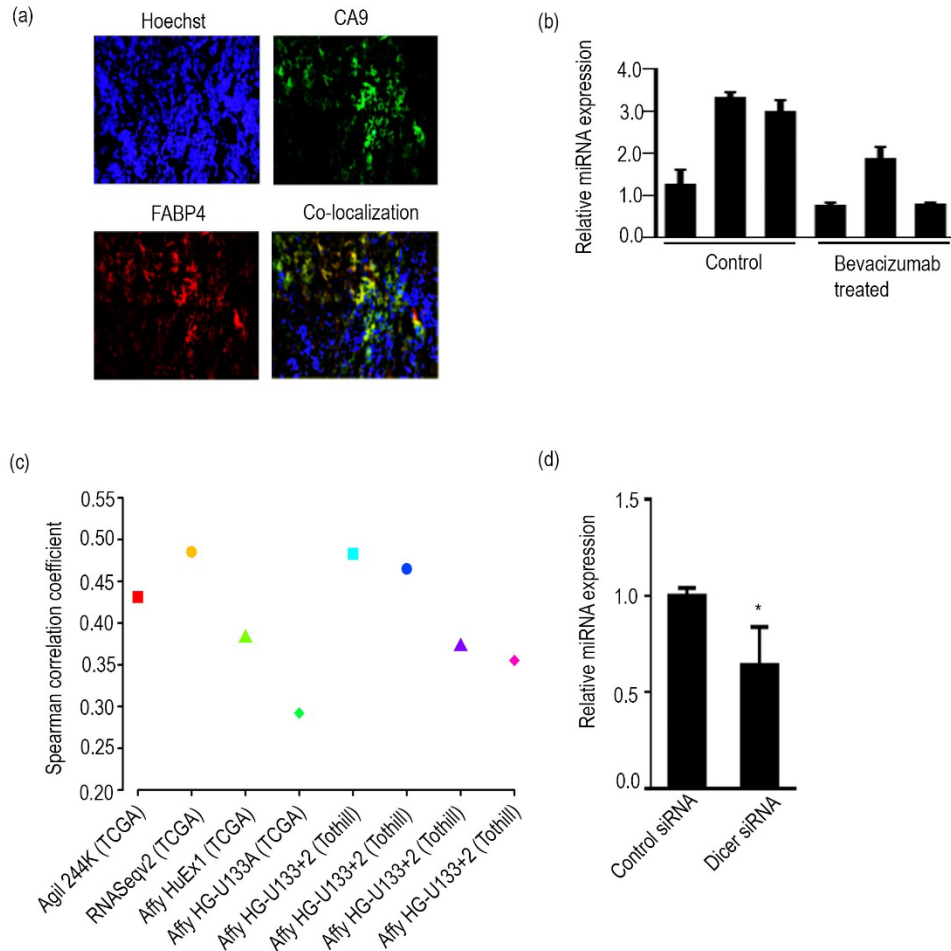
Figure 26 (a) Co-localization of CA9 (a hypoxia marker) and FABP4 in tumor tissues taken from mice treated with bevacizumab, which is known to induce hypoxia. Representative image is shown. (b) miR-409-3p expression levels in tumor tissues from mice treated with control vehicle or bevacizumab, which is known to induce hypoxia (n = 3 mice per group). (c) Direct correlation of FABP4 with PLAU (a hypoxia

signature gene) in patient samples across different platforms. (d) Downregulation of

miR409-3p after knockdown of dicer (*p<0.05)

Gene	Gene	Affy HuEx1		Affy HG-U133A		Agilent		RNASeqv2		Tothill	
		Spearman coef.	p value	Spearman coef.	p value	Spearman coef	p value	Spearman coef	p value	Spearman coef	p value
FABP4	**PLAU**	**0.381821**	**0**	**0.292179**	**1.85E-11**	**0.431181**	**9.27E-27**	**0.485024**	**3.63E-19**	**0.482964**	**8.68E-14**
FABP4	S100A3	0.220363	1.53E-07	-	-	0.252518	1.35E-09	0.291388	2.65E-07	0.319772	2.27E-06
FABP4	TPBG	0.250939	2.03E-09	-	-	0.223718	8.78E-08	-	-	0.287209	2.35E-05
FABP4	BCAR1	0.200654	1.82E-06	-	-	-	-	0.242984	2.02E-05	0.34571	2.42E-07
FABP4	PGF	0.251081	1.99E-09	-	-	-	-	0.351984	3.31E-10	-	-
FABP4	TUBB2A	0.2454	4.64E-09	-	-	0.281223	1.22E-11	-	-	0.41673	3.73E-10
FABP4	EIF2S1	-	-	-	-	0.220044	1.44E-07	-	-	0.230791	0.000708
FABP4	ANGPTL4	-	-	-	-	-	-	0.253214	8.69E-06	0.298421	9.85E-06
FABP4	PTGFRN	-	-	-	-	-	-	0.239304	2.72E-05	0.278031	4.32E-05
FABP4	TANC2	-	-	-	-	-	-	0.235108	3.79E-05	0.317551	2.68E-06
FABP4	PYGL	-	-	-	-	-	-	-	-	0.22888	0.000809
FABP4	VEZT	-	-	-	-	-	-	-	-	0.219382	0.001337
FABP4	PPARD	-	-	-	-	-	-	-	-	0.212546	0.001896

Table 5 Correlation of FABP4 gene expression with the expression of genes listed in

Winter hypoxia metagene signature across various data platforms

Chapter 7: Downstream effects of FABP4 in cancer cells

We conducted reverse phase protein array (RPPA) to identify signaling pathways regulated by FABP4. We compared two groups- HeyA8 MDR cells transfected by control siRNA or by FABP4 siRNA. The heat map is shown in Figure 27 a. The confirmation of downregulation of FABP4 is presented in the western blot (Figure 27 c). Several metastasis related proteins were suppressed in the cells where FABP4 expression was silenced (Figure 27 b). We analyzed the RPPA data using Ingenuity pathway analysis (IPA) and Netwalker softwares. The results from the IPA analysis is presented in Figure 27 d. We noticed that several key pathways related to cancer metastasis are downregulated in the cells where FABP4 is inhibited. The results from Netwalker analysis also supported this results and revealed that several subpathways related to metastasis are significantly downregulated in FABP4 siRNA transfected cells (Figure 27 e).
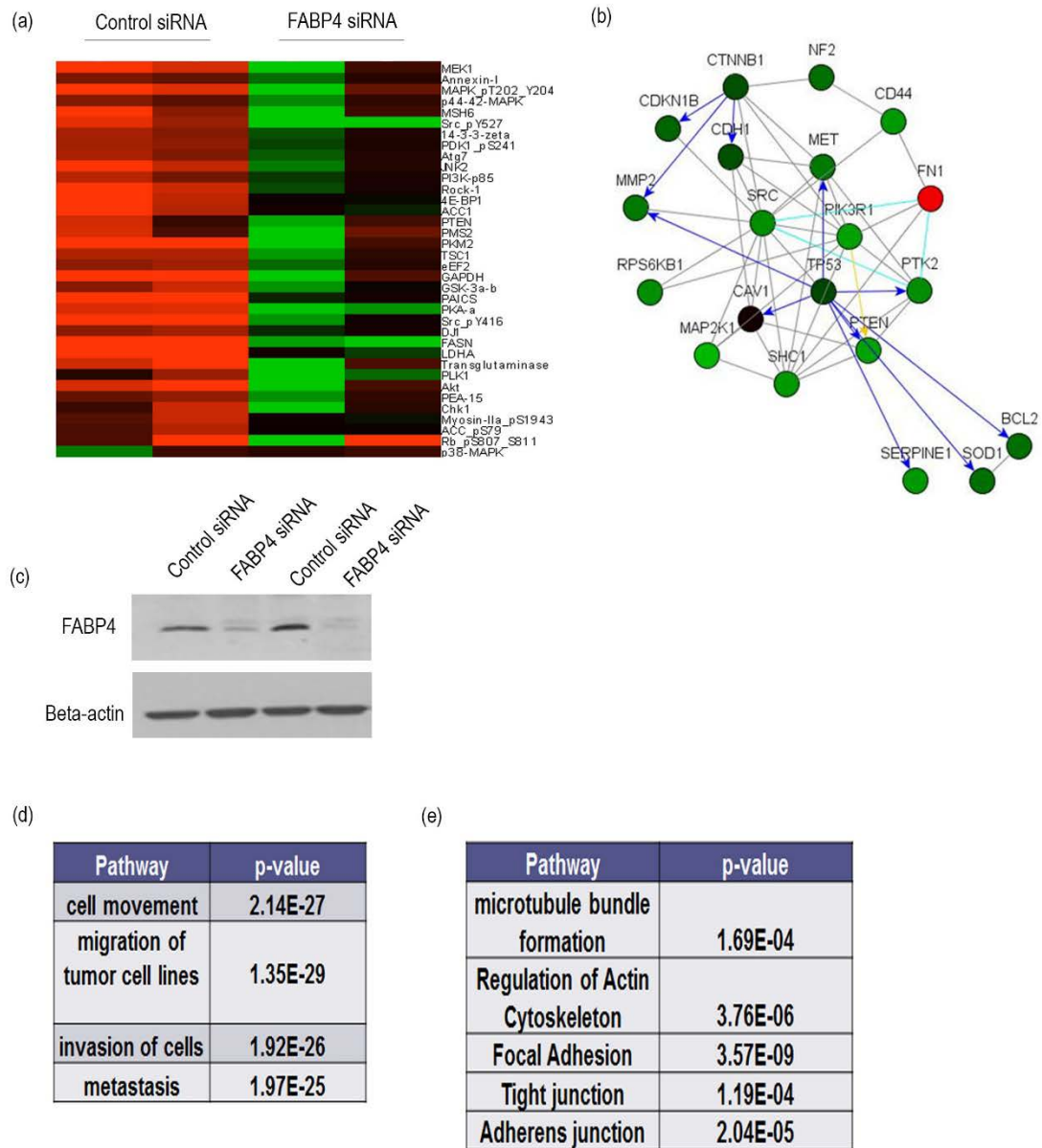
Figure 27 (a) RPPA data for downregulated proteins in the FABP4 siRNA and control

siRNA groups. (b) Proteins that were downregulated in the FABP4 siRNA group are

related to the metastasis pathway (c) Western blot for confirmation of downregulation

of FABP4 in the samples submitted to RPPA (d) Ingenuity pathway analysis of RPPA

data. (e) Netwalker analysis of RPPA data.

We next sought to identify the metabolomics changes regulated by FABP4. We first analyzed the metabolite and gene array presented in [58, 86, 87]. We sorted the patient tumor samples based on their expression of FABP4. Samples with FABP4 expression lower than the median were grouped in 'Low FABP4' group while those with higher FABP4 expression than the median were grouped in 'High FABP4' group. We then calculated median expression for each metabolite for samples present in each group. Table 6 lists the metabolites that have different expressions depending on the expression of FABP4. Low antilog value indicates low expression in low FABP4 group. We saw that several metabolites are different in high versus low FABP4 groups.

BIOCHEMICAL NAME	Antilog
glutathione, reduced (GSH)	0.01906
N-acetylaspartate (NAA)	0.15397
glycerophosphorylcholine (GPC)	0.27502
glycerol 3-phosphate (G3P)	0.30117
ascorbate (Vitamin C)	0.31861
N-acetyl-aspartyl-glutamate-NAAG-	0.49411
glucose 6-phosphate (G6P)	0.51071
glutathione, oxidized (GSSG)	0.54313
fructose-6-phosphate	0.56294
1-palmitoylglycerophosphoethanolamine	0.5662
adenosine-3-monophosphate-3 (AMP)	0.57108
dehydroascorbate	0.57873
obar-ribulose-5-phosphate-xylulose-5-phospha	0.5815
1-arachidonoylglycerophosphoinositol-	0.58669
2-oleoylglycerophosphoethanolamine-	0.59617
glycerol 2-phosphate	0.60175
1-palmitoylplasmenylethanolamine-	0.61374
1-oleoylglycerophosphoethanolamine	0.61412
dihydroxyacetone-phosphate-DHAP-	0.61641
S-adenosylhomocysteine (SAH)	0.62201
p-cresol-sulfate	0.67683
phosphoenolpyruvate (PEP)	0.67818
mannose-6-phosphate	0.68185
1-palmitoylglycerophosphoinositol-	0.68692
2-hydroxystearate	0.70347
carnitine	0.70723
gluconate	0.73625
2-hydroxypalmitate	0.73722
choline-phosphate	0.73992
1-stearoylglycerophosphoethanolamine	0.74021
butyrylcarnitine	0.74046
docosahexaenoate (DHA; 22:6n3)	0.74079
behenate-22-0-	0.74804
2-phosphoglycerate	0.75226
7-alpha-hydroxy-3-oxo-4-cholestenoate-7-Hoca	0.75483
4-hydroxybutyrate-GHB-	0.7568
2-hydroxyglutarate	0.76382
xylulose	0.77906
erythronate*	0.78137

1-linoleoylglycerophosphoethanolamine-	0.78458
propionylcarnitine	0.78633
ribitol	0.78647
1-stearoylglycerophosphoinositol	0.78654
inosine	0.78697
6-phosphogluconate	0.78916
dihomo-linolenate-20-3n3-or-n6-	0.79142
adrenate (22:4n6)	0.79299
arachidonate (20:4n6)	0.79409
docosapentaenoate-n6-DPA-22-5n6-	0.79532
ribose	0.79596
1,3-dihydroxyacetone	0.79703
phenylacetylglutamine	0.81738
3-phosphoglycerate	0.81998
spermidine	0.82124
alpha-hydroxyisovalerate	0.8232
bilirubin*E-E-	0.82466
adenosine-2-monophosphate-2 (AMP)	0.82958
isobutyrylcarnitine	0.83273
gamma-glutamylglutamate	0.83707
1-oleoylglycerophosphoinositol-	0.83845
isovalerylcarnitine	0.8385
pyruvate	0.84004
palmitoyl-sphingomyelin	0.84332
ophthalmate	0.84399
arabitol	0.8462
4-androsten-3beta-17beta-diol-disulfate-1-	0.85172
guanosine	0.85421
malate	0.85855
3-(4-hydroxyphenyl)lactate	0.86185
succinylcarnitine	0.86332
3-aminoisobutyrate	0.86378
fumarate	0.86417
flavin adenine dinucleotide (FAD+)	0.86571
1-arachidonoylglycerophosphoethanolamine-	0.86664
2-hydroxybutyrate (AHB)	0.87137
pantothenate	0.8716
eicosapentaenoate (EPA; 20:5n3)	0.87434
beta-hydroxyisovalerate	0.87622
caproate (6:0)	0.87751

glycylglycine	0.8796
cholesterol	0.8799
undecanedioate	0.88118
glycerate	0.88232
N1-methyladenosine	0.88694
2-aminobutyrate	0.8875
inositol-1-phosphate (I1P)	0.88849
uridine	0.88874
pyroglutamine*	0.88912
pregnen-diol-disulfate-	0.89145
nicotinamide	0.89562
choline	0.89575
glutamine	0.89829
alanine	0.90003
cytidine 5'-monophosphate-5-CMP-	0.90154
cysteine-glutathione-disulfide	0.90385
threonine	0.90621
hypoxanthine	0.90661
xanthosine	0.90721
xanthine	0.90767
acetylphosphate	0.9186
pyrosphosphate (PPi)	0.92256
leucine	0.92607
isoleucine	0.92645
cystathionine	0.92675
myo-inositol	0.9276
kynurenine	0.93418
hippurate	0.93739
urea	0.9379
heptaethylene-glycol	0.93795
methionine	0.93892
gamma-glutamylleucine	0.94026
acetylcarnitine	0.94029
creatine	0.94166
fructose	0.94302
glutamate	0.94468
N-formylmethionine	0.94594
tryptophan-betaine-	0.94846
5-oxoproline	0.95119
glycine	0.95285

azelate (nonanedioate)	0.95372
docosatrienoate-22-3n3-	0.95406
N-acetylglycine	0.95473
proline	0.95505
phenylalanine	0.95584
histidine	0.95635
aspartate	0.95794
pipecolate	0.95885
N-acetylneuraminate	0.95938
serine	0.95978
1,5-anhydroglucitol (1,5-AG)	0.96095
valine	0.9626
glycolate (hydroxyacetate)	0.96378
C-glycosyltryptophan-	0.9671
mannose	0.9691
mannitol	0.97312
3-dehydrocarnitine*	0.97348
2-aminoadipate	0.97574
gamma-glutamylphenylalanine	0.97589
stearate (18:0)	0.9774
ribulose	0.97766
5,6-dihydrouracil	0.98053
pelargonate (9:0)	0.98125
gamma-glutamylglutamine	0.9821
tyrosine	0.98455
putrescine	0.98462
lactate	0.98478
uracil	0.98781
phosphoethanolamine	0.98814
erythritol	0.99101
urate	0.99101
hexaethylene-glycol	0.9922
N-acetylserine	0.99228
ornithine	0.99386
phosphate	0.99474
sorbitol	0.99577
ribose-5-phosphate	0.99604
cystine	0.99679
caprylate (8:0)	0.99829
margarate (17:0)	0.9988

rboxy-4-methyl-5-propyl-2-furanpropanoate (CI	1
biliverdin	1
tetradecanedioate	1
ethanolamine	1.00054
asparagine	1.0009
myristate (14:0)	1.00993
hydroxyisovaleroyl-carnitine	1.01115
N-acetylthreonine	1.01121
palmitoyl-ethanolamide	1.01534
taurine	1.01649
gamma-aminobutyrate (GABA)	1.01724
arginine	1.01765
N6-acetyllysine	1.01896
laurate (12:0)	1.01939
creatinine	1.02247
N-acetylalanine	1.02297
hypotaurine	1.02305
assymetric-dimethylarginine (ADMA)	1.02316
nonadecanoate (19:0)	1.02736
methylphosphate	1.0274
tryptophan	1.0274
docosadienoate-22-2n6-	1.03034
myristoleate (14:1n5)	1.03036
lysine	1.03382
argininosuccinate	1.03817
glycerol	1.03922
cysteine	1.03926
ergothioneine	1.04088
caprate (10:0)	1.04506
trans-4-hydroxyproline	1.0482
scyllo-inositol	1.04943
eicosenoate (20:1n9 or 11)	1.0505
riboflavin (Vitamin B2)	1.05709
gamma-glutamylvaline	1.05969
fructose-1-phosphate	1.06182
3-hydroxybutyrate (BHBA)	1.06391
palmitate (16:0)	1.06449
docosapentaenoate (n3-DPA; 22:5n3)	1.06805
maltose	1.0704
dihomo-linoleate-20-2n6-	1.07442

N-acetylmethionine	1.07588
N-acetylornithine	1.08646
15-HETE	1.09975
citrate	1.11086
pseudouridine	1.11583
stearidonate (18:4n3)	1.11806
5-methylpalmitate-isobar-with-2-methylpalmitat	1.11878
pentadecanoate (15:0)	1.12253
beta-alanine	1.12512
13-HODE-9-HODE	1.12574
cortisol	1.12874
3-methyl-2-oxovalerate	1.12939
succinate	1.13281
oleate (18:1n9)	1.13819
4-methyl-2-oxopentanoate	1.15256
2-linoleoylglycerophosphoethanolamine-	1.15983
N-acetylglucosamine-6-phosphate	1.1648
betaine	1.17065
glucose	1.17257
alpha-tocopherol	1.174
octadecanedioate	1.18455
linoleate (18:2n6)	1.19287
osphate-glucose-1,6-diphosphate-myo-inosito	1.19868
phenol sulfate	1.2092
10-nonadecenoate (19:1n9)	1.22548
guanine	1.23592
hexadecanedioate	1.23857
linolenate [alpha or gamma] (18:3n3 or 6)	1.25673
palmitoleate (16:1n7)	1.26189
1-2-propanediol	1.26983
threonate	1.27318
maltotriose	1.30167
17-methylstearate	1.35496
stachydrine	1.38221
10-heptaadecenoate (17:1n7)	1.38914
1-stearoylglycerophosphocholine	1.4357
maltotetraose	1.63675
docosahexaenoylglycerophosphoethanolamin	1.67267
2-arachidonoylglycerophosphocholine*	1.75107
1-palmitoylglycerophosphocholine	2.54398
2-arachidonoylglycerophosphoethanolamine-	6.09392

Table 6 Metabolites differentially expressed in patient samples belonging to low- and high-FABP4-expression groups. Lower antilog value represents lower expression in the low-FABP4 group.

One of the limitations of this analysis was that the gene and metabolites arrays were conducted on the entire tumor tissues. Thus, the data could have been influenced by the genes or metabolites present in the stromal cells. To address this concern, we used Desorption Electrospray Ionization-Mass Spectrometry (DESI-MS imaging) technique. The technique not only identifies metabolites present in a tissue but gives the spatial information of the metabolite as well. For this experiment, we used the chemotherapy naïve, high grade ovarian tumor samples used in our initial biomarker discovery study. Based on their FABP4 expression, top 25% tumor samples were classified in 'high FABP4' group while the rest of the samples were classified in 'Low FABP4' group. We then conducted DESI-MS imaging in both, negative and positive polarities on 31 tumor samples.

The first step in the analysis was to check if there are sufficient differences in the metabolites and lipids that can correlate with the changes in FABP4 expression. Lasso (Least absolute shrinkage and selector operator) method was used to explore the correlations between lipids, metabolites and FABP4 levels. The samples were divided into training and validation groups. First, the training set was used to build a molecular model. The coefficient of variation analysis on the negative ion mode data from the training set, showed an overall agreement of 81.6%. The area under curve (AUC) was 0.79. The result thus suggested an association between the expression and composition of metabolites, and the expression of FABP4 in ovarian tumor tissues. The model generated from the training set was used for the samples from the validation set. When the negative ion mode data for the validation set was analyzed, the overall agreement of was found to be 51.6% and AUC was 0.60 (Table 7 a). Similar

methods were used for to analyze the positive ion mode data. The overall agreement for the training set was 74.2% with AUC=0.73 while the validation set yielded the overall agreement of 61.7% and AUC of 0.58 (Table 7 b). Thus, in both positive as well as in negative ion mode, the results indicate an association between metabolites and FABP4 expression.

We then decided to investigate if FABP4 levels can be predicted from the metabolite information (Table 7). We combined positive and negative ion mode data and built a comprehensive model. The data was then analyzed for each patient by cross-validation method. The analysis successfully classified 66.7% of high FABP4 samples and 100% of low samples in the right categories. Molecular models based on the lipid and metabolite data thus established that FABP4 expression can alter metabolic profiles of ovarian cancer tissues.

		Pathology	High FABP4	Low FABP4	Agreement (%)	Overall Agreement (%)	AUC
For pixels	Cross-Validation	High FABP4	1925	671	74.2	81.6	0.79
		Low FABP4	1218	6450	84.1		
	Validation Set	High FABP4	1003	1189	45.8	56.1	0.60
		Low FABP4	1084	1906	63.8		
For patients	Cross-Validation	High FABP4	5	1	83.3	80.0	0.79
		Low FABP4	3	11	78.6		
	Validation Set	High FABP4	4	2	66.7	63.6	0.60
		Low FABP4	2	3	60.0		

		Pathology	High FABP4	Low FABP4	Agreement (%)	Overall Agreement (%)	AUC
For pixels	Cross-Validation	High FABP4	1248	531	70.2	74.2	0.73
		Low FABP4	2271	6823	75.0		
	Validation Set	High FABP4	661	705	48.4	61.7	0.58
		Low FABP4	1049	2169	67.4		
For patients	Cross-Validation	High FABP4	5	1	83.3	73.7	0.73
		Low FABP4	4	9	69.2		
	Validation Set	High FABP4	2	2	50.0	50.0	0.58
		Low FABP4	3	3	50.0		

Table 7 (a) Model correlating molecular profiles and FABP4 expression based on negative ion mode data

(b) Model correlating molecular profiles and FABP4 expression based on positive ion mode data

The next step was to identify the metabolites that are altered by FABP4 expression. We hence analyzed the data by SAM (Significant analysis of Microarray) method and identified m/z values (mass to charge ratios) of the metabolites that differ in their expression in low and high FABP4 groups. With the false discovery rate of 3.8%, we were able to identify 122 unique monoisotonic m/z values characteristic of low FABP4 expression and 118 values characteristic of high FABP4 expression. We then used high mass accuracy/high mass resolution and tandem mass spectrometry analysis to identify the metabolite species associated with the m/z values. The species identified belong to the following classes of metabolites- small metabolites, fatty acids (FA), sterol lipids (ST), ceramides (Cer), glycerolipids (GL), monoacylglycerophosphates (PA), glycerophosphoethanolamines (PE), glycerophosphoglycerols (PG), glycerophosphoinositols (PI), glycerophosphoserines (PS), and cardiolipins (CL).

There were several metabolites that were uniquely different in both the groups. Table 8 and 9 lists all the metabolites present in low and high FABP4 groups. The composition of fatty acids was significantly different in low vs. high FABP4 groups. An increased number of highly unsaturated fatty acids was observed in high FABP4. Oxidation of fatty acids was also specifically observed in high FABP4 group. Glycerolipids, glycerophosphoethanolamines, glycerophosphoglycerols and lysophospholipid species, including LysoPE, LysoPG, and LysoPI were abundantly present in high FABP4 group compared to low FABP4 group. Conversely, the number of non-oxidized glycerophosphoinositols and glycerophosphoserines species was higher in the low FABP4 samples compared to the high FABP4 group and cardiolipins

were exclusively present in the low FABP4 samples. These observations suggest that changes in the metabolic profiles of ovarian cancer tissues are associated with variations in FABP4 expression.

HUMAN SAMPLES - HIGH FABP4 EXPRESSION				
Attribution	Molecular Formula	Detected *m/z*	Mass error (ppm)	SAM Score
Metabolites				
N-acetylaspartic acid	$C_6H_8NO_5$	174.0408	0.0	-17.207
Ascorbic acid	$C_6H_7O_6$	175.0252	2.3	-5.943
Gluconic acid	$C_6H_{11}O_7$	195.0509	0.5	-41.91
Phosphatidic acid	$C_6H_8O_7Cl$	226.9962	0.9	-6.776
Fatty Acids				
FA 14:1	$C_{14}H_{25}O_2$	225.1862	-0.9	-23.744
FA 17:0	$C_{17}H_{33}O_2$	269.2484	0.7	-0.514
FA hydroxy 16:0	$C_{16}H_{31}O_3$	271.2279	0.4	-13.784
FA 18:3	$C_{18}H_{29}O_2$	277.2171	0.7	-4.145
FA 18:2	$C_{18}H_{31}O_2$	279.2327	1.1	-11.127
FA 18:1	$C_{18}H_{32}O_2$	281.2484	0.7	-5.365
FA 18:0	$C_{18}H_{35}O_2$	283.2640	1.1	-3.589
FA 20:5	$C_{20}H_{29}O_2$	301.2171	0.7	-12.165
FA 20:4	$C_{20}H_{31}O_2$	303.2327	1.0	-27.378
FA 18:2	$C_{18}H_{32}O_2Cl$	315.2092	1.3	-17.244
FA 18:1	$C_{18}H_{34}O_2Cl$	317.2249	1.3	-21.336
FA hydroxy 20:4	$C_{20}H_{31}O_3$	319.2284	-1.6	-18.929
FA 18:0	$C_{18}H_{36}O_2Cl$	319.2407	0.6	-22.176
FA hydroxy 20:3	$C_{20}H_{33}O_3$	321.2427	2.5	-8.559
FA 22:6	$C_{22}H_{31}O_2$	327.2326	1.2	-21.309
FA 22:5	$C_{22}H_{33}O_2$	329.2482	1.2	-22.572
FA 22:4	$C_{22}H_{35}O_2$	331.2639	1.2	-37.569
FA 22:3	$C_{22}H_{37}O_2$	333.2794	1.5	-6.211
FA 20:4	$C_{20}H_{32}O_2Cl$	339.2093	0.9	-32.242
FA hydroxy 22:6	$C_{22}H_{31}O_3$	343.2296	-5.0	-5.971
FA 24:5	$C_{24}H_{37}O_2$	357.2795	1.1	-16.621
FA 24:4	$C_{24}H_{39}O_2$	359.2953	0.8	-17.472
FA 24:3	$C_{24}H_{41}O_2$	361.3106	1.7	-0.934
FA 22:4	$C_{22}H_{36}O_2Cl$	367.2416	-1.9	-33.351
FA hydroxy 24:0	$C_{24}H_{47}O_3$	383.3526	1.3	-2.796
Glycerolipids				
MG 18:0	$C_{21}H_{40}O_4Cl$	391.2615	1.5	-7.537
MG 22:6	$C_{25}H_{38}O_4Cl$	437.2459	1.1	-6.813
DG 32:1/0:0	$C_{35}H_{66}O_5Cl$	601.4594	1.7	-8.245
DG 32:0/0:0	$C_{35}H_{68}O_5Cl$	603.4758	0.5	-3.515
DG 34:3/0:0	$C_{37}H_{66}O_5Cl$	625.4594	1.6	-2.261
DG 34:2/0:0	$C_{37}H_{68}O_5Cl$	627.4754	1.1	-6.743
DG 34:1/0:0	$C_{37}H_{70}O_5Cl$	629.4913	0.6	-14.24
DG 36:4/0:0	$C_{39}H_{68}O_5Cl$	651.4753	1.2	-13.268
DG 36:3/0:0	$C_{39}H_{70}O_5Cl$	653.4916	0.2	-4.762
DG 36:2/0:0	$C_{39}H_{72}O_5Cl$	655.5072	0.3	-15.714
DG 38:6/0:0	$C_{41}H_{68}O_5Cl$	675.4752	1.3	-18.92
DG 38:5/0:0	$C_{41}H_{70}O_5Cl$	677.4932	-2.2	-15.97
DG 38:4/0:0	$C_{41}H_{72}O_5Cl$	679.5089	-2.2	-15.44

DG 40:7/0:0	C$_{43}$H$_{70}$O$_5$Cl	701.4892	3.6	**-2.8**
DG 40:6/0:0	C$_{43}$H$_{72}$O$_5$Cl	703.5063	1.6	**-15.599**
DG 40:5/0:0	C$_{43}$H$_{74}$O$_5$Cl	705.5230	1.1	**-15.089**
Glycerophosphoethanolamines				
LysoPE P-16:0	C$_{21}$H$_{43}$NO$_6$P	436.2843	-2.3	**-3.539**
LysoPE O-18:1	C$_{23}$H$_{47}$NO$_6$P	464.3159	-2.8	**-30.415**
LysoPE 18:1	C$_{23}$H$_{45}$NO$_7$P	478.2951	-2.5	**-4.209**
LysoPE 18:0	C$_{23}$H$_{47}$NO$_7$P	480.3109	-2.7	**-5.842**
LysoPE 20:4	C$_{23}$H$_{43}$NO$_7$P	500.2796	-2.6	**-18.64**
PE 20:4/1:0	C$_{26}$H$_{43}$NO$_8$P	528.2728	-0.8	**-36.177**
PE 34:0	C$_{23}$H$_{47}$NO$_6$P	718.5378	1.9	**-0.697**
PE P-18:0/18:4	C$_{41}$H$_{73}$NO$_7$Cl	722.5116	1.9	**-10.493**
PE O-38:5 or PE P-38:4	C$_{43}$H$_{77}$NO$_7$P	750.5432	-1.2	**-35.708**
PE 38:5	C$_{43}$H$_{75}$NO$_8$P	764.5224	-3.2	**-24.395**
PE 38:4	C$_{43}$H$_{77}$NO$_8$P	766.5382	6.2	**-6.357**
PE 38:2	C$_{43}$H$_{81}$NO$_8$P	770.5657	1.2	**-4.115**
PE 38:1	C$_{43}$H$_{83}$NO$_8$P	772.5853	1.9	**-19.182**
PE 39:6	C$_{44}$H$_{75}$NO$_8$P	776.5221	1.8	**-17.599**
PE 39:5	C$_{44}$H$_{77}$NO$_8$P	778.5378	-1.0	**-17.599**
PE O-40:5 or PE P-40:4	C$_{45}$H$_{81}$NO$_7$P	778.5764	0.5	**-20.071**
PE 40:5	C$_{45}$H$_{79}$NO$_8$P	792.5545	-1.6	**-10.169**
PE 37:1	C$_{42}$H$_{82}$NO$_8$PCl	794.5485	-0.8	**-4.871**
PE 40:4	C$_{45}$H$_{81}$NO$_8$P	794.5711	0.7	**-20.835**
PE 39:4	C$_{44}$H$_{80}$NO$_8$PCl	816.5310	0.7	**-4.447**
PE 39:2	C$_{44}$H$_{84}$NO$_8$PCl	820.5623	2.9	**-12.74**
PE 39:1	C$_{44}$H$_{86}$NO$_8$PCl	822.5761	-4.0	**-16.628**
PE 41:6	C$_{46}$H$_{80}$NO$_8$PCl	840.5350	-2.7	**-14.693**
PE 41:5	C$_{46}$H$_{82}$NO$_8$PCl	842.5495	1.1	**-26.422**
PE 41:4	C$_{46}$H$_{84}$NO$_8$PCl	844.5620	-1.4	**-25.036**
PE 43:6	C$_{48}$H$_{84}$NO$_8$PCl	868.5641	-3.4	**-7.314**
PE 43:2	C$_{48}$H$_{92}$NO$_8$PCl	876.6285	0.8	**-8.158**
Glycerophosphoglycerols				
LysoPG 16:0	C$_{22}$H$_{44}$O$_9$P	483.2734	-2.1	**-7.141**
LysoPG 18:2	C$_{24}$H$_{44}$O$_9$P	507.2744	-3.1	**-20.225**
LysoPG 18:1	C$_{24}$H$_{46}$O$_9$P	509.2881	-2.9	**-18.358**
LysoPG 22:6	C$_{28}$H$_{44}$O$_9$P	555.2744	-0.7	**-11.491**
PG 34:3	C$_{40}$H$_{72}$O$_{10}$P	743.4890	-2.8	**-0.683**
PG 34:2	C$_{40}$H$_{74}$O$_{10}$P	745.5015	1.5	**-1.249**
PG 16:0/18:1	C$_{40}$H$_{76}$O$_{10}$P	747.5196	1.6	**-4.319**
PG 36:4	C$_{42}$H$_{74}$O$_{10}$P	769.5007	2.3	**-18.539**
PG 18:2/18:1	C$_{42}$H$_{76}$O$_{10}$P	771.5201	-2.5	**-4.819**
PG 18:1/18:1	C$_{42}$H$_{78}$O$_{10}$P	773.5331	0.9	**-2.341**
PG 38:6	C$_{44}$H$_{74}$O$_{10}$P	793.5010	1.9	**-7.587**
PG 38:5	C$_{44}$H$_{76}$O$_{10}$P	795.5145	4.7	**-2.768**
PG 40:8	C$_{46}$H$_{74}$O$_{10}$P	817.5011	1.7	**-6.187**
PG 40:7	C$_{46}$H$_{76}$O$_{10}$P	819.5160	2.7	**-2.822**
PG 40:6	C$_{46}$H$_{78}$O$_{10}$P	821.5309	3.5	**-0.714**
PG 40:5	C$_{46}$H$_{80}$O$_{10}$P	823.5480	1.8	**-0.707**
PG 22:6/22:6	C$_{50}$H$_{74}$O$_{10}$P	865.4996	3.4	**-7.994**
Ceramides				
Cer d32:1	C$_{32}$H$_{63}$NO$_3$Cl	544.4519	0.9	**-8.899**
Cer d16:1/17:0	C$_{33}$H$_{65}$NO$_3$Cl	558.4663	0.7	**-16.215**
Cer d34:2	C$_{34}$H$_{65}$NO$_3$Cl	570.4655	1.8	**-8.47**
Cer d34:1	C$_{34}$H$_{67}$NO$_3$Cl	572.4809	0.5	**-1.065**
Cer d36:2	C$_{36}$H$_{69}$NO$_3$Cl	598.4960	-1.7	**-4.673**
Cer d36:1	C$_{36}$H$_{71}$NO$_3$Cl	600.5118	-2.4	**-17.626**

Cer d38:1	$C_{40}H_{79}NO_3Cl$	656.5752	-0.1	**-8.174**
Cer d41:2	$C_{41}H_{79}NO_3Cl$	668.5766	-0.4	**-1.288**
Cer d42:0	$C_{42}H_{81}NO_3Cl$	682.5901	1.3	**-0.513**
Cer d42:1	$C_{42}H_{83}NO_3Cl$	684.6068	1.0	**-1.236**
PE-Cer d36:1	$C_{38}H_{76}N_2O_6P$	687.5449	-0.4	**-4.101**
Monoacylglycerophosphates				
PA 36:1	$C_{39}H_{74}O_8P$	701.5120	1.0	**-18.155**
PA O-38:2 or PA P-38:1	$C_{41}H_{79}O_7PCl$	749.5278	1.3	**-11.93**
Cardiolipins				
CL 72:4	$C_{81}H_{148}O_{17}P_2$	727.5070	-1.9	**-7.459**
Glycerophosphoinositols				
LysoPI 15:0	$C_{24}H_{46}O_{12}P$	557.2729	0.5	**-16.255**
LysoPI O-16:0	$C_{25}H_{50}O_{11}P$	557.3091	0.9	**-5.78**
LysoPI 18:0	$C_{27}H_{52}O_{12}P$	599.3199	0.5	**-20.061**
Lyso PI 20:4	$C_{29}H_{48}O_{12}P$	619.2904	-2.4	**-15.733**
PI O-33:2 or PI P-33:1	$C_{42}H_{79}O_{12}PCl$	841.5011	-1.0	**-13.023**
PI P-18:0/17:2	$C_{44}H_{81}O_{12}PCl$	867.5158	0.2	**-15.209**
PI O-35:2 or PI P-35:1	$C_{44}H_{83}O_{12}PCl$	869.5312	0.5	**-1.013**
PI 37:4	$C_{46}H_{80}O_{13}P$	871.5342	3.3	**-3.616**
PI 38:6	$C_{47}H_{78}O_{13}P$	881.5159	3.1	**-15.606**
PI 38:5	$C_{47}H_{80}O_{13}P$	883.5332	1.1	**-15.194**
PI 38:4	$C_{47}H_{82}O_{13}P$	885.5483	1.8	**-27.615**
PI 40:4	$C_{49}H_{86}O_{13}P$	913.5793	2.1	**-18.087**
PI 40:3	$C_{49}H_{88}O_{13}P$	915.5952	1.7	**-8.514**
Glycerophosphoserines				
PS O-36:4 or PS P-36:3	$C_{42}H_{75}NO_9P$	768.5211	-3.4	**-6.698**
PS 38:4	$C_{44}H_{77}O_{10}NP$	810.5279	1.5	**-0.461**
PS O-39:0	$C_{45}H_{89}NO_9P$	818.6245	4.3	**-0.518**
PS O-40:4 or PS P-40:3	$C_{46}H_{83}NO_9P$	824.5810	0.1	**-12.284**
PS 39:2	$C_{45}H_{83}NO_{10}P$	828.5724	4.3	**-4.851**

Table 8. High FABP4– human data – 122 *m/z* values

HUMAN SAMPLES - LOW FABP4 EXPRESSION				
Attribution	**Molecular Formula**	**Detected _m/z_**	**Mass error (ppm)**	**SAM Score**
Metabolites				
Fumarate	$C_{47}H_{84}O_{13}P$	115.0039	-1.7	**18.081**
Acetyl-glycine	$C_4H_6NO_3$	116.0351	1.7	**11.101**
Succinate	$C_4H_5O_4$	117.0195	-1.7	**31.003**
2-Hydroxy-3-methylbutyric acid	$C_5H_9O_3$	117.0559	-1.7	**19.079**
Taurine	$C_2H_6NO_3S$	124.008	-0.8	**27.304**
Pyroglutamate	$C_5H_6NO_3$	128.0355	-1.6	**8.295**
Aspartate	$C_4H_6NO_4$	132.0305	-2.3	**18.919**
3-Hydroxypicolinic acid	$C_6H_4NO_3$	138.0198	-0.7	**40.807**
Glutamine	$C_5H_9N_2O_3$	145.0621	-1.4	**20.826**
Glutamic acid	$C_5H_8NO_4$	146.0460	0.7	**26.925**
2-Hydroxyglutarate	$C_5H_7O_5$	147.0302	-2.0	**21.018**
Xanthine	$C_5H_3N_4O_2$	151.0263	-1.3	**37.65**
Glycerophosphoglycerol	$C_6H_{14}O_8P$	245.0430	-0.8	**18.354**

Glutathione	$C_{10}H_{82}N_3O_6S$	306.0762	2.6	**42.764**
Fatty Acids				
FA 8:0	$C_8H_{15}O_2$	143.1079	0.7	**29.669**
FA 9:0	$C_9H_{17}O_2$	157.1235	-0.6	**29.847**
FA 15:0	$C_{15}H_{29}O_2$	241.2183	4.1	**4.87**
FA 16:1	$C_{16}H_{29}O_2$	253.2171	-0.8	**3.483**
FA 20:3	$C_{20}H_{33}O_2$	305.2483	-1.0	**15.075**
FA 20:2	$C_{20}H_{35}O_2$	307.2638	-1.6	**11.185**
FA 20:1	$C_{20}H_{37}O_2$	309.2795	2.3	**20.186**
FA 20:0	$C_{20}H_{39}O_2$	311.2952	-1.3	**8.804**
FA 22:0	$C_{22}H_{43}O_2$	339.3264	1.5	**10.756**
FA 23:1	$C_{23}H_{43}O_2$	351.3261	2.3	**11.157**
FA 23:0	$C_{23}H_{45}O_2$	353.3420	1.4	**7.575**
FA 24:1	$C_{24}H_{45}O_2$	365.3420	1.4	**21.275**
FA 24:0	$C_{24}H_{47}O_2$	367.3578	1.1	**21.739**
FA 26:3	$C_{26}H_{45}O_2$	389.3422	0.8	**11.355**
FA 26:2	$C_{26}H_{47}O_2$	391.3578	1.0	**17.688**
FA 26:1	$C_{26}H_{49}O_5$	393.3734	1.0	**11.657**
FA 26:0	$C_{26}H_{51}O_2$	395.3889	1.5	**29.87**
Glycerolipids				
DG 24:0/0:0	$C_{27}H_{51}O_5$	455.3760	4.0	**10.533**
Glycerophosphoethanolamines				
PE 18:1/1:0	$C_{24}H_{45}NO_8P$	506.2882	1.2	**11.03**
PE 20:3/1:0	$C_{26}H_{45}NO_8P$	530.2912	-4.5	**21.256**
PE O-34:3 or PE P-34:2	$C_{39}H_{73}NO_7P$	698.5153	3.3	**23.028**
PE O-34:2 or PE P-34:1	$C_{39}H_{75}NO_7P$	700.5272	2.1	**21.527**
PE 34:2	$C_{39}H_{73}NO_8P$	714.5052	3.8	**25.328**
PE 34:1	$C_{39}H_{75}NO_8P$	716.5221	2.1	**21.369**
PE O-36:3 or P-36:2	$C_{41}H_{77}NO_7P$	726.5449	0.8	**15.769**
PE 35:1	$C_{40}H_{77}NO_8P$	730.5368	3.3	**9.588**
PE 36:3	$C_{41}H_{75}NO_8P$	740.5208	3.8	**27.408**
PE 36:2	$C_{41}H_{77}NO_8P$	742.5378	1.9	**18.265**
PE 38:3	$C_{43}H_{79}NO_8P$	768.5574	-3.3	**27.714**
Glycerophosphoglycerols				
PG 18:0/18:1	$C_{42}H_{80}O_{10}P$	775.5482	1.7	**19.923**
PG 18:0/18:0	$C_{42}H_{82}O_{10}P$	777.5651	0.3	**13.591**
PG 38:4	$C_{44}H_{78}O_{10}P$	797.5313	3.1	**6.512**
PG 38:3	$C_{44}H_{80}O_{10}P$	799.5467	3.5	**13.973**
PG 38:2	$C_{44}H_{82}O_{10}P$	801.5634	2.1	**12.159**
PG 42:7	$C_{48}H_{80}O_{10}P$	847.5463	3.8	**9.462**
Ceramides				
Cer d18:16:0	$C_{34}H_{69}NO_3Cl$	574.4962	1.6	**13.104**
Cer m18:1/22:0	$C_{40}H_{79}NO_2Cl$	640.5796	1.4	**7.264**
Cer m18:1/24:1	$C_{42}H_{81}NO_2Cl$	666.5975	2.1	**20.026**
Cer m42:1	$C_{42}H_{83}NO_2Cl$	668.6109	1.3	**16.913**
Cer d18:1/23:0	$C_{41}H_{81}NO_2Cl$	670.5895	2.4	**5.698**
Cer d40:0(2OH)	$C_{40}H_{81}NO_4Cl$	674.5874	-2.1	**16.897**
Cer d42:1	$C_{42}H_{83}NO_3Cl$	684.6068	0.1	**10.001**
Cer d42:0	$C_{42}H_{85}NO_3Cl$	686.6221	0.3	**21.885**
Cer d18:1/25:0	$C_{43}H_{85}NO_3Cl$	698.6223	0.3	**11.719**
Cer d18:1/26:1	$C_{44}H_{85}NO_3Cl$	710.6258	4.9	**11.435**
Cer d18:1/26:0	$C_{44}H_{87}NO_3Cl$	712.6369	1.5	**6.835**
PE - Cer 36:3	$C_{38}H_{73}N_2O_6PCl$	719.4881	2.6	**11.341**
GlcCer d34:1	$C_{40}H_{77}NO_8Cl$	734.5323	2.7	**5.86**
PE-Cer d37:1	$C_{39}H_{79}N_2O_6PCl$	737.5359	1.5	**14.674**
Monoacylglycerophosphates				

PA 32:0	C$_{35}$H$_{68}$O$_8$P	647.4678	3.2	**17.343**
PA 24:2	C$_{37}$H$_{68}$O$_8$P	671.4642	2.2	**17.925**
PA 24:1	C$_{37}$H$_{70}$O$_8$P	673.4814	1.6	**22.269**
PA 36:4	C$_{39}$H$_{68}$O$_8$P	695.4646	1.6	**11.851**
PA 36:3	C$_{39}$H$_{70}$O$_8$P	697.4801	1.9	**12.823**
Cardiolipins				
CL 68:5	C$_{77}$H$_{138}$O$_{17}$P$_2$	698.4716	0.9	**5.183**
CL 70:7	C$_{79}$H$_{138}$O$_{17}$P$_2$	710.4697	1.8	**25.307**
CL 70:6	C$_{79}$H$_{140}$O$_{17}$P$_2$	711.4767	3.0	**20.886**
CL 70:5	C$_{79}$H$_{142}$O$_{17}$P$_2$	712.4837	4.2	**11.261**
CL 72:8	C$_{81}$H$_{140}$O$_{17}$P$_2$	723.4791	0.4	**20.666**
CL 72:7	C$_{81}$H$_{142}$O$_{17}$P$_2$	724.4841	3.6	**26.85**
CL 72:6	C$_{81}$H$_{144}$O$_{17}$P$_2$	725.4941	0.6	**25.978**
CL 74:10	C$_{83}$H$_{140}$O$_{17}$P$_2$	735.4779	1.2	**13.261**
CL 74:9	C$_{83}$H$_{142}$O$_{17}$P$_2$	736.4852	2.0	**22.139**
CL 74:8	C$_{83}$H$_{144}$O$_{17}$P$_2$	737.4921	3.3	**22.478**
CL 74:7	C$_{83}$H$_{146}$O$_{17}$P$_2$	738.5015	1.1	**18.876**
CL 76:10	C$_{85}$H$_{144}$O$_{17}$P$_2$	749.4924	2.8	**19.881**
CL 76:9	C$_{85}$H$_{146}$O$_{17}$P$_2$	750.5045	2.9	**15.033**
CL 76:8	C$_{85}$H$_{148}$O$_{17}$P$_2$	751.5086	2.0	**14.259**
CL 76:7	C$_{85}$H$_{150}$O$_{17}$P$_2$	752.5161	2.5	**13.432**
CL 36:4	C$_{45}$H$_{82}$O$_{15}$P$_2$Cl	959.4823	2.4	**2.809**
Glycerophosphoinositols				
LysoPI (16:0/0:0)	C$_{25}$H$_{48}$O$_{12}$P	571.2899	1.8	**4.408**
PI (32:1)	C$_{41}$H$_{76}$O$_{13}$P	807.5016	1.6	**22.334**
PI (32:0)	C$_{41}$H$_{78}$O$_{13}$P	809.5141	5.6	**25.352**
PI (34:2)	C$_{43}$H$_{78}$O$_{13}$P	833.5166	2.4	**28.065**
PI (34:1)	C$_{43}$H$_{80}$O$_{13}$P	835.5321	2.5	**25.546**
PI (O-23:0)	C$_{42}$H$_{83}$O$_{12}$PCl	845.5318	0.2	**7.793**
PI (25:1)	C$_{44}$H$_{82}$O$_{13}$P	849.5519	-2.4	**21.476**
PI (36:4)	C$_{45}$H$_{78}$O$_{13}$P	857.5172	1.6	**2.918**
PI (36:3)	C$_{45}$H$_{80}$O$_{13}$P	859.5347	-0.6	**31.721**
PI (36:2)	C$_{45}$H$_{82}$O$_{13}$P	861.5486	1.5	**45.539**
PI (36:1)	C$_{45}$H$_{84}$O$_{13}$P	863.5655	2.8	**25.679**
PI (37:3)	C$_{46}$H$_{82}$O$_{13}$P	873.5506	-0.8	**17.932**
PI (38:6)	C$_{47}$H$_{78}$O$_{13}$P	881.5196	1.1	**20.554**
PI (38:3)	C$_{47}$H$_{84}$O$_{13}$P	887.5653	-0.2	**18.707**
PI (40:6)	C$_{49}$H$_{82}$O$_{13}$P	909.5472	-3.0	**9.853**
PI (39:4)	C$_{48}$H$_{85}$O$_{13}$PCl	935.5441	2.0	**20.006**
C13 PI (40:7)	C$_{49}$H$_{81}$O$_{13}$PCl	943.5110	0.1	**9.499**
Glycerophosphoserines				
PS P-34:1	C$_{40}$H$_{75}$NO$_9$P	744.5177	1.1	**4.274**
PS 16:0/18:1	C$_{40}$H$_{75}$NO$_{10}$P	760.5149	2.0	**18.59**
PS P-36:2 or PS O-36:3	C$_{42}$H$_{77}$NO$_9$P	770.5324	2.2	**14.362**
PS O-36:2 or PS P-36:1	C$_{42}$H$_{79}$NO$_9$P	772.5490	1.0	**4.287**
PS 36:3	C$_{42}$H$_{75}$NO$_{10}$P	784.5133	0.1	**28.208**
PS 36:2	C$_{42}$H$_{77}$NO$_{10}$P	786.5279	1.5	**34.307**
PS 18:0/18:1	C$_{42}$H$_{79}$NO$_{10}$P	788.5466	-2.4	**17.526**
PS O-38:4 or P-38:3	C$_{44}$H$_{79}$NO$_9$P	796.5467	3.9	**4.253**
PS 38:3	C$_{44}$H$_{79}$NO$_{10}$P	812.5437	1.2	**31.901**
PS 38:2	C$_{44}$H$_{81}$NO$_{10}$P	814.5577	3.3	**30.261**
PS 38:1	C$_{44}$H$_{83}$O$_{10}$NP	816.5745	1.8	**23.544**
PS 40:6	C$_{46}$H$_{77}$O$_{10}$NP	834.5271	2.4	**13.286**
PS 40:2	C$_{46}$H$_{85}$O$_{10}$NP	842.5906	1.3	**17.723**
PS 40:1	C$_{46}$H$_{87}$O$_{10}$NP	844.6056	2.0	**21.329**
PS 42:3	C$_{48}$H$_{87}$O$_{10}$NP	868.6029	-5.1	**15.417**

PS 42:2	$C_{48}H_{89}O_{10}NP$	870.6220	-1.1	**17.786**
PS 42:1	$C_{48}H_{91}O_{10}NP$	872.6369	-1.9	**20.275**

Table 9. Low FABP4 – human data 118 *m/z* values

For our next step of analysis, we decided to conduct DESI-MS imaging on *in vivo* tumor tissues from one of our experiments. The two groups that we selected were- Control siRNA and FABP4 siRNA. The metabolite profiles of these tissues would be a direct result of the changes in FABP4 expression and hence is crucial to understand how knocking down FABP4 can affect the metabolomics of cancer cells. The primary results from these analyses are presented in Figure 28 and the detailed analysis is presented in Table 10 and 11. There were 125 metabolites that were unique to the control siRNA group while 59 metabolites were only present in the FABP4 siRNA group. Similar to the patient analysis, we noticed more fatty acids and glycerolipids in control siRNA (i.e. high FABP4 group) than FABP4 siRNA group (i.e. Low FABP4 group). There was an enrichment of unsaturated and oxidated fatty acids and lysophospholipids species in the control siRNA group. Interestingly we did not see any fatty acid in FABP4 siRNA treated group. There were 50 metabolites that were common between mice and human data when high FABP4 was considered while 26 species were found to be common in mice and human samples when low FABP4 data was considered (Table 12 and 13).

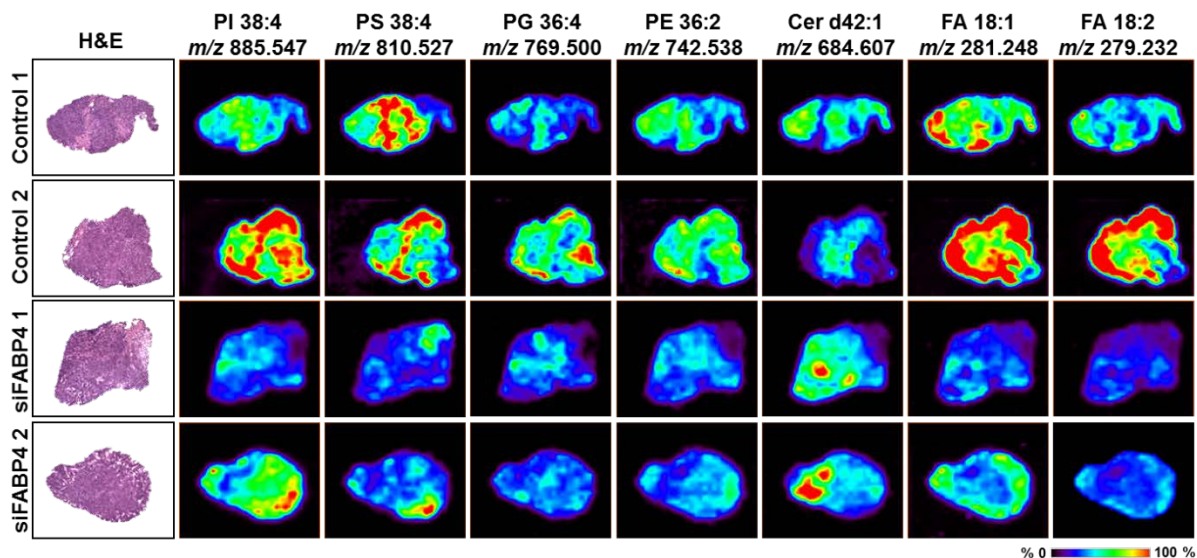**Figure 28** DESI-MS imaging pictures of *in vivo* tumor tissues. Representative pictures show metabolites like glycerophosphoinositols (PI), glycerophosphoserines (PS), glycerophosphoethanolamines (PE), glycerophosphoglycerols (PG) and fatty acids (FA) are suppressed after FABP4 is knocked down with FABP4 siRNA. On the other hand, ceramides are present in more abundance in FABP4 siRNA group compared to the control group.

MICE SAMPLES - CONTROL - HIGH FABP4 EXPRESSION				
Attribution	**Molecular Formula**	**Detected _m/z_**	**Mass error (ppm)**	**SAM Score**
Metabolites				
Uracil	$C_4H_3O_2N_2$	111.0199	0.9	**-7.573**
Taurine	$C_2H_6NO_3S$	124.0073	0.8	**-5.756**
Xanthine	$C_5H_3O_2N_4$	151.0260	-0.7	**-6.716**
Ascorbic acid	$C_6H_7O_6$	175.0245	-1.7	**-2.442**
Citrate	$C_6H_7O_7$	191.0193	-2.1	**-9.995**
Lauric Acid	$C_{12}H_{23}O_2$	199.1699	-2.5	**-10.98**
Glycerophosphoethanolamine	$C_5H_{13}NO_6P$	214.0481	-2.3	**-12.602**
Glucose	$C_6H_{12}O_6Cl$	215.0323	-2.3	**-4.518**
Norselic acid A	$C_{29}H_{39}O_2$	451.2859	-1.1	**-11.045**
Fatty Acids				
FA 8:0	$C_8H_{15}O_2$	143.1076	-1.4	**-10.212**
FA 14:0	$C_{14}H_{27}O_2$	227.2011	-2.6	**-15.768**
FA 15:0	$C_{15}H_{29}O_2$	241.2166	-2.9	**-13.172**
FA 16:2	$C_{16}H_{27}O_2$	251.2008	-3.6	**-9.152**
FA 16:1	$C_{16}H_{29}O_2$	253.2167	-2.4	**-16.69**
FA 16:0	$C_{16}H_{31}O_2$	255.2324	-2.4	**-22.387**
FA 18:3	$C_{18}H_{29}O_2$	277.2167	-2.2	**-14.723**
FA 18:2	$C_{18}H_{31}O_2$	279.2324	-2.1	**-22.826**
FA 18:1	$C_{18}H_{33}O_2$	281.2480	-2.1	**-22.745**
FA 18:0	$C_{18}H_{35}O_2$	283.2636	-2.1	**-21.869**
FA hydroxy 18:2	$C_{18}H_{31}O_3$	295.2271	-2.7	**-8.968**
FA 19:1	$C_{19}H_{35}O_2$	295.2635	-2.7	**-19.208**
FA 19:0	$C_{19}H_{37}O_2$	297.2792	-2.4	**-16.768**
FA 20:5	$C_{20}H_{29}O_2$	301.2165	2.7	**-7.552**
FA 20:4	$C_{20}H_{31}O_2$	303.2322	2.6	**-22.184**
FA 20:3	$C_{20}H_{33}O_2$	305.2477	2.9	**-20.094**
FA 20:2	$C_{20}H_{35}O_2$	307.2634	2.9	**-21.457**
FA 20:1	$C_{20}H_{37}O_2$	309.2791	2.6	**-21.247**
FA 20:0	$C_{20}H_{39}O_2$	311.2946	3.2	**-15.449**
FA 18:2	$C_{18}H_{32}O_2Cl$	315.2087	2.9	**-6.647**
FA 18:1	$C_{18}H_{34}O_2Cl$	317.2245	2.5	**-6.058**
FA hydroxy 20:4	$C_{20}H_{31}O_3$	319.2273	1.9	**-6.266**
FA 22:6	$C_{22}H_{31}O_2$	327.2321	2.8	**-16.919**
FA 22:5	$C_{22}H_{33}O_2$	329.2477	2.7	**-17.188**
FA 22:4	$C_{22}H_{35}O_2$	331.2639	1.2	**-20.922**
FA 22:3	$C_{22}H_{37}O_2$	333.279	2.7	**-17.56**
FA 22:2	$C_{22}H_{39}O_2$	335.2952	1.2	**-18.522**
FA 22:1	$C_{22}H_{41}O_2$	337.3102	3.0	**-15.492**
FA 20:4	$C_{20}H_{32}O_2Cl$	339.2088	2.4	**-6.08**
FA 22:0	$C_{22}H_{43}O_2$	339.3258	3.2	**-9.48**
FA 24:6	$C_{24}H_{35}O_2$	355.2634	2.5	**-16.981**
FA 24:5	$C_{24}H_{37}O_2$	357.2789	2.8	**-16.732**
FA 24:4	$C_{24}H_{39}O_2$	359.2947	2.5	**-21.34**
FA 24:3	$C_{24}H_{41}O_2$	361.3103	2.5	**-17.218**
FA 24:2	$C_{24}H_{43}O_2$	363.3262	1.9	**-17.659**
FA 24:1	$C_{24}H_{45}O_2$	365.3416	2.5	**-15.144**
FA 22:4	$C_{22}H_{36}O_2Cl$	367.2421	-3.3	**-7.137**

FA 24:0	$C_{24}H_{47}O_2$	367.3578	1.1	**-6.06**
FA 25:1	$C_{25}H_{47}O_2$	379.3573	2.4	**-5.221**
FA methyl 24:0	$C_{25}H_{49}O_2$	381.3731	1.8	**-7.862**
FA 26:5	$C_{26}H_{41}O_2$	385.3105	1.8	**-16.964**
FA 26:4	$C_{26}H_{43}O_2$	387.3260	2.3	**-20.89**
FA 26:3	$C_{26}H_{45}O_2$	389.3416	2.3	**-16.232**
FA 26:2	$C_{26}H_{47}O_2$	391.3573	2.3	**-17.552**
FA 26:1	$C_{26}H_{49}O_2$	393.3734	1.0	**-12.345**
FA 28:2	$C_{26}H_{51}O_2$	395.3884	2.8	**-14.191**
FA 26:0	$C_{26}H_{51}O_2$	395.3885	2.5	**-6.23**
Glycerolipids				
MG 18:0/0:0	$C_{21}H_{40}O_4Cl$	391.2610	2.8	**-11.384**
DG 36:3/0:0	$C_{39}H_{70}O_5Cl$	653.4908	1.4	**-3.08**
DG 36:2/0:0	$C_{39}H_{72}O_5Cl$	655.5075	-0.2	**-2.453**
Glycerophosphoethanolamines				
LysoPE 16:0	$C_{21}H_{43}NO_6P$	436.2821	2.8	**-10.52**
LysoPE 18:0	$C_{23}H_{47}NO_7P$	480.3084	2.5	**-13.315**
PE 34:2	$C_{39}H_{73}NO_8P$	714.5062	2.4	**-6.228**
PE P-18:0/18:4	$C_{41}H_{73}NO_7P$	722.5111	2.6	**-18.191**
PE O-36:3 or P-36:2	$C_{41}H_{77}NO_7P$	726.5417	-3.6	**-5.228**
PE 36:3	$C_{41}H_{75}NO_8P$	740.5217	2.6	**-9.691**
PE 36:2	$C_{41}H_{77}NO_8P$	742.5372	2.7	**-14.611**
PE 36:1	$C_{41}H_{79}NO_8P$	744.552	3.9	**-10.896**
PE O-38:5 or PE P-38:4	$C_{43}H_{77}NO_7P$	750.5423	2.7	**-22.396**
PE 38:5	$C_{43}H_{75}NO_8P$	764.5217	2.5	**-11.709**
PE 38:4	$C_{43}H_{77}NO_8P$	766.5374	2.3	**-24.932**
PE 40:6	$C_{45}H_{77}NO_8P$	790.5403	-1.4	**-15.82**
PE 40:5	$C_{45}H_{79}NO_8P$	792.5550	-0.1	**-6.361**
PE 40:4	$C_{45}H_{81}NO_8P$	794.5707	-0.3	**-18.501**
Glycerophosphoglycerols				
LysoPG 18:2	$C_{24}H_{44}O_9P$	507.2718	2.0	**-8.529**
LysoPG 18:1	$C_{24}H_{46}O_9P$	509.2876	1.8	**-4.018**
LysoPG 22:6	$C_{28}H_{44}O_9P$	555.2720	1.4	**-7.775**
PG 16:0/18:1	$C_{40}H_{76}O_{10}P$	747.5160	2.9	**-8.047**
PG 36:4	$C_{42}H_{74}O_{10}P$	769.5002	3.0	**-12.51**
PG 18:2/18:1	$C_{42}H_{76}O_{10}P$	771.5152	3.9	**-4.627**
PG 18:1/18:1	$C_{42}H_{78}O_{10}P$	773.5316	2.8	**-5.956**
PG 38:2	$C_{44}H_{82}O_{10}P$	801.5639	1.5	**-10.651**
PG 40:8	$C_{46}H_{74}O_{10}P$	817.5004	2.6	**-6.68**
Monoacylglycerophosphates				
PA 32:0	$C_{35}H_{68}O_8P$	647.4639	-2.8	**-5.362**
PA 24:2	$C_{37}H_{68}O_8P$	671.4641	2.4	**-5.662**
PA 36:4	$C_{39}H_{68}O_8P$	695.4643	2.0	**-8.407**
PA 36:3	$C_{39}H_{70}O_8P$	697.4804	1.4	**-9.11**
PA 36:2	$C_{39}H_{72}O_8P$	699.4948	3.1	**-6.552**
Cardiolipins				
CL 72:8	$C_{81}H_{140}O_{17}P_2$	723.4766	-3.0	**-7.731**
CL 72:7	$C_{81}H_{142}O_{17}P_2$	724.4834	4.6	**-8.549**
CL 72:4	$C_{81}H_{148}O_{17}P_2$	727.5070	4.3	**-4.471**
CL 74:10	$C_{83}H_{140}O_{17}P_2$	735.4758	4.1	**-6.673**
CL 74:9	$C_{83}H_{142}O_{17}P_2$	736.4847	2.7	**-8.388**

CL 74:8	$C_{83}H_{144}O_{17}P_2$	737.4922	3.1	**-16.348**
CL 74:7	$C_{83}H_{146}O_{17}P_2$	738.5022	0.1	**-18.066**
CL 74:6	$C_{83}H_{148}O_{17}P_2$	739.5074	3.7	**-16.188**
CL 79:10	$C_{85}H_{144}O_{17}P_2$	749.4924	2.8	**-8.087**
CL 79:9	$C_{85}H_{146}O_{17}P_2$	750.5026	-0.4	**-5.903**
CL 79:8	$C_{85}H_{148}O_{17}P_2$	751.5077	3.2	**-9.615**
CL 79:7	$C_{85}H_{150}O_{17}P_2$	752.5180	0.1	**-5.77**
Glycerophosphoinositols				
LysoPI 18:0	$C_{27}H_{52}O_{12}P$	599.3189	2.2	**-13.656**
LysoPI 20:4	$C_{29}H_{48}O_{12}P$	619.2868	3.4	**-7.542**
PI 36:4	$C_{45}H_{78}O_{13}P$	857.5163	2.7	**-12.731**
PI 36:3	$C_{45}H_{80}O_{13}P$	859.5312	3.5	**-8.368**
PI 36:2	$C_{45}H_{82}O_{13}P$	861.5475	2.8	**-9.857**
PI 37:4	$C_{46}H_{80}O_{13}P$	871.5332	1.1	**-7.472**
PI 38:5	$C_{47}H_{80}O_{13}P$	883.5321	2.4	**-10.395**
PI 38:4	$C_{47}H_{82}O_{13}P$	885.5474	2.8	**-17.953**
PI 38:3	$C_{47}H_{84}O_{13}P$	887.5653	-0.2	**-13.431**
PI 39:4	$C_{48}H_{84}O_{13}P$	899.5629	2.9	**-8.627**
PI 40:6	$C_{49}H_{82}O_{13}P$	909.5480	-2.1	**-10.136**
PI 40:5	$C_{49}H_{84}O_{13}P$	911.5627	-3.1	**-11.638**
PI 40:4	$C_{49}H_{86}O_{13}P$	913.5783	3.2	**-19.748**
Glycerophosphoserines				
PS 36:4	$C_{42}H_{73}NO_{10}P$	782.4961	2.2	**-6.987**
PS 36:3	$C_{42}H_{75}NO_{10}P$	784.5119	1.9	**-4.53**
PS 36:2	$C_{42}H_{77}NO_{10}P$	786.5270	2.7	**-13.616**
PS 18:0/18:1	$C_{42}H_{79}NO_{10}P$	788.5429	2.3	**-10.371**
PS 38:4	$C_{44}H_{77}O_{10}NP$	810.5269	2.7	**-21.491**
PS 38:3	$C_{44}H_{79}NO_{10}P$	812.5416	3.8	**-12.988**
PS 38:2	$C_{44}H_{81}NO_{10}P$	814.5577	3.3	**-8.516**
PS 39:4	$C_{45}H_{79}NO_{10}P$	824.5432	1.8	**-9.394**
PS 39:3	$C_{45}H_{81}NO_{10}P$	826.5628	-2.9	**-4.376**
PS 40:6	$C_{46}H_{77}O_{10}NP$	834.5269	2.6	**-12.156**
PS 40:4	$C_{46}H_{81}O_{10}NP$	838.5578	3.1	**-20.635**
PS 22:6/19:0	$C_{46}H_{81}O_{10}NP$	848.5439	0.9	**-10.301**
PS 41:4	$C_{47}H_{83}O_{10}NP$	852.5732	3.3	**-7.748**

Table 10. Mice samples – Control - highFABP4 – 125 *m/z* values

MICE SAMPLES – siFABP4 - LOW FABP4 EXPRESSION				
Attribution	**Molecular Formula**	**Detected *m/z***	**Mass error (ppm)**	**SAM Score**
Metabolites				
Succinate	$C_4H_5O_4$	117.0193	0.6	**14.447**
Glutathione	$C_{10}H_{16}N_3O_6S$	306.0756	-2.9	**2.372**
Methymycin	$C_{25}H_{43}NO_7Cl$	504.2720	-2.8	**3.565**
Glycerolipids				
DG 32:1/0:0	$C_{35}H_{66}O_5Cl$	601.4593	1.8	**5.518**
DG 34:2/0:0	$C_{37}H_{68}O_5Cl$	627.4747	-2.2	**4.196**

110

DG 34:1/0:0	$C_{37}H_{70}O_5Cl$	629.4914	-0.5	**5.772**
DG 36:4/0:0	$C_{39}H_{68}O_5Cl$	651.4748	2.0	**1.339**
DG 36:1/0:0	$C_{39}H_{74}O_5Cl$	657.5229	0.2	**3.089**
DG 38:6/0:0	$C_{41}H_{68}O_5Cl$	675.4751	1.5	**4.087**
DG 38:5/0:0	$C_{41}H_{70}O_5Cl$	677.4903	2.1	**5.15**
DG 38:4/0:0	$C_{41}H_{72}O_5Cl$	679.5057	2.5	**3.376**
DG 40:8/0:0	$C_{43}H_{68}O_5Cl$	699.4742	2.7	**4.638**
DG 40:7/0:0	$C_{43}H_{70}O_5Cl$	701.4901	2.3	**3.189**
DG 40:7/0:0	$C_{43}H_{72}O_5Cl$	703.5063	1.6	**3.147**
Glycerophosphoethanolamines				
PE 18:1	$C_{24}H_{45}NO_8P$	506.2876	2.4	**2.363**
PE 36:2	$C_{41}H_{77}NO_8P$	742.5378	1.9	**2.007**
PE 38:6	$C_{43}H_{73}NO_8P$	762.5040	5.1	**4.499**
PE 37:1	$C_{42}H_{82}NO_8PCl$	794.5444	3.5	**2.379**
PE 38:6	$C_{43}H_{73}NO_8P$	762.5040	5.1	**4.499**
PE 39:2	$C_{44}H_{84}NO_8PCl$	820.5595	4.1	**2.855**
Glycerophosphoglycerol *s*				
PG 22:1	$C_{38}H_{72}O_{10}P$	719.4857	1.7	**2.984**
PG 34:1	$C_{40}H_{72}O_{10}P$	743.4850	2.6	**2.738**
PG P-26:2 or PG O-36:3	$C_{42}H_{78}O_9P$	757.5385	0.5	**8.120**
PG P-36:1 or PG O-36:2	$C_{42}H_{80}O_9P$	759.5526	2.5	**3.118**
PG 18:0/18:1	$C_{42}H_{80}O_{10}P$	775.5482	1.7	**4.647**
PG 18:0/18:0	$C_{42}H_{82}O_{10}P$	777.5651	0.3	**5.331**
PG 38:7	$C_{44}H_{72}O_{10}P$	791.4848	2.7	**2.043**
PG 38:5	$C_{44}H_{76}O_{10}P$	795.5145	4.7	**2.059**
PG 42:9	$C_{48}H_{76}O_{10}P$	843.5146	4.3	**5.532**
Ceramides				
Cer d32:1	$C_{32}H_{63}NO_3Cl$	544.4492	1.8	**2.891**
Cer 34:2	$C_{34}H_{65}NO_3Cl$	570.4644	2.5	**5.907**
Cer 34:1	$C_{34}H_{67}NO_3Cl$	572.4802	2.3	**5.537**
Cer d18/16:0	$C_{34}H_{69}NO_3Cl$	574.4960	1.9	**3.892**
Cer m18:1/22:0	$C_{40}H_{79}NO_2Cl$	640.5790	2.3	**3.255**
Cer d40:2	$C_{40}H_{77}NO_3Cl$	654.5585	1.8	**5.066**
Cer d40:2	$C_{40}H_{77}NO_3Cl$	656.5741	2.0	**2.583**
Cer m42:1	$C_{42}H_{83}NO_2Cl$	668.6107	1.6	**6.489**
Cer d42:1	$C_{42}H_{83}NO_3Cl$	684.6071	0.6	**9.328**
Cer d42:0	$C_{42}H_{85}NO_3Cl$	686.6207	2.3	**6.922**
Cer m44:1	$C_{44}H_{87}NO_2Cl$	696.6413	2.6	**5.418**
Cer d18:1/26:1	$C_{44}H_{85}NO_3Cl$	710.6239	2.3	**3.455**
Cer d18:1/26:0	$C_{44}H_{87}NO_3Cl$	712.6379	0.1	**7.647**
GlcCer d34:2	$C_{50}H_{95}NO_8Cl$	872.6757	-0.6	**4.767**
GlcCer d34:1	$C_{50}H_{97}NO_8Cl$	874.6869	4.5	**6.519**
Cardiolipins				
CL 70:7	$C_{79}H_{138}O_{17}P_2$	710.4689	3.0	**4.073**
CL 70:6	$C_{79}H_{140}O_{17}P_2$	711.4755	4.6	**2.794**
CL 74:10	$C_{83}H_{140}O_{17}P_2$	735.4779	1.2	**0.599**
CL 74:9	$C_{83}H_{142}O_{17}P_2$	736.4852	2.0	**1.58**

Glycerophosphoinositols				
PI O-31:1 or PI P-31:0	$C_{40}H_{77}O_{12}PCl$	815.4856	-1.1	**2.002**
Glycerophosphoserines				
PS P-33:0	$C_{39}H_{75}NO_9P$	732.5171	1.9	**5.018**
PS P-36:2 or PS O-36:3	$C_{42}H_{77}NO_9P$	770.5324	2.2	**3.814**
PS O-36:2 or PS P-36:1	$C_{42}H_{79}NO_9P$	772.5490	1.0	**2.084**
PS 18:0/18:1	$C_{42}H_{79}NO_{10}P$	788.5466	-2.4	**4.731**
PS O-39:0	$C_{45}H_{89}NO_9P$	818.6258	2.7	**1.992**
PS 40:2	$C_{46}H_{85}O_{10}NP$	842.5894	2.7	**2.74**
PS 40:1	$C_{46}H_{87}O_{10}NP$	844.6056	2.0	**3.798**
PS O-41:0	$C_{47}H_{93}O_9NP$	846.6582	1.3	**9.73**
PS 42:2	$C_{48}H_{89}O_{10}NP$	870.6213	2.0	**4.253**
PS 42:1	$C_{48}H_{91}O_{10}NP$	872.6357	3.3	**3.518**

Table 11 Mice samples – siFABP4 - lowFABP4 – 59 *m/z* values

AGREEMENTS WITH HUMAN - CONTROL - HIGH FABP4 EXPRESSION				
Attribution	**Molecular Formula**	**Detected *m/z***	**Mass error (ppm)**	**SAM Score**
Metabolites				
Taurine	$C_2H_6NO_3S$	124.0073	0.8	**-5.756**
Xanthine	$C_5H_3O_2N_4$	151.026	-0.7	**-6.716**
Fatty Acids				
FA 18:3	$C_{18}H_{29}O_2$	277.2167	-2.2	**-14.723**
FA 18:2	$C_{18}H_{31}O_2$	279.2324	-2.1	**-22.826**
FA 18:1	$C_{18}H_{33}O_2$	281.248	-2.1	**-22.745**
FA 18:0	$C_{18}H_{35}O_2$	283.2636	-2.1	**-21.869**
FA 19:0	$C_{19}H_{37}O_2$	297.2792	-2.4	**-16.768**
FA 20:5	$C_{20}H_{29}O_2$	301.2165	2.7	**-7.552**
FA 20:4	$C_{20}H_{31}O_2$	303.2322	2.6	**-22.184**
FA 18:2	$C_{18}H_{32}O_2Cl$	315.2087	2.9	**-6.647**
FA 18:1	$C_{18}H_{34}O_2Cl$	317.2245	2.5	**-6.058**
FA hydroxy 20:4	$C_{20}H_{31}O_3$	319.2273	1.9	**-6.266**
FA 22:6	$C_{22}H_{31}O_2$	327.2321	2.8	**-16.919**
FA 22:5	$C_{22}H_{33}O_2$	329.2477	2.7	**-17.188**
FA 22:4	$C_{22}H_{35}O_2$	331.2639	1.2	**-20.922**
FA 22:3	$C_{22}H_{37}O_2$	333.2790	2.7	**-17.56**
FA 20:4	$C_{20}H_{32}O_2Cl$	339.2088	2.4	**-6.08**
FA 24:5	$C_{24}H_{37}O_2$	357.2789	2.8	**-16.732**
FA 24:4	$C_{24}H_{39}O_2$	359.2947	2.5	**-21.34**
FA 22:4	$C_{22}H_{36}O_2Cl$	367.2421	-3.3	**-7.137**
Glycerolipids				
MG 18:0/0:0	$C_{21}H_{40}O_4Cl$	391.2610	2.8	**-11.384**
DG 36:3/0:0	$C_{39}H_{70}O_5Cl$	653.4908	1.4	**-3.08**
DG 36:2/0:0	$C_{39}H_{72}O_5Cl$	655.5075	-0.2	**-2.453**
Glycerophosphoethanolamines				
LysoPE 16:0	$C_{21}H_{43}NO_6P$	436.2821	2.8	**-10.52**

LysoPE 18:0	$C_{23}H_{47}NO_7P$	480.3084	2.5	**-13.315**
PE P-18:0/18:4	$C_{41}H_{73}NO_7P$	722.5111	2.6	**-18.191**
PE O-38:5 or PE P-38:4	$C_{43}H_{77}NO_7P$	750.5423	2.7	**-22.396**
PE 38:5	$C_{43}H_{75}NO_8P$	764.5217	2.5	**-11.709**
PE 40:5	$C_{45}H_{79}NO_8P$	792.5550	-0.1	**-6.361**
PE 40:4	$C_{45}H_{81}NO_8P$	794.5707	-0.3	**-18.501**
Glycerophosphoglycerols				
LysoPG 18:2	$C_{24}H_{44}O_9P$	507.2718	2.0	**-8.529**
LysoPG 18:1	$C_{24}H_{46}O_9P$	509.2876	1.8	**-4.018**
LysoPG 22:6	$C_{28}H_{44}O_9P$	555.2720	1.4	**-7.775**
PG 16:0/18:1	$C_{40}H_{76}O_{10}P$	747.5160	2.9	**-8.047**
PG 36:4	$C_{42}H_{74}O_{10}P$	769.5002	3.0	**-12.51**
PG 18:2/18:1	$C_{42}H_{76}O_{10}P$	771.5152	3.9	**-4.627**
PG 18:1/18:1	$C_{42}H_{78}O_{10}P$	773.5316	2.8	**-5.956**
PG 40:8	$C_{46}H_{74}O_{10}P$	817.5004	2.6	**-6.68**
Cardiolipins				
CL 72:4	$C_{81}H_{148}O_{17}P_2$	727.5070	4.3	**-4.471**
Glycerophosphoinositols				
LysoPI 18:0	$C_{27}H_{52}O_{12}P$	599.3189	2.2	**-13.656**
LysoPI 20:4	$C_{29}H_{48}O_{12}P$	619.2868	3.4	**-7.542**
PI 37:4	$C_{46}H_{80}O_{13}P$	871.5332	1.1	**-7.472**
PI 38:5	$C_{47}H_{80}O_{13}P$	883.5321	2.4	**-10.395**
PI 38:4	$C_{47}H_{82}O_{13}P$	885.5474	2.8	**-17.953**
PI 38:3	$C_{47}H_{84}O_{13}P$	887.5653	-0.2	**-13.431**
PI 40:6	$C_{49}H_{82}O_{13}P$	909.5480	-2.1	**-10.136**
PI 40:4	$C_{49}H_{86}O_{13}P$	913.5783	3.2	**-19.748**
Glycerophosphoserines				
PS 36:3	$C_{42}H_{75}NO_{10}P$	784.5119	1.9	**-4.53**
PS 38:4	$C_{44}H_{77}O_{10}NP$	810.5269	2.7	**-21.491**
PS 39:4	$C_{45}H_{79}NO_{10}P$	824.5432	1.8	**-9.394**

Table 12. Same species for human and mice samples - highFABP4 – 50 *m/z* values

AGREEMENTS WITH HUMAN - siFABP4 - LOW FABP4 EXPRESSION				
Attribution	**Molecular Formula**	**Detected *m/z***	**Mass error (ppm)**	**SAM Score**
Metabolites				
Succinate	$C_4H_5O_4$	117.0193	0.6	**14.447**
Glutathione	$C_{10}H_{16}N_3O_6S$	306.0756	-2.9	**2.372**
Glycerophosphoethanolamines				
PE 18:1	$C_{24}H_{45}NO_8P$	506.2876	2.4	**2.363**
PE 36:2	$C_{41}H_{77}NO_8P$	742.5378	1.9	**2.007**
PE 38:6	$C_{43}H_{73}NO_8P$	762.5040	5.1	**4.499**
Glycerophosphoglycerols				
PG 18:0/18:1	$C_{42}H_{80}O_{10}P$	775.5482	1.7	**4.647**
PG 18:0/18:0	$C_{42}H_{82}O_{10}P$	777.5651	0.3	**5.331**
PG 42:7	$C_{48}H_{80}O_{10}P$	847.5431	7.6	**6.468**

Ceramides				
Cer d18/16:0	$C_{34}H_{69}NO_3Cl$	574.4960	1.9	**3.892**
Cer m18:1/22:0	$C_{40}H_{79}NO_2Cl$	640.5790	2.3	**3.255**
Cer m42:1	$C_{42}H_{83}NO_2Cl$	668.6107	1.6	**6.489**
Cer d42:1	$C_{42}H_{83}NO_3Cl$	684.6071	0.6	**9.328**
Cer d42:0	$C_{42}H_{85}NO_3Cl$	686.6207	2.3	**6.922**
Cer d18:1/26:1	$C_{44}H_{85}NO_3Cl$	710.6239	2.3	**3.455**
Cer d18:1/26:0	$C_{44}H_{87}NO_3Cl$	712.6379	0.1	**7.647**
Cardiolipins				
CL 70:7	$C_{79}H_{138}O_{17}P_2$	710.4689	3.0	**4.073**
CL 70:6	$C_{79}H_{140}O_{17}P_2$	711.4755	4.6	**2.794**
CL 74:10	$C_{83}H_{140}O_{17}P_2$	735.4779	1.2	**0.599**
CL 74:9	$C_{83}H_{142}O_{17}P_2$	736.4852	2.0	**1.58**
Glycerophosphoserines				
PS P-36:2 or PS O-36:3	$C_{42}H_{77}NO_9P$	770.5324	2.2	**3.814**
PS O-36:2 or PS P-36:1	$C_{42}H_{79}NO_9P$	772.5490	1.0	**2.084**
PS 18:0/18:1	$C_{42}H_{79}NO_{10}P$	788.5466	-2.4	**4.731**
PS 40:2	$C_{46}H_{85}O_{10}NP$	842.5894	2.7	**2.74**
PS 40:1	$C_{46}H_{87}O_{10}NP$	844.6056	2.0	**3.798**
PS 42:2	$C_{48}H_{89}O_{10}NP$	870.6213	2.0	**4.253**
PS 42:1	$C_{48}H_{91}O_{10}NP$	872.6357	3.3	**3.518**

Table 13. Same species for human and mice samples - lowFABP4 – 26 _m/z_ values

Effect of FABP4 expression on overall and progression-free survival

We queried Tothill ovarian cancer patient data set to investigate the association between FABP4 and overall and progression-free survival. The data were available for 2 probesets for FABP4. Using multi-variate analysis, we observed that there was a significant correlation between high FABP4 expression and overall survival (Figure 29 a) and with progression-free survival (Figure 29 b) for both the probe-sets. For the univariate analysis as well, high FABP4 correlated with poor overall (Figure 29 c) and progression-free survival (Figure 29 d).

(a)

Variable	HR	lower .95	upper .95	p-value
Stage (III-IV vs I-II)	5.209	1.275	21.275	0.0215
Age (continuous)	1.022	1.0001	1.044	0.0476
FABP4 (203980_at)	1.071	1.004	1.141	0.0369

Variable	HR	lower .95	upper .95	p-value
Stage (III-IV vs I-II)	5.345	1.313	21.769	0.0193
Age (continuous)	1.021	0.9997	1.043	0.05347
FABP4 (235978_at)	1.281	1.075	1.526	0.00564

(b)

Variable	HR	lower .95	upper .95	p-value
Stage (III-IV vs I-II)	4.11	1.668	10.127	0.00212
FABP4 (203980_at)	1.098	1.042	1.157	0.00047

Variable	HR	lower .95	upper .95	p-value
Stage (III-IV vs I-II)	4.374	1.782	10.736	0.00127
FABP4 (235978_at)	1.329	1.147	1.539	0.00015

(c)

Variable	HR	lower .95	upper .95	p-value
Stage (III-IV vs I-II)	6.023	1.483	24.463	0.01205
Grade (3 vs 1-2)	1.199	0.788	1.824	0.39762
Age (continuous)	1.022	1.001	1.043	0.04430
FABP4 (203980_at)	1.085	1.019	1.156	0.01146
FABP4 (235978_at)	1.320	1.106	1.574	0.00203

(d)

Variable	HR	lower .95	upper .95	p-value
Stage (III-IV vs I-II)	4.866	1.988	11.907	0.00053
Grade (3 vs 1-2)	1.078	0.775	1.498	0.65548
Age (continuous)	1.002	0.986	1.018	0.79086
FABP4 (203980_at)	1.120	1.064	1.180	0.00002
FABP4 (235978_at)	1.383	1.196	1.600	0.00001

Figure 29 (a) Multivariate analysis of FABP4 (for two probes) for overall survival using Tothill data set. (b) Multivariate analysis of FABP4 (for two probes) for progression-free survival using Tothill data set (c) Univariate analysis for FABP4 using Tothill data set for overall survival (d) Univariate analysis for FABP4 using Tothill data set for progression-free survivalFABP4 in uterine cancer

Chapter 8: FABP4 as a predictor of residual disease in uterine cancer

Having established the importance of FABP4 in residual disease of ovarian cancer, we decided to investigate if it can be used as a predictor for other cancer types as well. We selected uterine cancer since the standard of care for this cancer is similar to that of ovarian cancer (Primary debulking surgery followed by adjuvant chemotherapy). We initially checked FABP4 expression in uterine cancer cell lines and noticed that the expression is considerably low (Figure 30 a). However, sometimes tumor micro-environment can induce certain gene expressions. We hence decided to check expression of FABP4 in tumor samples collected from uterine cancer mouse models. We checked the expression on tumor collected from SKUT2, HEC1a, ISHIKAWA and SPEC2 mouse models and compared it to the HeyA8 MDR mouse model (Positive control) staining. We noticed that uterine tumor tissues do express FABP4 *in vivo* (Figure 30 b). The next step was to investigate patient data base and explore the association between FABP4 expression and incidences of residual disease. We analyzed TCGA data and segregated the samples as endometrioid or serous. The samples were then divided into residual disease (RD) or no residual disease (R0) groups. There was however, no significant correlation between FABP4 expression and residual disease incidences in both of these groups (Figure 30 c and d). We thus concluded that relation between FABP4 and RD is unique for ovarian cancer.
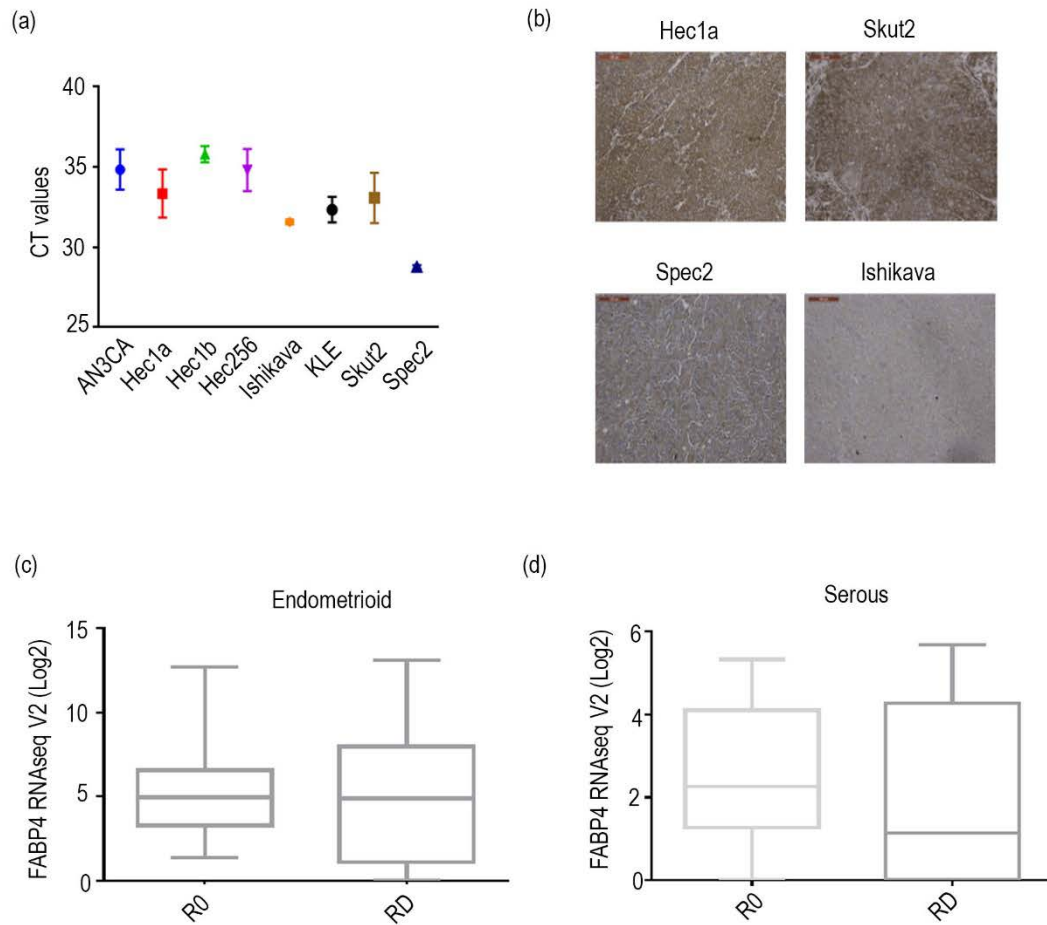
Figure 30 (a) Expression of FABP4 in a uterine cancer cell line panel. (b) Immunohistochemical staining showing expression of FABP4 in *in vivo* mouse models of uterine cancer. (c, d) Relation between FABP4 and residual disease status in (c) endometrioid and (d) serous subtypes of uterine cancer, R0- No residual disease, RD- Residual disease (TCGA patient database).

Chapter 9: Therapeutic options to target FABP4 in patients

Our results thus far recognize FABP4 as a promising therapeutic target for ovarian cancer patients. Our next step, therefore, was to search for clinically approved drugs that can target FABP4. In a recent study, tamoxifen, a selective estrogen modulator, has been shown to inhibit FABP4 in macrophages [92]. We decided to check if it can suppress FABP4 in ovarian cancer cells. We used physiologically relevant concentrations of tamoxifen and checked its effects on FABP4 expression. We treated HeyA8 MDR cells with various concentrations of tamoxifen, for different time intervals. At a concentration of 3.5 uM, after 24 hours, tamoxifen inhibited FABP4 expression by more than 50% ($p<0.0.5$) (Figure 31 a). We then decided to check if this inhibition was functionally relevant. We first conducted free fatty acid uptake assay. Since FABP4 plays a key role in uptake and metabolism of fatty acids, this assay reflects if inhibition of FABP4 was sufficient enough to affect its functions. Tamoxifen inhibition of FABP4 significantly impaired the ability of cancer cells to uptake free fatty acids as shown in Figure 30 b ($p<0.01$). We also checked if we see any effect on metastasis related pathways. We noticed that inhibition of FABP4 by Tamoxifen suppressed migratory ability by cancer cells significantly $p< 0.05$ (Figure 30 c). Tamoxifen is thus a potential candidate for FABP4 inhibition in ovarian cancer.
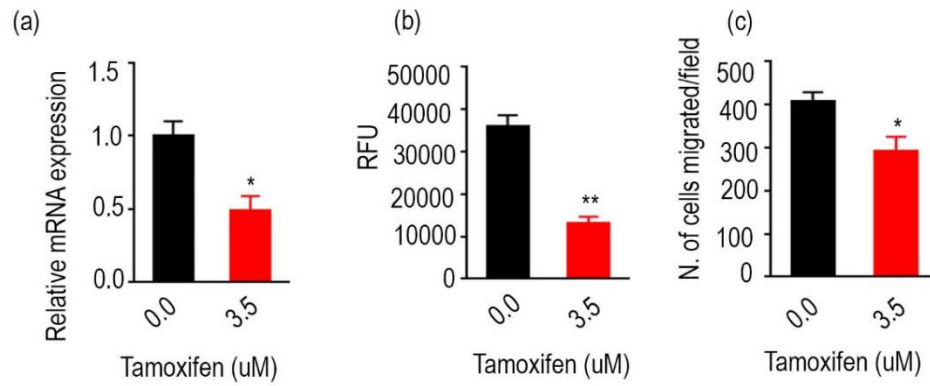
Figure 31 (a) Effect of tamoxifen treatment on the expression of FABP4 in HeyA8 MDR cells. *$p<0.05$. (b) Effect of tamoxifen treatment on the ability of cancer cells to take up free fatty acids (HeyA8 MDR cells). **$p<0.01$. (c) Change in the migratory potential of cancer cells after tamoxifen treatment (HeyA8 MDR cells). *$p<0.05$.

Chapter 10: Discussion

Systematically combining clinical data, experimental models and bioinformatics, we explored the underlying biology of residual disease in ovarian cancer. Using publicly available datasets we have shown that high expression of FABP4 and ADH1B can predict increased likelihood of residual disease in ovarian cancer patients. The results were also validated by additional patient cohorts taken from two cancer institutes. If confirmed by additional external validations, this study has potential applications in the clinical settings for personalized treatment approaches. If a patient has high likelihood of having residual disease after the debulking surgery, it would be more beneficial to give her neoadjuvant chemotherapy first. It might increase chances of achieving complete cytoreduction at interval debulking thus improving patient prognosis. Avoiding unnecessary surgeries will also reduce the surgery-associated morbidities in patients. Thus, it is crucial to personalize the treatment options (NACT or PDS) based the residual disease predictions for a given patient.

Previous studies have employed CT scans or CA-125 levels for prediction of suboptimal cytoreduction, but they do have certain limitations [20, 29, 30]. Most of the studies used old classifications of 'optimal' and 'suboptimal' cytoreduction. Recent studies have established the importance of R0 resection making the old classification system inadequate to assess prognostic impact. Thus, some of the earlier studies may not be valid any longer since the markers were not particularly used to study R0/RD status. Many CT scan based studies also lack external validity [13, 34] .

Recent studies have explored the gene signatures of residual tumors of ovarian cancer. A study of 213 ovarian cancer patients showed that tumor samples simultaneously overexpressing GLUT-1 and Ki-67 were more likely to get suboptimally cytoreduced than other tumor samples [93]. Another study with 44 advanced serous ovarian cancers identified 120 genes that were differentially expressed between optimally and suboptimally cytoreduced tumors. A predictive model consisting of 32 genes was able to predict optimal or suboptimal debulking with 72.7% accuracy [94]. Several of the genes found to be predictors of suboptimal disease were linked with increased metastasis in ovarian cancer. The study however did not validate in internal cross-validation. Other genes including IGF1R, VEGF-C, SRA1, TGFβ1, CAR3/7, CAR4/7, RNAse III Dicer have been found to be associated with suboptimal debulking of ovarian cancer [95-100]. Certain proteins such as cyclin E, c-erb-B-2, Twist, p63α, ERCC1, AEG-1, P130cas have also been found to be correlated with increased likelihood of suboptimal cytoreduction [101-107]. Immunoprofiling of 232 ovarian tumors have shown increased number of T-regulatory cells (CD4+CD25+ T cells) in suboptimally resected patient samples compared to the samples from optimally debulked patients [108]. Epigenetic modifications have also been linked with surgical outcome. HOXA11 methylation levels have been found to be significantly different between <2cm residual disease and > 2cm residual disease [109]. A large study based on meta-analysis of 1525 samples of primary, late stage high-grade serous ovarian tumors has revealed a gene signature that is differentially expressed in optimally suboptimally cytoreduced tumors. Validations studies using qRT-PCR and immunohistochemical staining have revealed POSTN, CXCL14, phosphorylated

Smad2/3 as independent predictors of debulking status. The model based on these three proteins was able to classify high and low risk samples with 92.8% accuracy. Pathways analysis of this gene signature revealed activation of TGF-β1/Smad signaling pathway, RTK/Ras/MAPK/Erg-1, AMPK/Erg-1 and Hedgehog/Gli signaling in tumors taken from suboptimally cytoreduced patients [110]. Although these studies have several limitations; such as small number of samples, lack of independent validation, inclusion of heterogeneous tumor types, grades and varying definitions of optimal, suboptimal instead of R0, RD cases etc.; they indicate that tumor biology plays a crucial role in determining the surgical outcome of ovarian cancer patients.

In the light of the limitations of other studies, our study to identify molecular predictors is unique for the following reasons: 1) We used R0 and RD as our clinical endpoints. Various studies have shown that there is a larger difference in overall survival between R0 and RD patients compared to the difference between optimal and suboprimal surgeries. Moreover, the definition of R0 is consistent across all the centers contrary to the definitions of optimal cytoreduction which vary. 2) The assay if approved will be used for patients who had not received any prior chemotherapy. Hence, we only focused on primary tumors of high grade serous ovarian cancer from patients who had not received any neoadjuvant chemotherapy or surgery. 3) To avoid batch effects, we used two different datasets, confirmed the results in a separate patient dataset and validated it experimentally using another separate patient cohort. 4) To make the test clinically feasible, we restricted the selection to a small number of predictors. 5) The odds ratio for prediction by CA-125 levels are lower than our prediction of residual disease using FABP4 expression [24, 111].

However, compared to the clinical data such as CT-scans, CA-125 levels or laparoscopic measurements; information about molecular predictors would be less readily available to the surgeons. Hence, predictions using molecular biomarkers would probably be combined with laparoscopic assessment to predict RD status of a patient.

Little is known about the biology of residual disease in ovarian cancer. This study not only delineates the downstream signaling of FABP4 leading to residual disease, it also investigates the regulation of FABP4. Hypoxia has been known to promote tumor progression however, its exact role in the pattern of metastasis was not known. We show that hypoxia suppresses miR-409-3p thus removing FABP4 inhibition which leads to FABP4 upregulation ultimately leading to residual disease.

miR-409-3p has also been studied in various types of cancers such as gastric, colorectal, breast, prostate, glioblastoma, fibrosarcoma and osteosarcoma. In glioblastoma, miR-409-3p has been shown to regulate O6-methylguanine-DNA methyltransferase (MGMT) [112]. It also suppresses glioma cell proliferation and invasion by targeting HMGN5 [113]. In colon cancer, miR-409-3p can suppress Beclin-1 and thus inhibits chemotherapy induced autophagy and sensitizes the cancer cells to chemotherapy. Its expression is also lower in colorectal cancer tissues compared to the adjacent non-tumor tissues. In addition to Beclin, NLK and GAB1 have been shown to be targets of miR-409-3p [114-116]. In fibrosarcoma cell line HT1080; miR-409-3p suppresses tumor growth, vascularization and metastasis by targeting angiogenesis (ANG) [117]. miR-409-3p has been extensively studied in breast cancer. It has been shown to suppress proliferation, migration and invasion of breast cancer

cell lines and shown to inhibit tumor progression possibly by downregulating its target genes such as AKT and ZEB1 [118, 119]. Patient sample analyses have also shown that its expression is low in tumor tissues compared to normal breast tissue specimens. Moreover, it has also been suggested as a detection and prognostic marker of breast cancer since its plasma levels are found to be lower in cancer patients compared to the normal controls [120, 121]. The importance of miR-409-3p as a tumor suppressor has also been studied in gastric cancer. It is significantly downregulated in gastric cancer cell lines and tumor tissues compared to non-tumorous samples. Moreover, its expression is lower in patients with lymph node metastasis compared to the patients without lymph node metastasis [122]. In gastric cancer, radixin and PHF10 are shown to be the targets of mir-409-3p [122, 123] whereas in osteosarcoma it inhibits metastasis and tumor progression by targeting CTNND1 [124]. In addition, it also acts as a tumor suppressor in lung adenosarcoma and bladder cancer by targeting c-Met [125]. While it acts as a tumor suppressor miRNA in glioblastoma, osteosarcoma, fibrosarcoma, lung, breast, gastric and colon cancers, it is known to promote tumor progression in prostate cancer. Higher expression of miR-409-3p has been observed in prostate cancer cell lines and tissues than the normal controls. It increases expression of EMT and stemness markers in cancer cells and. Delivery of miR-409-3p/5p induced tumors in mice *in vivo*. Conversely inhibition of miR-409-5p led to reduced metastasis and improved survival [126, 127]. The role of miR-409-3p in ovarian cancer has not been studied yet and our study describes its role in regulation of FABP4 and residual disease of ovarian cancer.

FABP4 has been shown to be present in adipocytes, macrophages, endothelial cells as well as in dendritic cells. In these cell types as well, it is known to promote tumor progression by increasing angiogenesis, inflammation or by providing energy from adipocytes to the cancer cells. Our selection of primary tumors for the initial biomarker discovery made sure that the data mainly came from tumor cells than stromal cells. Our *in vitro* studies focused on how changes in FABP4 expression in cancer cells affects their metastatic potential. In our *in vivo* studies as well, we utilized DOPC nanoliposomes which are known to be specifically uptaken by cancer cell. Thus inhibition of tumor progression can be attributed to the inhibition of FABP4 in cancer cells than stromal cells. Further, we used DESI-MS imaging technique to study the metabolic changes associated with FABP4 and we extracted data specifically from cancer cell compartment of the tumor tissues. None of the previous studies used such sophisticated techniques to delineate the spatial information about the functions of FABP4. We here present evidences that FABP4 specifically present in cancer cells can regulate multiple proteins and metabolites to increase infiltrative behavior and metastatic potential of cancer cells. We thus show that FABP4 present in cancer cells is responsible for residual disease while stromal FABP4 might play a secondary role in this pathway.

DESI-MS imaging showed that lipidomic profiles of R0 and RD patients differ significantly. Mice data also revealed that FABP4 manipulation had significant effects on the metabolites present in cancer cells. Higher unsaturation and oxidation of fatty acids and lysophospholipids were observed in higher relative abundance in samples with high FABP4 expression. Studies have suggested that unsaturated fatty acids can

126

activate the beta catenin pathway, downregulate PTEN or increase cancer cell adhesion and thus play a key role in pathways leading to tumor progression by [128-130]. Fatty acid oxidation has been linked with increased metastasis in breast and ovarian cancer models [52, 131]. Lysophospholipids are considered potential biomarkers for ovarian cancer. They have also been known to increase cancer cell migration thus helping tumor progression [132, 133]. High expression of FABP4 can thus regulate various metabolites and protein pathways that can lead to aggressive disease.

Future directions

Our study has shown FABP4 and ADH1B as promising molecular biomarkers for prediction of residual disease. However, in order to for these markers to be included in the clinical settings, the study needs external validation and development of CLIA (Clinical Laboratory Improvement Amendments)-compliant assay to assess FABP4 or ADH1B expression. A prospective trial analyzing FABP4 expression prior to triaging and comparing it with the surgical outcome of patients will be a great step forward in establishing the specificity and sensitivity of these markers. Our study used primary ovarian tumor samples to check FABP4 expression and we showed that expression of FABP4 in omental tissue is drastically different than its levels in ovarian tissues. A comprehensive study analyzing FABP4 expression in various metastatic tissues can further indicate whether similar results can be obtained using metastatic nodules. On a similar note, serum levels of FABP4 and ADH1B can also be compared between R0 and RD patients. If similar results can be obtained using serum samples, the non-invasive approach will make the study more applicable in clinics.

A recent study elucidating the role of stromal cell gene signature in residual disease biology is of particular interest [134]. It will be interesting and informative to study the interaction between FABP4 present in cancer cells and these genes present in stromal cells, and how this interplay might play a role in residual disease occurrence.

Our DESI-MS data reveal many metabolites relevant for residual disease. The data thus lay foundation for future studies which can focus in depth on these metabolites and the pathways they regulate. Understanding the metabolic determinants of ovarian cancer growth and of leaving residual disease will further elucidate underlying mechanisms and open avenues for the development of therapeutic options targeting these moieties.

Therapeutic strategies using siRNA and miRNAs have proven themselves to be attractive treatment options for a variety of diseases. In cancer therapeutics, where there are several undrggable targets, these miRNA and siRNA based options are of particular advantage. However, there are challenges in making them clinical feasible. Mir-34 is one of the very few miRNAs that have entered the clinical trials. Studies of mir-200, miR-192 and mir-630 have proven the potential of miRNA in cancer therapeutics [82, 135, 136]. Several siRNAs therapies including EphA2 siRNA, ELK1 siRNA, EZH2 siRNA have been able to inhibit tumor progression [137, 138]. Few studies have been successful in devising delivery vehicles to carry miRNAs and siRNAs. The DOPC nanoliposomes used in our study have shown promising results in many prior preclinical studies [136-139]. The liposomes are currently being tested in Phase 1 clinical trials for delivery of EphA2 siRNAs (NCT01591356). Our study

utilizing DOPC nanoliposomes encapsulating FABP4 siRNA and miR-409-3p mimic thus provides further evidence that siRNA and miRNA based treatment options have potential as cancer therapeutics, specifically for the management of metastatic disease.

Significance and translational relevance

Residual disease following primary debulking has been associated with poor prognosis of cancer patients. Patients with high risk of residual disease should ideally be treated with neoadjuvant chemotherapy to increase the chances of R0 resection at interval debulking surgery and avoid unnecessary morbidities associated with cytoreductive surgeries. In this study, we developed molecular biomarkers that can predict the likelihood of residual disease in ovarian cancer patients. Use of these biomarkers can help clinicians in triaging patients to personalized treatment option. Patients with high expression of FABP4 and ADH1B can be at high risk of residual disease, hence will be ideal candidates for neoadjuvant chemotherapy instead of unwarranted aggressive primary surgery. This approach will not only increase overall survival but can also improve quality of life of ovarian cancer patients.

Little is known about the underlying biology of residual disease. Our study uses various in *vitro* and *in vivo* techniques to investigate the pathways that lead to residual disease and demonstrates the crucial role FABP4 plays in promoting invasiveness and infiltration of cancer cells. Moreover, ours is the first study to use *in vivo* mouse models to study this clinically observed phenomenon. Since the exact replication of aggressive cytoreduction and assessment of residual disease is not possible in mice; we devised a modified version of a clinically validated method to predict the likelihood

of leaving residual disease in *in vivo* experiments. We hope that this new modified scoring systems proves useful in initiating more *in vivo* experiments to study yet unknown aspects of residual disease pathophysiology.

We also explore the upstream regulatory mechanisms of FABP4 and identified hypoxia as a major tumor micro-environmental factor regulating FABP4. We further show that miR-409-3p directly targets FABP4 and in turn is regulated by hypoxia. We thus provide several lines of evidence that hypoxia-miR-409-3p-FABP4 is the major axis regulating residual disease in ovarian cancer. Downstream of FABP4, we investigated protein and lipid pathways regulated by FABP4. Although studies have focused on the metabolomics of ovarian cancer [56-58]; they don't identify specific tumor compartments where the metabolic changes occur. We thus used DESI-MS imaging technique to get the spatial information of the metabolites. The use of DESI-MS technique was mainly considered in identifying tumor margins in surgical resection or in disease diagnosis [65]. We successfully applied this technique 1) To identify cancer cell-specific metabolomics associated with FABP4 expression in ovarian cancer patients 2) To identify metabolomics changes occurring in the cancer cell compartment after inhibiting FABP4 expression *in vivo*. Identifying the exact location of metabolic changes is crucial, not only in understanding how a gene's functions influence and shape the cancer biology but it will also help in future therapeutic development.

We identify FABP4 and miR-409-3p as promising therapeutic targets in ovarian cancer and using DOPC nanoliposomes containing targeted siRNA and miRNA molecules, we establish their importance in inhibiting tumor progression. We also

130

tested a clinically approved drug to target FABP4. Tamoxifen has mainly been used in the treatment of breast cancer[140].Some clinical trials have used tamoxifen for ovarian cancer treatment, but the results of those trials were mixed[141-143]. However, it is important to note that those patients had advanced stage ovarian cancer and no specific biomarker was used to select patients who would respond to tamoxifen treatment. Our preliminary experiments suggest that tamoxifen can suppress expression and functions of FABP4 and can inhibit tumor progression. Future studies are essential to establish tamoxifen as a part of ovarian cancer management, but our study lays the foundation for repurposing tamoxifen, a clinically approved drug for additional usage and also proposes a biomarker (FABP4) to select patients who will benefit the most with tamoxifen treatment.

Figure 32 gives a summary of results of our study.
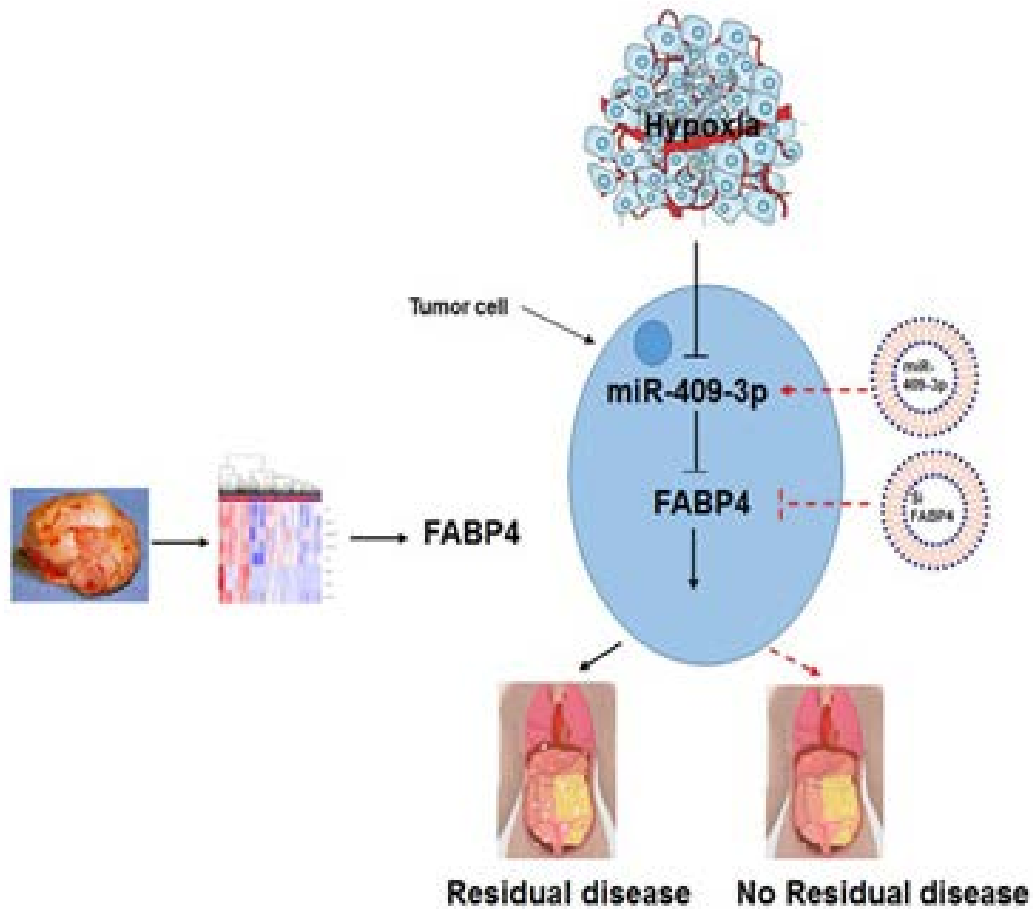
Figure 32 Summary model

We, thus, provide an important conceptual advance in understanding the causal biology of residual disease, a molecular biomarker based method to predict the RD status and new therapeutic avenues for ovarian cancer treatment.

Bibliography

1.   Griffiths, C.T., *Surgical resection of tumor bulk in the primary treatment of ovarian carcinoma.* Natl Cancer Inst Monogr, 1975. **42**: p. 101-4.

2.   Chi, D.S., J.B. Liao, L.F. Leon, E.S. Venkatraman, M.L. Hensley, D. Bhaskaran, and W.J. Hoskins, *Identification of prognostic factors in advanced epithelial ovarian carcinoma.* Gynecol Oncol, 2001. **82**(3): p. 532-7.

3.   Hoskins, W.J., W.P. McGuire, M.F. Brady, H.D. Homesley, W.T. Creasman, M. Berman, H. Ball, and J.S. Berek, *The effect of diameter of largest residual disease on survival after primary cytoreductive surgery in patients with suboptimal residual epithelial ovarian carcinoma.* Am J Obstet Gynecol, 1994. **170**(4): p. 974-9; discussion 979-80.

4.   Aletti, G.D., S.C. Dowdy, B.S. Gostout, M.B. Jones, C.R. Stanhope, T.O. Wilson, K.C. Podratz, and W.A. Cliby, *Aggressive surgical effort and improved survival in advanced-stage ovarian cancer.* Obstet Gynecol, 2006. **107**(1): p. 77-85.

5.   Bookman, M.A., M.F. Brady, W.P. McGuire, P.G. Harper, D.S. Alberts, M. Friedlander, N. Colombo, J.M. Fowler, P.A. Argenta, K. De Geest, D.G. Mutch, R.A. Burger, A.M. Swart, E.L. Trimble, C. Accario-Winslow, and L.M. Roth, *Evaluation of new platinum-based treatment regimens in advanced-stage ovarian cancer: a Phase III Trial of the Gynecologic Cancer Intergroup.* J Clin Oncol, 2009. **27**(9): p. 1419-25.

6.   Bristow, R.E., R.S. Tomacruz, D.K. Armstrong, E.L. Trimble, and F.J. Montz, *Survival effect of maximal cytoreductive surgery for advanced ovarian*

carcinoma during the platinum era: a meta-analysis. J Clin Oncol, 2002. **20**(5): p. 1248-59.

7.   Chang, S.J., M. Hodeib, J. Chang, and R.E. Bristow, *Survival impact of complete cytoreduction to no gross residual disease for advanced-stage ovarian cancer: a meta-analysis.* Gynecol Oncol, 2013. **130**(3): p. 493-8.

8.   Alberts, D.S., P.Y. Liu, E.V. Hannigan, R. O'Toole, S.D. Williams, J.A. Young, E.W. Franklin, D.L. Clarke-Pearson, V.K. Malviya, and B. DuBeshter, *Intraperitoneal cisplatin plus intravenous cyclophosphamide versus intravenous cisplatin plus intravenous cyclophosphamide for stage III ovarian cancer.* N Engl J Med, 1996. **335**(26): p. 1950-5.

9.   Armstrong, D.K., B. Bundy, L. Wenzel, H.Q. Huang, R. Baergen, S. Lele, L.J. Copeland, J.L. Walker, R.A. Burger, and G. Gynecologic Oncology, *Intraperitoneal cisplatin and paclitaxel in ovarian cancer.* N Engl J Med, 2006. **354**(1): p. 34-43.

10.   Chang, S.J., R.E. Bristow, and H.S. Ryu, *Impact of complete cytoreduction leaving no gross residual disease associated with radical cytoreductive surgical procedures on survival in advanced ovarian cancer.* Ann Surg Oncol, 2012. **19**(13): p. 4059-67.

11.   Polterauer, S., I. Vergote, N. Concin, I. Braicu, R. Chekerov, S. Mahner, L. Woelber, I. Cadron, T. Van Gorp, R. Zeillinger, D.C. Castillo-Tong, and J. Sehouli, *Prognostic value of residual tumor size in patients with epithelial ovarian cancer FIGO stages IIA-IV: analysis of the OVCAD data.* Int J Gynecol Cancer, 2012. **22**(3): p. 380-5.

12. du Bois, A., A. Reuss, E. Pujade-Lauraine, P. Harter, I. Ray-Coquard, and J. Pfisterer, *Role of surgical outcome as prognostic factor in advanced epithelial ovarian cancer: a combined exploratory analysis of 3 prospectively randomized phase 3 multicenter trials: by the Arbeitsgemeinschaft Gynaekologische Onkologie Studiengruppe Ovarialkarzinom (AGO-OVAR) and the Groupe d'Investigateurs Nationaux Pour les Etudes des Cancers de l'Ovaire (GINECO).* Cancer, 2009. **115**(6): p. 1234-44.

13. Nick, A.M., R.L. Coleman, P.T. Ramirez, and A.K. Sood, *A framework for a personalized surgical approach to ovarian cancer.* Nat Rev Clin Oncol, 2015. **12**(4): p. 239-45.

14. Vergote, I., C.G. Trope, F. Amant, G.B. Kristensen, T. Ehlen, N. Johnson, R.H. Verheijen, M.E. van der Burg, A.J. Lacave, P.B. Panici, G.G. Kenter, A. Casado, C. Mendiola, C. Coens, L. Verleye, G.C. Stuart, S. Pecorelli, N.S. Reed, R. European Organization for, G. Treatment of Cancer-Gynaecological Cancer, and N.C.T. Group, *Neoadjuvant chemotherapy or primary surgery in stage IIIC or IV ovarian cancer.* N Engl J Med, 2010. **363**(10): p. 943-53.

15. Kang, S. and B.H. Nam, *Does neoadjuvant chemotherapy increase optimal cytoreduction rate in advanced ovarian cancer? Meta-analysis of 21 studies.* Ann Surg Oncol, 2009. **16**(8): p. 2315-20.

16. Bian, C., K. Yao, L. Li, T. Yi, and X. Zhao, *Primary debulking surgery vs. neoadjuvant chemotherapy followed by interval debulking surgery for patients with advanced ovarian cancer.* Arch Gynecol Obstet, 2016. **293**(1): p. 163-8.

17.   Sato, S. and H. Itamochi, *Neoadjuvant chemotherapy in advanced ovarian cancer: latest results and place in therapy.* Ther Adv Med Oncol, 2014. **6**(6): p. 293-304.

18.   Loizzi, V., L. Leone, A. Camporeale, L. Resta, L. Selvaggi, E. Cicinelli, and G. Cormio, *Neoadjuvant Chemotherapy in Advanced Ovarian Cancer: A Single-Institution Experience and a Review of the Literature.* Oncology, 2016. **91**(4): p. 211-216.

19.   Brockbank, E.C., T.E. Ind, D.P. Barton, J.H. Shepherd, M.E. Gore, R. A'Hern, and J.E. Bridges, *Preoperative predictors of suboptimal primary surgical cytoreduction in women with clinical evidence of advanced primary epithelial ovarian cancer.* Int J Gynecol Cancer, 2004. **14**(1): p. 42-50.

20.   Chi, D.S., E.S. Venkatraman, V. Masson, and W.J. Hoskins, *The ability of preoperative serum CA-125 to predict optimal primary tumor cytoreduction in stage III epithelial ovarian carcinoma.* Gynecol Oncol, 2000. **77**(2): p. 227-31.

21.   Vorgias, G., C. Iavazzo, P. Savvopoulos, E. Myriokefalitaki, M. Katsoulis, N. Kalinoglou, and T. Akrivos, *Can the preoperative Ca-125 level predict optimal cytoreduction in patients with advanced ovarian carcinoma? A single institution cohort study.* Gynecol Oncol, 2009. **112**(1): p. 11-5.

22.   Rodriguez, N., J.A. Rauh-Hain, M. Shoni, R.S. Berkowitz, M.G. Muto, C. Feltmate, J.O. Schorge, M.G. del Carmen, U.A. Matulonis, and N.S. Horowitz, *Changes in serum CA-125 can predict optimal cytoreduction to no gross residual disease in patients with advanced stage ovarian cancer treated with neoadjuvant chemotherapy.* Gynecologic Oncology. **125**(2): p. 362-366.

23.   Barlow, T.S., M. Przybylski, J.M. Schilder, D.H. Moore, and K.Y. Look, *The utility of presurgical CA125 to predict optimal tumor cytoreduction of epithelial ovarian cancer.* Int J Gynecol Cancer, 2006. **16**(2): p. 496-500.

24.   Memarzadeh, S., S.B. Lee, J.S. Berek, and R. Farias-Eisner, *CA125 levels are a weak predictor of optimal cytoreductive surgery in patients with advanced epithelial ovarian cancer.* Int J Gynecol Cancer, 2003. **13**(2): p. 120-4.

25.   Arits, A.H., J.E. Stoot, A.A. Botterweck, F.J. Roumen, and A.C. Voogd, *Preoperative serum CA125 levels do not predict suboptimal cytoreductive surgery in epithelial ovarian cancer.* Int J Gynecol Cancer, 2008. **18**(4): p. 621-8.

26.   Rossi, A.C., G. Di Vagno, G. Cormio, A. Cazzolla, S. Stefanelli, E. D'Elia, and L. Selvaggi, *A retrospective study of preoperative CA 125 levels in 82 patients with ovarian cancer.* Arch Gynecol Obstet, 2004. **269**(4): p. 263-5.

27.   Angioli, R., F. Plotti, S. Capriglione, A. Aloisi, R. Montera, D. Luvero, A. Miranda, E.V. Cafa, P. Damiani, and P. Benedetti-Panici, *Can the preoperative HE4 level predict optimal cytoreduction in patients with advanced ovarian carcinoma?* Gynecol Oncol, 2013. **128**(3): p. 579-83.

28.   Kim, H.J., C.H. Choi, Y.Y. Lee, T.J. Kim, J.W. Lee, D.S. Bae, and B.G. Kim, *Surgical outcome prediction in patients with advanced ovarian cancer using computed tomography scans and intraoperative findings.* Taiwan J Obstet Gynecol, 2014. **53**(3): p. 343-7.

29.   Nelson, B.E., A.T. Rosenfield, and P.E. Schwartz, *Preoperative abdominopelvic computed tomographic prediction of optimal cytoreduction in epithelial ovarian carcinoma.* J Clin Oncol, 1993. **11**(1): p. 166-72.

30.   Dowdy, S.C., S.A. Mullany, K.R. Brandt, B.J. Huppert, and W.A. Cliby, *The utility of computed tomography scans in predicting suboptimal cytoreductive surgery in women with advanced ovarian carcinoma.* Cancer, 2004. **101**(2): p. 346-52.

31.   Bristow, R.E., L.R. Duska, N.C. Lambrou, E.K. Fishman, M.J. O'Neill, E.L. Trimble, and F.J. Montz, *A model for predicting surgical outcome in patients with advanced ovarian carcinoma using computed tomography.* Cancer, 2000. **89**(7): p. 1532-40.

32.   Suidan, R.S., P.T. Ramirez, D.M. Sarasohn, J.B. Teitcher, S. Mironov, R.B. Iyer, Q. Zhou, A. Iasonos, H. Paul, M. Hosaka, C.A. Aghajanian, M.M. Leitao, Jr., G.J. Gardner, N.R. Abu-Rustum, Y. Sonoda, D.A. Levine, H. Hricak, and D.S. Chi, *A multicenter prospective trial evaluating the ability of preoperative computed tomography scan and serum CA-125 to predict suboptimal cytoreduction at primary debulking surgery for advanced ovarian, fallopian tube, and peritoneal cancer.* Gynecol Oncol, 2014. **134**(3): p. 455-61.

33.   Janco, J.M., G. Glaser, B. Kim, M.E. McGree, A.L. Weaver, W.A. Cliby, S.C. Dowdy, and J.N. Bakkum-Gamez, *Development of a prediction model for residual disease in newly diagnosed advanced ovarian cancer.* Gynecol Oncol, 2015. **138**(1): p. 70-7.

34.   Gomez-Hidalgo, N.R., B.A. Martinez-Cannon, A.M. Nick, K.H. Lu, A.K. Sood, R.L. Coleman, and P.T. Ramirez, *Predictors of optimal cytoreduction in patients with newly diagnosed advanced-stage epithelial ovarian cancer: Time to incorporate laparoscopic assessment into the standard of care.* Gynecol Oncol, 2015. **137**(3): p. 553-8.

35.   Fagotti, A., F. Fanfani, M. Ludovisi, R. Lo Voi, G. Bifulco, A.C. Testa, and G. Scambia, *Role of laparoscopy to assess the chance of optimal cytoreductive surgery in advanced ovarian cancer: a pilot study.* Gynecol Oncol, 2005. **96**(3): p. 729-35.

36.   Fagotti, A., G. Ferrandina, F. Fanfani, A. Ercoli, D. Lorusso, M. Rossi, and G. Scambia, *A laparoscopy-based score to predict surgical outcome in patients with advanced ovarian carcinoma: a pilot study.* Ann Surg Oncol, 2006. **13**(8): p. 1156-61.

37.   Angioli, R., I. Palaia, M.A. Zullo, L. Muzii, N. Manci, M. Calcagno, and P.B. Panici, *Diagnostic open laparoscopy in the management of advanced ovarian cancer.* Gynecol Oncol, 2006. **100**(3): p. 455-61.

38.   Brun, J.L., R. Rouzier, S. Uzan, and E. Darai, *External validation of a laparoscopic-based score to evaluate resectability of advanced ovarian cancers: clues for a simplified score.* Gynecol Oncol, 2008. **110**(3): p. 354-9.

39.   Fagotti, A., G. Vizzielli, P. De Iaco, D. Surico, A. Buda, V.D. Mandato, F. Petruzzelli, F. Ghezzi, S. Garzarelli, L. Mereu, R. Vigano, S. Tateo, F. Fanfani, and G. Scambia, *A multicentric trial (Olympia-MITO 13) on the accuracy of*

laparoscopy to assess peritoneal spread in ovarian cancer. Am J Obstet Gynecol, 2013. **209**(5): p. 462 e1-462 e11.

40.   Fagotti, A., G. Ferrandina, G. Vizzielli, F. Fanfani, V. Gallotta, V. Chiantera, B. Costantini, P.A. Margariti, S. Gueli Alletti, F. Cosentino, L. Tortorella, and G. Scambia, *Phase III randomised clinical trial comparing primary surgery versus neoadjuvant chemotherapy in advanced epithelial ovarian cancer with high tumour load (SCORPION trial): Final analysis of peri-operative outcome.* Eur J Cancer, 2016. **59**: p. 22-33.

41.   Makowski, L., J.B. Boord, K. Maeda, V.R. Babaev, K.T. Uysal, M.A. Morgan, R.A. Parker, J. Suttles, S. Fazio, G.S. Hotamisligil, and M.F. Linton, *Lack of macrophage fatty-acid-binding protein aP2 protects mice deficient in apolipoprotein E against atherosclerosis.* Nat Med, 2001. **7**(6): p. 699-705.

42.   Rolph, M.S., T.R. Young, B.O. Shum, C.Z. Gorgun, C. Schmitz-Peiffer, I.A. Ramshaw, G.S. Hotamisligil, and C.R. Mackay, *Regulation of dendritic cell function and T cell priming by the fatty acid-binding protein AP2.* J Immunol, 2006. **177**(11): p. 7794-801.

43.   Elmasri, H., E. Ghelfi, C.W. Yu, S. Traphagen, M. Cernadas, H. Cao, G.P. Shi, J. Plutzky, M. Sahin, G. Hotamisligil, and S. Cataltepe, *Endothelial cell-fatty acid binding protein 4 promotes angiogenesis: role of stem cell factor/c-kit pathway.* Angiogenesis, 2012. **15**(3): p. 457-68.

44.   Furuhashi, M. and G.S. Hotamisligil, *Fatty acid-binding proteins: role in metabolic diseases and potential as drug targets.* Nat Rev Drug Discov, 2008. **7**(6): p. 489-503.

45.   Hotamisligil, G.S. and D.A. Bernlohr, *Metabolic functions of FABPs--mechanisms and therapeutic implications.* Nat Rev Endocrinol, 2015. **11**(10): p. 592-605.

46.   Spiegelman, B.M. and H. Green, *Control of specific protein biosynthesis during the adipose conversion of 3T3 cells.* J Biol Chem, 1980. **255**(18): p. 8811-18.

47.   Shaughnessy, S., E.R. Smith, S. Kodukula, J. Storch, and S.K. Fried, *Adipocyte metabolism in adipocyte fatty acid binding protein knockout mice (aP2-/-) after short-term high-fat feeding: functional compensation by the keratinocyte [correction of keritinocyte] fatty acid binding protein.* Diabetes, 2000. **49**(6): p. 904-11.

48.   Ghelfi, E., C.W. Yu, H. Elmasri, M. Terwelp, C.G. Lee, V. Bhandari, S.A. Comhair, S.C. Erzurum, G.S. Hotamisligil, J.A. Elias, and S. Cataltepe, *Fatty acid binding protein 4 regulates VEGF-induced airway angiogenesis and inflammation in a transgenic mouse model: implications for asthma.* Am J Pathol, 2013. **182**(4): p. 1425-33.

49.   Makowski, L., K.C. Brittingham, J.M. Reynolds, J. Suttles, and G.S. Hotamisligil, *The fatty acid-binding protein, aP2, coordinates macrophage cholesterol trafficking and inflammatory activity. Macrophage expression of aP2 impacts peroxisome proliferator-activated receptor gamma and IkappaB kinase activities.* J Biol Chem, 2005. **280**(13): p. 12888-95.

50.   Furuhashi, M., G. Tuncman, C.Z. Gorgun, L. Makowski, G. Atsumi, E. Vaillancourt, K. Kono, V.R. Babaev, S. Fazio, M.F. Linton, R. Sulsky, J.A. Robl, R.A. Parker, and G.S. Hotamisligil, *Treatment of diabetes and atherosclerosis*

by inhibiting fatty-acid-binding protein aP2. Nature, 2007. **447**(7147): p. 959-65.

51.   Harjes, U., E. Bridges, K.M. Gharpure, I. Roxanis, H. Sheldon, F. Miranda, L.S. Mangala, S. Pradeep, G. Lopez-Berestein, A. Ahmed, B. Fielding, A.K. Sood, and A.L. Harris, *Antiangiogenic and tumour inhibitory effects of downregulating tumour endothelial FABP4.* Oncogene, 2017. **36**(7): p. 912-921.

52.   Nieman, K.M., H.A. Kenny, C.V. Penicka, A. Ladanyi, R. Buell-Gutbrod, M.R. Zillhardt, I.L. Romero, M.S. Carey, G.B. Mills, G.S. Hotamisligil, S.D. Yamada, M.E. Peter, K. Gwin, and E. Lengyel, *Adipocytes promote ovarian cancer metastasis and provide energy for rapid tumor growth.* Nat Med, 2011. **17**(11): p. 1498-503.

53.   Lee, D., K. Wada, Y. Taniguchi, H. Al-Shareef, T. Masuda, Y. Usami, T. Aikawa, M. Okura, Y. Kamisaki, and M. Kogo, *Expression of fatty acid binding protein 4 is involved in the cell growth of oral squamous cell carcinoma.* Oncol Rep, 2014. **31**(3): p. 1116-20.

54.   Guaita-Esteruelas, S., A. Bosquet, P. Saavedra, J. Guma, J. Girona, E.W. Lam, K. Amillano, J. Borras, and L. Masana, *Exogenous FABP4 increases breast cancer cell proliferation and activates the expression of fatty acid transport proteins.* Mol Carcinog, 2017. **56**(1): p. 208-217.

55.   Alo, P.L., P. Visca, M.L. Framarino, C. Botti, S. Monaco, V. Sebastiani, D.E. Serpieri, and U. Di Tondo, *Immunohistochemical study of fatty acid synthase in ovarian neoplasms.* Oncol Rep, 2000. **7**(6): p. 1383-8.

56.   Han, C., L. Yang, H.H. Choi, J. Baddour, A. Achreja, Y. Liu, Y. Li, J. Li, G. Wan, C. Huang, G. Ji, X. Zhang, D. Nagrath, and X. Lu, *Amplification of USP13 drives ovarian cancer metabolism.* Nat Commun, 2016. **7**: p. 13525.

57.   Yang, L., T. Moss, L.S. Mangala, J. Marini, H. Zhao, S. Wahlig, G. Armaiz-Pena, D. Jiang, A. Achreja, J. Win, R. Roopaimoole, C. Rodriguez-Aguayo, I. Mercado-Uribe, G. Lopez-Berestein, J. Liu, T. Tsukamoto, A.K. Sood, P.T. Ram, and D. Nagrath, *Metabolic shifts toward glutamine regulate tumor growth, invasion and bioenergetics in ovarian cancer.* Mol Syst Biol, 2014. **10**: p. 728.

58.   Zand, B., R.A. Previs, N.M. Zacharias, R. Rupaimoole, T. Mitamura, A.S. Nagaraja, M. Guindani, H.J. Dalton, L. Yang, J. Baddour, A. Achreja, W. Hu, C.V. Pecot, C. Ivan, S.Y. Wu, C.R. McCullough, K.M. Gharpure, E. Shoshan, S. Pradeep, L.S. Mangala, C. Rodriguez-Aguayo, Y. Wang, A.M. Nick, M.A. Davies, G. Armaiz-Pena, J. Liu, S.K. Lutgendorf, K.A. Baggerly, M.B. Eli, G. Lopez-Berestein, D. Nagrath, P.K. Bhattacharya, and A.K. Sood, *Role of Increased n-acetylaspartate Levels in Cancer.* J Natl Cancer Inst, 2016. **108**(6): p. djv426.

59.   Blanksby, S.J. and T.W. Mitchell, *Advances in mass spectrometry for lipidomics.* Annu Rev Anal Chem (Palo Alto Calif), 2010. **3**: p. 433-65.

60.   Wiseman, J.M., D.R. Ifa, Q. Song, and R.G. Cooks, *Tissue imaging at atmospheric pressure using desorption electrospray ionization (DESI) mass spectrometry.* Angew Chem Int Ed Engl, 2006. **45**(43): p. 7188-92.

61.   Manicke, N.E., J.M. Wiseman, D.R. Ifa, and R.G. Cooks, *Desorption electrospray ionization (DESI) mass spectrometry and tandem mass*

spectrometry (MS/MS) of phospholipids and sphingolipids: ionization, adduct formation, and fragmentation. J Am Soc Mass Spectrom, 2008. **19**(4): p. 531-43.

62.   Zhang, J.I., N. Talaty, A.B. Costa, Y. Xia, W.A. Tao, R. Bell, J.H. Callahan, and R.G. Cooks, *Rapid direct lipid profiling of bacteria using desorption electrospray ionization mass spectrometry.* International Journal of Mass Spectrometry, 2011. **301**(1–3): p. 37-44.

63.   Jackson, A.U., A. Tata, C. Wu, R.H. Perry, G. Haas, L. West, and R.G. Cooks, *Direct analysis of Stevia leaves for diterpene glycosides by desorption electrospray ionization mass spectrometry.* Analyst, 2009. **134**(5): p. 867-74.

64.   Lane, A.L., L. Nyadong, A.S. Galhena, T.L. Shearer, E.P. Stout, R.M. Parry, M. Kwasnik, M.D. Wang, M.E. Hay, F.M. Fernandez, and J. Kubanek, *Desorption electrospray ionization mass spectrometry reveals surface-mediated antifungal chemical defense of a tropical seaweed.* Proc Natl Acad Sci U S A, 2009. **106**(18): p. 7314-9.

65.   Eberlin, L.S., C.R. Ferreira, A.L. Dill, D.R. Ifa, and R.G. Cooks, *Desorption electrospray ionization mass spectrometry for lipid characterization and biological tissue imaging.* Biochim Biophys Acta, 2011. **1811**(11): p. 946-60.

66.   Badu-Tawiah, A., C. Bland, D.I. Campbell, and R.G. Cooks, *Non-aqueous spray solvents and solubility effects in desorption electrospray ionization.* J Am Soc Mass Spectrom, 2010. **21**(4): p. 572-9.

67.   Green, F.M., T.L. Salter, I.S. Gilmore, P. Stokes, and G. O'Connor, *The effect of electrospray solvent composition on desorption electrospray ionisation (DESI) efficiency and spatial resolution.* Analyst, 2010. **135**(4): p. 731-7.

68.   Takats, Z., J.M. Wiseman, B. Gologan, and R.G. Cooks, *Mass spectrometry sampling under ambient conditions with desorption electrospray ionization.* Science, 2004. **306**(5695): p. 471-3.

69.   Zhang, J., W. Yu, S.W. Ryu, J. Lin, G. Buentello, R. Tibshirani, J. Suliburk, and L.S. Eberlin, *Cardiolipins Are Biomarkers of Mitochondria-Rich Thyroid Oncocytic Tumors.* Cancer Res, 2016. **76**(22): p. 6588-6597.

70.   Girod, M., Y. Shi, J.X. Cheng, and R.G. Cooks, *Mapping lipid alterations in traumatically injured rat spinal cord by desorption electrospray ionization imaging mass spectrometry.* Anal Chem, 2011. **83**(1): p. 207-15.

71.   Eberlin, L.S., D.R. Ifa, C. Wu, and R.G. Cooks, *Three-Dimensional Vizualization of Mouse Brain by Lipid Analysis using Ambient Ionization Mass Spectrometry.* Angewandte Chemie (International ed. in English), 2010. **49**(5): p. 873-876.

72.   Dill, A.L., L.S. Eberlin, A.B. Costa, C. Zheng, D.R. Ifa, L. Cheng, T.A. Masterson, M.O. Koch, O. Vitek, and R.G. Cooks, *Multivariate statistical identification of human bladder carcinomas using ambient ionization imaging mass spectrometry.* Chemistry, 2011. **17**(10): p. 2897-902.

73.   Cooks, R.G., N.E. Manicke, A.L. Dill, D.R. Ifa, L.S. Eberlin, A.B. Costa, H. Wang, G. Huang, and Z. Ouyang, *New ionization methods and miniature mass spectrometers for biomedicine: DESI imaging for cancer diagnostics and paper*

spray ionization for therapeutic drug monitoring. Faraday Discuss, 2011. **149**: p. 247-67; discussion 333-56.

74.   Eberlin, L.S., A.L. Dill, A.B. Costa, D.R. Ifa, L. Cheng, T. Masterson, M. Koch, T.L. Ratliff, and R.G. Cooks, *Cholesterol sulfate imaging in human prostate cancer tissue by desorption electrospray ionization mass spectrometry.* Anal Chem, 2010. **82**(9): p. 3430-4.

75.   Eberlin, L.S., A.L. Dill, A.J. Golby, K.L. Ligon, J.M. Wiseman, R.G. Cooks, and N.Y. Agar, *Discrimination of human astrocytoma subtypes by lipid analysis using desorption electrospray ionization imaging mass spectrometry.* Angew Chem Int Ed Engl, 2010. **49**(34): p. 5953-6.

76.   Masterson, T.A., A.L. Dill, L.S. Eberlin, M. Mattarozzi, L. Cheng, S.D. Beck, F. Bianchi, and R.G. Cooks, *Distinctive glycerophospholipid profiles of human seminoma and adjacent normal tissues by desorption electrospray ionization imaging mass spectrometry.* J Am Soc Mass Spectrom, 2011. **22**(8): p. 1326-33.

77.   *Integrated genomic analyses of ovarian carcinoma.* Nature, 2011. **474**(7353): p. 609-615.

78.   Tothill, R.W., A.V. Tinker, J. George, R. Brown, S.B. Fox, S. Lade, D.S. Johnson, M.K. Trivett, D. Etemadmoghadam, B. Locandro, N. Traficante, S. Fereday, J.A. Hung, Y.E. Chiew, I. Haviv, G. Australian Ovarian Cancer Study, D. Gertig, A. DeFazio, and D.D. Bowtell, *Novel molecular subtypes of serous and endometrioid ovarian cancer linked to clinical outcome.* Clin Cancer Res, 2008. **14**(16): p. 5198-208.

79. Lee, J.W., H.D. Han, M.M.K. Shahzad, S.W. Kim, L.S. Mangala, A.M. Nick, C.H. Lu, R.R. Langley, R. Schmandt, H.S. Kim, S.L. Mao, J. Gooya, C. Fazenbaker, D. Jackson, D.A. Tice, C.N. Landen, R.L. Coleman, and A.K. Sood, *EphA2 Immunoconjugate as Molecularly Targeted Chemotherapy for Ovarian Carcinoma.* Journal of the National Cancer Institute, 2009. **101**(17): p. 1193-1205.

80. Landen, C.N., Jr., A. Chavez-Reyes, C. Bucana, R. Schmandt, M.T. Deavers, G. Lopez-Berestein, and A.K. Sood, *Therapeutic EphA2 gene targeting in vivo using neutral liposomal small interfering RNA delivery.* Cancer Res, 2005. **65**(15): p. 6910-8.

81. Reshef, D.N., Y.A. Reshef, H.K. Finucane, S.R. Grossman, G. McVean, P.J. Turnbaugh, E.S. Lander, M. Mitzenmacher, and P.C. Sabeti, *Detecting novel associations in large data sets.* Science, 2011. **334**(6062): p. 1518-24.

82. Rupaimoole, R., C. Ivan, D. Yang, K.M. Gharpure, S.Y. Wu, C.V. Pecot, R.A. Previs, A.S. Nagaraja, G.N. Armaiz-Pena, M. McGuire, S. Pradeep, L.S. Mangala, C. Rodriguez-Aguayo, L. Huang, M. Bar-Eli, W. Zhang, G. Lopez-Berestein, G.A. Calin, and A.K. Sood, *Hypoxia-upregulated microRNA-630 targets Dicer, leading to increased tumor progression.* Oncogene, 2016. **35**(33): p. 4312-20.

83. Wyman, S.K., R.K. Parkin, P.S. Mitchell, B.R. Fritz, K. O'Briant, A.K. Godwin, N. Urban, C.W. Drescher, B.S. Knudsen, and M. Tewari, *Repertoire of microRNAs in Epithelial Ovarian Cancer as Determined by Next Generation Sequencing of Small RNA cDNA Libraries.* Plos One, 2009. **4**(4).

84. Winter, S.C., F.M. Buffa, P. Silva, C. Miller, H.R. Valentine, H. Turley, K.A. Shah, G.J. Cox, R.J. Corbridge, J.J. Homer, B. Musgrove, N. Slevin, P. Sloan, P. Price, C.M. West, and A.L. Harris, *Relation of a hypoxia metagene derived from head and neck cancer to prognosis of multiple cancers.* Cancer Res, 2007. **67**(7): p. 3441-9.

85. Cancer Genome Atlas Research, N., *Integrated genomic analyses of ovarian carcinoma.* Nature, 2011. **474**(7353): p. 609-15.

86. Cole, S.W., J.M. Arevalo, R. Takahashi, E.K. Sloan, S.K. Lutgendorf, A.K. Sood, J.F. Sheridan, and T.E. Seeman, *Computational identification of gene-social environment interaction at the human IL6 locus.* Proc Natl Acad Sci U S A, 2010. **107**(12): p. 5681-6.

87. Lutgendorf, S.K., K. DeGeest, C.Y. Sung, J.M. Arevalo, F. Penedo, J. Lucci, 3rd, M. Goodheart, D. Lubaroff, D.M. Farley, A.K. Sood, and S.W. Cole, *Depression, social support, and beta-adrenergic transcription control in human ovarian cancer.* Brain Behav Immun, 2009. **23**(2): p. 176-83.

88. Eberlin, L.S., R.J. Tibshirani, J. Zhang, T.A. Longacre, G.J. Berry, D.B. Bingham, J.A. Norton, R.N. Zare, and G.A. Poultsides, *Molecular assessment of surgical-resection margins of gastric cancer by mass-spectrometric imaging.* Proc Natl Acad Sci U S A, 2014. **111**(7): p. 2436-41.

89. Cordero, A.B., Y. Kwon, X. Hua, and A.K. Godwin, *In vivo imaging and therapeutic treatments in an orthotopic mouse model of ovarian cancer.* J Vis Exp, 2010(42).

90. Greenaway, J., R. Moorehead, P. Shaw, and J. Petrik, *Epithelial-stromal interaction increases cell proliferation, survival and tumorigenicity in a mouse model of human epithelial ovarian cancer.* Gynecol Oncol, 2008. **108**(2): p. 385-94.

91. Loges, S., M. Mazzone, P. Hohensinner, and P. Carmeliet, *Silencing or fueling metastasis with VEGF inhibitors: antiangiogenesis revisited.* Cancer Cell, 2009. **15**(3): p. 167-70.

92. Jiang, M., L. Zhang, X. Ma, W. Hu, Y. Chen, M. Yu, Q. Wang, X. Li, Z. Yin, Y. Zhu, X. Gao, D.P. Hajjar, Y. Duan, and J. Han, *Tamoxifen inhibits macrophage FABP4 expression through the combined effects of the GR and PPARgamma pathways.* Biochem J, 2013. **454**(3): p. 467-77.

93. Semaan, A., A.R. Munkarah, H. Arabi, S. Bandyopadhyay, S. Seward, S. Kumar, A. Qazi, Y. Hussein, R.T. Morris, and R. Ali-Fehmi, *Expression of GLUT-1 in epithelial ovarian carcinoma: correlation with tumor cell proliferation, angiogenesis, survival and ability to predict optimal cytoreduction.* Gynecol Oncol, 2011. **121**(1): p. 181-6.

94. Berchuck, A., E.S. Iversen, J.M. Lancaster, H.K. Dressman, M. West, J.R. Nevins, and J.R. Marks, *Prediction of optimal versus suboptimal cytoreduction of advanced-stage serous ovarian cancer with the use of microarrays.* Am J Obstet Gynecol, 2004. **190**(4): p. 910-25.

95. An, Y., L. Cai, Y. Wang, D. Zhu, Y. Guan, and J. Zheng, *Local expression of insulin-like growth factor-I, insulin-like growth factor-I receptor, and estrogen receptor alpha in ovarian cancer.* Onkologie, 2009. **32**(11): p. 638-44.

96.   Sinn, B.V., S. Darb-Esfahani, R.M. Wirtz, A. Faggad, W. Weichert, A.C. Buckendahl, A. Noske, B.M. Muller, J. Budczies, J. Sehouli, E.I. Braicu, M. Dietel, and C. Denkert, *Vascular endothelial growth factor C mRNA expression is a prognostic factor in epithelial ovarian cancer as detected by kinetic RT-PCR in formalin-fixed paraffin-embedded tissue.* Virchows Arch, 2009. **455**(6): p. 461-7.

97.   Leoutsakou, T., M. Talieri, and A. Scorilas, *Expression analysis and prognostic significance of the SRA1 gene, in ovarian cancer.* Biochem Biophys Res Commun, 2006. **344**(2): p. 667-74.

98.   Komiyama, S., T. Kurahashi, M. Ishikawa, K. Tanaka, M. Komiyama, M. Mikami, and Y. Udagawa, *Expression of TGFss1 and its receptors is associated with biological features of ovarian cancer and sensitivity to paclitaxel/carboplatin.* Oncol Rep, 2011. **25**(4): p. 1131-8.

99.   Reimer, D., I. Steppan, A. Wiedemair, N. Concin, G. Hofstetter, C. Marth, E. Muller-Holzner, and A.G. Zeimet, *Soluble isoforms but not the transmembrane form of coxsackie-adenovirus receptor are of clinical relevance in epithelial ovarian cancer.* Int J Cancer, 2007. **120**(12): p. 2568-75.

100.   Merritt, W.M., Y.G. Lin, L.Y. Han, A.A. Kamat, W.A. Spannuth, R. Schmandt, D. Urbauer, L.A. Pennacchio, J.F. Cheng, A.M. Nick, M.T. Deavers, A. Mourad-Zeidan, H. Wang, P. Mueller, M.E. Lenburg, J.W. Gray, S. Mok, M.J. Birrer, G. Lopez-Berestein, R.L. Coleman, M. Bar-Eli, and A.K. Sood, *Dicer, Drosha, and outcomes in patients with ovarian cancer.* N Engl J Med, 2008. **359**(25): p. 2641-50.

101. Rosen, D.G., G. Yang, M.T. Deavers, A. Malpica, J.J. Kavanagh, G.B. Mills, and J. Liu, *Cyclin E expression is correlated with tumor progression and predicts a poor prognosis in patients with ovarian carcinoma.* Cancer, 2006. **106**(9): p. 1925-32.

102. Simpson, B.J., H.A. Phillips, A.M. Lessells, S.P. Langdon, and W.R. Miller, *c-erbB growth-factor-receptor proteins in ovarian tumours.* Int J Cancer, 1995. **64**(3): p. 202-6.

103. Hosono, S., H. Kajiyama, M. Terauchi, K. Shibata, K. Ino, A. Nawa, and F. Kikkawa, *Expression of Twist increases the risk for recurrence and for poor survival in epithelial ovarian carcinoma patients.* Br J Cancer, 2007. **96**(2): p. 314-20.

104. Jewell, E.L., K.M. Darcy, A. Hutson, P.S. Lee, L.J. Havrilesky, L.A. Grace, A. Berchuck, and A.A. Secord, *Association between the N-terminally truncated (DeltaN) p63alpha (DeltaNp63alpha) isoform and debulking status, VEGF expression and progression-free survival in previously untreated, advanced stage epithelial ovarian cancer: A Gynecologic Oncology Group study.* Gynecol Oncol, 2009. **115**(3): p. 424-9.

105. Lin, F., K. Lin, X. Xie, and C. Zhou, *Increased ERCC1 protein expression is associated with suboptimal debulking in advanced epithelial ovarian cancer.* Anticancer Res, 2010. **30**(6): p. 2447-52.

106. Li, C., J. Liu, R. Lu, G. Yu, X. Wang, Y. Zhao, H. Song, P. Lin, X. Sun, X. Yu, Y. Zhang, X. Ning, and J. Geng, *AEG -1 overexpression: a novel indicator for*

peritoneal dissemination and lymph node metastasis in epithelial ovarian cancers. Int J Gynecol Cancer, 2011. **21**(4): p. 602-8.

107. Nick, A.M., R.L. Stone, G. Armaiz-Pena, B. Ozpolat, I. Tekedereli, W.S. Graybill, C.N. Landen, G. Villares, P. Vivas-Mejia, J. Bottsford-Miller, H.S. Kim, J.S. Lee, S.M. Kim, K.A. Baggerly, P.T. Ram, M.T. Deavers, R.L. Coleman, G. Lopez-Berestein, and A.K. Sood, *Silencing of p130cas in ovarian carcinoma: a novel mechanism for tumor cell death.* J Natl Cancer Inst, 2011. **103**(21): p. 1596-612.

108. Barnett, J.C., S.M. Bean, R.S. Whitaker, E. Kondoh, T. Baba, S. Fujii, J.R. Marks, H.K. Dressman, S.K. Murphy, and A. Berchuck, *Ovarian cancer tumor infiltrating T-regulatory (T(reg)) cells are associated with a metastatic phenotype.* Gynecol Oncol, 2010. **116**(3): p. 556-62.

109. Fiegl, H., G. Windbichler, E. Mueller-Holzner, G. Goebel, M. Lechner, I.J. Jacobs, and M. Widschwendter, *HOXA11 DNA methylation--a novel prognostic biomarker in ovarian cancer.* Int J Cancer, 2008. **123**(3): p. 725-9.

110. Riester, M., W. Wei, L. Waldron, A.C. Culhane, L. Trippa, E. Oliva, S.H. Kim, F. Michor, C. Huttenhower, G. Parmigiani, and M.J. Birrer, *Risk prediction for late-stage ovarian cancer by meta-analysis of 1525 patient samples.* J Natl Cancer Inst, 2014. **106**(5).

111. Tucker, S.L., K. Gharpure, S.M. Herbrich, A.K. Unruh, A.M. Nick, E.K. Crane, R.L. Coleman, J. Guenthoer, H.J. Dalton, S.Y. Wu, R. Rupaimoole, G. Lopez-Berestein, B. Ozpolat, C. Ivan, W. Hu, K.A. Baggerly, and A.K. Sood, *Molecular*

biomarkers of residual disease after surgical debulking of high-grade serous ovarian cancer. Clin Cancer Res, 2014. **20**(12): p. 3280-8.

112. Khalil, S., E. Fabbri, A. Santangelo, V. Bezzerri, C. Cantù, G.D. Gennaro, A. Finotti, C. Ghimenton, A. Eccher, M. Dechecchi, A. Scarpa, B. Hirshman, C. Chen, M. Ferracin, M. Negrini, R. Gambari, and G. Cabrini, *miRNA array screening reveals cooperative MGMT-regulation between miR-181d-5p and miR-409-3p in glioblastoma.* Oncotarget, 2016. **7**(19): p. 28195-28206.

113. Cao, Y., L. Zhang, M. Wei, X. Jiang, and D. Jia, *MicroRNA-409-3p Represses Glioma Cell Invasion and Proliferation by Targeting High-mobility Group Nucleosome Binding Domain 5.* Oncol Res, 2017.

114. Tan, S., H. Shi, M. Ba, S. Lin, H. Tang, X. Zeng, and X. Zhang, *miR-409-3p sensitizes colon cancer cells to oxaliplatin by inhibiting Beclin-1-mediated autophagy.* Int J Mol Med, 2016. **37**(4): p. 1030-8.

115. Liu, M., A. Xu, X. Yuan, Q. Zhang, T. Fang, W. Wang, and C. Li, *Downregulation of microRNA-409-3p promotes aggressiveness and metastasis in colorectal cancer: an indication for personalized medicine.* J Transl Med, 2015. **13**: p. 195.

116. Bai, R., C. Weng, H. Dong, S. Li, G. Chen, and Z. Xu, *MicroRNA-409-3p suppresses colorectal cancer invasion and metastasis partly by targeting GAB1 expression.* Int J Cancer, 2015. **137**(10): p. 2310-22.

117. Weng, C., H. Dong, G. Chen, Y. Zhai, R. Bai, H. Hu, L. Lu, and Z. Xu, *miR-409-3p inhibits HT1080 cell proliferation, vascularization and metastasis by targeting angiogenin.* Cancer Lett, 2012. **323**(2): p. 171-9.

118. Zhang, G., Z. Liu, H. Xu, and Q. Yang, *miR-409-3p suppresses breast cancer cell growth and invasion by targeting Akt1.* Biochem Biophys Res Commun, 2016. **469**(2): p. 189-95.

119. Ma, Z., Y. Li, J. Xu, Q. Ren, J. Yao, and X. Tian, *MicroRNA-409-3p regulates cell invasion and metastasis by targeting ZEB1 in breast cancer.* IUBMB Life, 2016. **68**(5): p. 394-402.

120. Cao, G.H., X.L. Sun, F. Wu, W.F. Chen, J.Q. Li, and W.C. Hu, *Low expression of miR-409-3p is a prognostic marker for breast cancer.* Eur Rev Med Pharmacol Sci, 2016. **20**(18): p. 3825-3829.

121. Cuk, K., M. Zucknick, J. Heil, D. Madhavan, S. Schott, A. Turchinovich, D. Arlt, M. Rath, C. Sohn, A. Benner, H. Junkermann, A. Schneeweiss, and B. Burwinkel, *Circulating microRNAs in plasma as early detection markers for breast cancer.* Int J Cancer, 2013. **132**(7): p. 1602-12.

122. Zheng, B., L. Liang, S. Huang, R. Zha, L. Liu, D. Jia, Q. Tian, Q. Wang, C. Wang, Z. Long, Y. Zhou, X. Cao, C. Du, Y. Shi, and X. He, *MicroRNA-409 suppresses tumour cell invasion and metastasis by directly targeting radixin in gastric cancers.* Oncogene, 2012. **31**(42): p. 4509-16.

123. Li, C., H. Nie, M. Wang, L. Su, J. Li, B. Yu, M. Wei, J. Ju, Y. Yu, M. Yan, Q. Gu, Z. Zhu, and B. Liu, *MicroRNA-409-3p regulates cell proliferation and apoptosis by targeting PHF10 in gastric cancer.* Cancer Lett, 2012. **320**(2): p. 189-97.

124. Wu, S., X. Du, M. Wu, H. Du, X. Shi, and T. Zhang, *MicroRNA-409-3p inhibits osteosarcoma cell migration and invasion by targeting catenin-delta1.* Gene, 2016. **584**(1): p. 83-9.

125. Wan, L., L. Zhu, J. Xu, B. Lu, Y. Yang, F. Liu, and Z. Wang, *MicroRNA-409-3p functions as a tumor suppressor in human lung adenocarcinoma by targeting c-Met.* Cell Physiol Biochem, 2014. **34**(4): p. 1273-90.

126. Josson, S., M. Gururajan, P. Hu, C. Shao, G.Y. Chu, H.E. Zhau, C. Liu, K. Lao, C.L. Lu, Y.T. Lu, J. Lichterman, S. Nandana, Q. Li, A. Rogatko, D. Berel, E.M. Posadas, L. Fazli, D. Sareen, and L.W. Chung, *miR-409-3p/-5p promotes tumorigenesis, epithelial-to-mesenchymal transition, and bone metastasis of human prostate cancer.* Clin Cancer Res, 2014. **20**(17): p. 4636-46.

127. Josson, S., M. Gururajan, S.Y. Sung, P. Hu, C. Shao, H.E. Zhau, C. Liu, J. Lichterman, P. Duan, Q. Li, A. Rogatko, E.M. Posadas, C.L. Haga, and L.W. Chung, *Stromal fibroblast-derived miR-409 promotes epithelial-to-mesenchymal transition and prostate tumorigenesis.* Oncogene, 2015. **34**(21): p. 2690-9.

128. Johanning, G.L. and T.Y. Lin, *Unsaturated Fatty-Acid Effects on Human Breast-Cancer Cell-Adhesion.* Nutrition and Cancer-an International Journal, 1995. **24**(1): p. 57-66.

129. Kim, H., C. Rodriguez-Navas, R.K. Kollipara, P. Kapur, I. Pedrosa, J. Brugarolas, R. Kittler, and J. Ye, *Unsaturated Fatty Acids Stimulate Tumor Growth through Stabilization of beta-Catenin.* Cell Reports, 2015. **13**(3): p. 495-503.

130. Vinciguerra, M., F. Carrozzino, M. Peyrou, S. Carlone, R. Montesano, R. Benelli, and M. Foti, *Unsaturated fatty acids promote hepatoma proliferation*

and *progression through downregulation of the tumor suppressor PTEN.* Journal of Hepatology, 2009. **50**(6): p. 1132-1141.

131. Park, J.H., S. Vithayathil, S. Kumar, P.L. Sung, L.E. Dobrolecki, V. Putluri, V.B. Bhat, S.K. Bhowmik, V. Gupta, K. Arora, D. Wu, E. Tsouko, Y. Zhang, S. Maity, T.R. Donti, B.H. Graham, D.E. Frigo, C. Coarfa, P. Yotnda, N. Putluri, A. Sreekumar, M.T. Lewis, C.J. Creighton, L.J. Wong, and B.A. Kaipparettu, *Fatty Acid Oxidation-Driven Src Links Mitochondrial Energy Reprogramming and Oncogenic Properties in Triple-Negative Breast Cancer.* Cell Rep, 2016. **14**(9): p. 2154-65.

132. Monet, M., D. Gkika, V. Lehen'kyi, A. Pourtier, F. Vanden Abeele, G. Bidaux, V. Juvin, F. Rassendren, S. Humez, and N. Prevarsakaya, *Lysophospholipids stimulate prostate cancer cell migration via TRPV2 channel activation.* Biochim Biophys Acta, 2009. **1793**(3): p. 528-39.

133. Sutphen, R., Y. Xu, G.D. Wilbanks, J. Fiorica, E.C. Grendys, Jr., J.P. LaPolla, H. Arango, M.S. Hoffman, M. Martino, K. Wakeley, D. Griffin, R.W. Blanco, A.B. Cantor, Y.J. Xiao, and J.P. Krischer, *Lysophospholipids are potential biomarkers of ovarian cancer.* Cancer Epidemiol Biomarkers Prev, 2004. **13**(7): p. 1185-91.

134. Liu, Z., J.A. Beach, H. Agadjanian, D. Jia, P.J. Aspuria, B.Y. Karlan, and S. Orsulic, *Suboptimal cytoreduction in ovarian carcinoma is associated with molecular pathways characteristic of increased stromal activation.* Gynecol Oncol, 2015. **139**(3): p. 394-400.

135.   Wu, S.Y., R. Rupaimoole, F. Shen, S. Pradeep, C.V. Pecot, C. Ivan, A.S. Nagaraja, K.M. Gharpure, E. Pham, H. Hatakeyama, M.H. McGuire, M. Haemmerle, V. Vidal-Anaya, C. Olsen, C. Rodriguez-Aguayo, J. Filant, E.A. Ehsanipour, S.M. Herbrich, S.N. Maiti, L. Huang, J.H. Kim, X. Zhang, H.D. Han, G.N. Armaiz-Pena, E.G. Seviour, S. Tucker, M. Zhang, D. Yang, L.J. Cooper, R. Ali-Fehmi, M. Bar-Eli, J.S. Lee, P.T. Ram, K.A. Baggerly, G. Lopez-Berestein, M.C. Hung, and A.K. Sood, *A miR-192-EGR1-HOXB9 regulatory network controls the angiogenic switch in cancer.* Nat Commun, 2016. **7**: p. 11169.

136.   Pecot, C.V., R. Rupaimoole, D. Yang, R. Akbani, C. Ivan, C. Lu, S. Wu, H.D. Han, M.Y. Shah, C. Rodriguez-Aguayo, J. Bottsford-Miller, Y. Liu, S.B. Kim, A. Unruh, V. Gonzalez-Villasana, L. Huang, B. Zand, M. Moreno-Smith, L.S. Mangala, M. Taylor, H.J. Dalton, V. Sehgal, Y. Wen, Y. Kang, K.A. Baggerly, J.S. Lee, P.T. Ram, M.K. Ravoori, V. Kundra, X. Zhang, R. Ali-Fehmi, A.M. Gonzalez-Angulo, P.P. Massion, G.A. Calin, G. Lopez-Berestein, W. Zhang, and A.K. Sood, *Tumour angiogenesis regulation by the miR-200 family.* Nat Commun, 2013. **4**: p. 2427.

137.   Landen, C.N., A. Chavez-Reyes, C. Bucana, R. Schmandt, M.T. Deavers, G. Lopez-Berestein, and A.K. Sood, *Therapeutic EphA2 Gene Targeting In vivo Using Neutral Liposomal Small Interfering RNA Delivery.* Cancer Research, 2005. **65**(15): p. 6910-6918.

138.   Rupaimoole, R., S.Y. Wu, S. Pradeep, C. Ivan, C.V. Pecot, K.M. Gharpure, A.S. Nagaraja, G.N. Armaiz-Pena, M. McGuire, B. Zand, H.J. Dalton, J. Filant,

J.B. Miller, C. Lu, N.C. Sadaoui, L.S. Mangala, M. Taylor, T. van den Beucken, E. Koch, C. Rodriguez-Aguayo, L. Huang, M. Bar-Eli, B.G. Wouters, M. Radovich, M. Ivan, G.A. Calin, W. Zhang, G. Lopez-Berestein, and A.K. Sood, *Hypoxia-mediated downregulation of miRNA biogenesis promotes tumour progression.* Nat Commun, 2014. **5**: p. 5202.

139.   Merritt, W.M., Y.G. Lin, W.A. Spannuth, M.S. Fletcher, A.A. Kamat, L.Y. Han, C.N. Landen, N. Jennings, K. De Geest, R.R. Langley, G. Villares, A. Sanguino, S.K. Lutgendorf, G. Lopez-Berestein, M.M. Bar-Eli, and A.K. Sood, *Effect of interleukin-8 gene silencing with liposome-encapsulated small interfering RNA on ovarian cancer cell growth.* J Natl Cancer Inst, 2008. **100**(5): p. 359-72.

140.   *Tamoxifen for early breast cancer: an overview of the randomised trials. Early Breast Cancer Trialists' Collaborative Group.* Lancet, 1998. **351**(9114): p. 1451-67.

141.   Hatch, K.D., J.B. Beecham, J.A. Blessing, and W.T. Creasman, *Responsiveness of patients with advanced ovarian carcinoma to tamoxifen. A Gynecologic Oncology Group study of second-line therapy in 105 patients.* Cancer, 1991. **68**(2): p. 269-71.

142.   Markman, M., K.A. Iseminger, K.D. Hatch, W.T. Creasman, W. Barnes, and B. Dubeshter, *Tamoxifen in platinum-refractory ovarian cancer: a Gynecologic Oncology Group Ancillary Report.* Gynecol Oncol, 1996. **62**(1): p. 4-6.

143.   Perez-Gracia, J.L. and E.M. Carrasco, *Tamoxifen therapy for ovarian cancer in the adjuvant and advanced settings: systematic review of the literature and implications for future research.* Gynecol Oncol, 2002. **84**(2): p. 201-9.

Vita

Kshipra M. Gharpure was born in Thane, India on July 4th, 1987, the daughter of Dr. Makarand P. Gharpure and Mrunmayee M. Gharpure, and younger sister of Shantanu M. Gharpure. After completing her bachelor's degree in pharmaceutical sciences from Institute of Chemical Technology, India in 2009, she entered University at Buffalo, State University of New York. She received the degree of Master of Sciences in Biotechnology in August 2011. In August of 2011 she entered The University of Texas MD Anderson Cancer Center UTHealth Graduate School of Biomedical Sciences and joined Dr. Anil K. Sood's laboratory.

Permanent address:

7009 Almeda Road,

Houston, TX, 70054